Liposome-Anchored Local Delivery of Immunomodulatory Agents for Tumor Therapy

by

Brandon Kwong

B.A.Sc., Engineering Science
University of Toronto, 2005

Submitted to the Department of Biological Engineering
in Partial Fulfillment of the Requirements for the Degree of

Doctor of Philosophy

At the

Massachusetts Institute of Technology

June 2012

Signature of Author: _____
Department of Biological Engineering
May 4, 2012

Certified by: _____
Darrell J. Irvine
Professor of Biological Engineering and Materials Science
Thesis Supervisor

Accepted by: _____
Forest M. White
Associate Professor of Biological Engineering
Chairman, Graduate Program Committee for Biological Engineering

Members of Thesis Committee:

Darrell J. Irvine
Professor of Biological Engineering and Materials Science
Thesis Supervisor

K. Dane Wittrup
Associate Director, Koch Institute for Integrative Cancer Research
Carbon P. Dubbs Professor of Chemical Engineering and Biological Engineering
Thesis Committee Chair

Jianzhu Chen
Ivan R. Cottrell Professor of Immunology

Liposome-Anchored Local Delivery of Immunomodulatory Agents for Tumor Therapy

by

Brandon Kwong

Submitted to the Department of Biological Engineering
On May 4, 2012 in Partial Fulfillment of the Requirements for the Degree of
Doctor of Philosophy in Biological Engineering at the
Massachusetts Institute of Technology

ABSTRACT

Immunostimulatory therapies that activate immune response pathways are of great interest for overcoming the immunosuppression present in advanced tumors. Agonistic antibodies against the co-stimulatory receptors CD40 and CD137, Toll-Like Receptor (TLR) ligands such as CpG oligonucleotides, and immunostimulatory cytokines such as IL-2 have all previously demonstrated potent, synergistic anti-tumor effects. However, the clinical use of such therapies is significantly hampered by the severe, dose-limiting inflammatory toxicities provoked upon systemic exposure. We hypothesized that by anchoring immunomodulatory agents to lipid nanoparticles we could retain the bio-activity of therapeutics in the local tumor tissue and tumor-draining lymph node, but limit systemic exposure to these potent molecules. We first prepared liposomes bearing surface-conjugated anti-CD40 and CpG and assessed their therapeutic efficacy and systemic toxicity compared to soluble versions of the same immuno-agonists, injected intratumorally in established solid tumors in mice. Anti-CD40/CpG-coupled liposomes significantly inhibited primary tumor growth and induced a survival benefit similar to locally injected soluble anti-CD40+CpG. Biodistribution analyses following local delivery showed that the liposomal carriers successfully sequestered anti-CD40 and CpG *in vivo*, reducing leakage into systemic circulation while allowing draining to the tumor-proximal lymph node. Contrary to locally administered soluble immunotherapy, anti-CD40/CpG liposomes did not elicit significant increases in serum levels of ALT enzyme, systemic inflammatory cytokines, or overall weight loss, confirming that off-target inflammatory effects had been minimized. Thus, these results confirmed the development of a delivery strategy capable of inducing robust anti-tumor responses concurrent with minimal systemic side effects.

We next assessed the dissemination of the tumor-specific immune response that had been primed by locally administered, liposome-conjugated therapy. Since anti-CD40/CpG-coupled liposomes were unable to consistently induce the rejection of a secondary distal tumor challenge, we adapted the strategy of liposome-coupled delivery for the administration of anti-CD137 and IL-2, two potent T cell-stimulatory agents. Local intra-tumoral therapy using anti-CD137-liposomes + IL-2-liposomes induced the highly potent inhibition of primary treated tumors and achieved a majority of complete cures, while successfully minimizing systemic exposure and eliminating symptoms of inflammatory toxicity, including lethality. In addition, 100% of anti-CD137 + IL-2 liposome-treated mice were protected against a secondary distal tumor challenge, and demonstrated a significant delay in the progression of simultaneously inoculated, distal untreated

tumors. Subsequent analyses confirmed that anti-CD137-liposomes and IL-2-liposomes bound specifically to cytotoxic T cells (CTLs) within the treated tumor, and that the depletion of CTLs abrogated the therapeutic anti-tumor response. Overall, these results indicated the effective local priming of an adaptive tumor-specific response, capable of mediating local, systemic, and memory anti-tumor immunity. The versatility of this liposome conjugation strategy suggests that we have developed a generalizable tool enabling the local delivery of highly potent immunomodulatory agonists in the absence of systemic toxicity, which could substantially improve the clinical applicability of such agents in cancer therapy.

Thesis supervisor: Darrell J. Irvine
Title: Professor of Biological Engineering and Materials Science

TABLE OF CONTENTS

ACKNOWLEDGEMENTS

I would like to sincerely thank all the people who have provided so much support and guidance over the course of this thesis.

To my family: my parents, my brother and my sister-in-law, and my grandparents. You have all been constant sources of inspiration, encouragement, and support, without which I would not be where I am today.

To my fiancée Bonnie: all the way from first-year PhD classmates, to being office-mates and lab-mates, and now on our way to a life together, you have been with me through it all. Your love and support has been amazing, and I could not have done it without you.

To my advisor Darrell: beyond all the technical and scientific guidance you have given me over the years, your dedication and integrity provide an amazing role model for everyone in the lab, and I have the utmost admiration and respect for you.

To my friends at MIT, especially Abhinav – apartment-mate for 5 of these years; Alex (+family), James TM, Nidhi and Saurabh, and Ta, your friendship and support have made the tough times bearable, and the good times even better, and because of you I will always remember my years at MIT with much fondness.

To past and current members of the Irvine Lab, especially Adrienne and James, as well as (in no particular order) Chris, Haipeng, Maria, Erin, Yuki, Yana, Anna, Jamal, Sid, and everyone else, for the friendships and all the technical support I have gotten from you over the years.

To the other members of my thesis committee, Dr. Dane Wittrup and Dr. Jianzhu Chen, and Annie Gai from the Wittrup Lab, for all the technical support and the generous donations of cell lines and plasmid constructs.

To my extended family around Boston, especially my cousins Terence, Tim, and Serena, and Uncle Paul and Aunt Janis (and family), who have always been encouraging and welcoming during my time here.

To all other friends and family, for all your support.

I am forever grateful to all of you.

List of Figures

5.2. *In vitro* binding and bioactivity of anti-CD137-coupled liposomes on primary stimulated splenocyte cultures.
5.3. *In vitro* binding and bioactivity of IL-2/Fc-coupled liposomes on primary stimulated splenocyte cultures.
5.4. Highly potent inhibition of primary treated B16 tumors in the absence of systemic toxicity, via intra-tumoral liposome-coupled anti-CD137 + IL-2/Fc therapy.
5.5. Potent therapeutic efficacy concurrent with severe or lethal systemic toxicity induced by intra-tumorally injected, soluble anti-CD137 + IL-2/Fc combination therapy.
5.6. Systemic circulating levels of anti-CD137 and IL-2/Fc following intra-tumoral soluble or liposome-anchored delivery.
5.7. Rejection of distal secondary tumor challenge in mice, following local anti-CD137 + IL-2/Fc primary therapy in soluble or liposome-coupled form.
5.8. Inhibition of simultaneous distal tumors following liposome-coupled anti-CD137 + IL-2/Fc therapy at a primary tumor site.
5.9. Modified therapeutic regimens fail to significantly improve on the efficacy of liposome-coupled anti-CD137 + IL-2/Fc treatment.
5.10. Lack of an effective therapeutic window for the addition of systemic soluble anti-CD137 + IL-2/Fc therapy to the established regimen of local liposome-coupled therapy.
5.11. Binding specificity of anti-CD137-liposomes and IL-2/Fc liposomes for $CD8^+$ CTLs at the treated tumor and proximal LN.
5.12. Specific binding or non-specific uptake of therapeutic vs. IgG liposomes by NK cells, DCs, and macrophages, at the treated tumor and proximal LN.
5.13. Liposome-coupled anti-CD137 + IL-2/Fc therapy induced an increase in tumor-infiltrating CTLs, but not NK cells, at the treated and distal tumors.
5.14. Reduced infiltration of regulatory T cells and the overall priming of increased CTL:Treg ratios in therapeutic liposome-treated tumors.
5.15. Requirement for $CD8^+$ CTLs but not NK cells in the priming of an effective anti-tumor immune response, via liposome-coupled anti-CD137 + IL-2/Fc therapy.

CHAPTER 1: Background and Motivation

1.1. Immunomodulatory therapies for tumor treatment

Tumors possess a wide variety of mechanisms to enable evasion from detection and elimination by the host immune system.[1,2] These mechanisms include the impairment of tumor-infiltrating effector cells such as NK cells and cytotoxic T cells (CTLs) either directly (via induction of apoptosis or anergy) or indirectly (via secretion of inhibitory cytokines leading to tolerance); the downregulation of antigen expression, antigen presentation, and co-stimulatory pathways to hinder induction of tumor antigen-specific immune responses; and the recruitment of immuno-suppressive cells such as regulatory T cells and myeloid-derived suppressor cells. Therefore, a potentially powerful therapeutic strategy for tumor treatment is to stimulate the host immune system in order to counteract these mechanisms of tumor-induced suppression, while allowing the tumor itself to act as a depot site of tumor antigen release.

Previous studies have successfully demonstrated this strategy with the administration of non-cell-based biologic therapies, such as cytokines, siRNA, monoclonal antibodies, or Toll-like Receptor (TLR) agonists, as well as small-molecule drugs. For example, antibodies against CTLA-4, PD-1, or IL-10 receptor can counteract tumor-associated immune tolerance by blocking tumor-induced suppressive effects on CTLs, dendritic cells, and other immune subsets.[3,4] Similarly, siRNA or small-molecule compounds that inhibit the immuno-suppressive STAT3 pathway can induce significant anti-tumor responses, from the delay of tumor progression up to the complete regression of established tumors.[5] On the other hand, cytokines such as GM-CSF, interferon-alpha (IFN-α), IL-2, or IL-12, antibodies such as anti-CD40, anti-OX40, or anti-CD137, and TLR agonists such as CpG oligonucleotides can directly provide

costimulatory signals to antigen-presenting cells (APCs) or tumor-specific T cells, to trigger the effective priming of an anti-tumor immune response.[6-9] Furthermore, these therapies can be combined with cell-based therapies, such as the adoptive transfer of *ex vivo*-primed tumor antigen-specific T cells or *ex vivo*-activated antigen-primed APCs, thereby delivering a potent strike against the tumor and re-activating various facets of anti-tumor immunity.[10,11] Over the past two decades, these strategies of anti-tumor immunotherapy have shown enormous promise in successfully treating a wide variety of pre-clinical animal tumor models, as well as in a growing number of clinical trials.[12-14]

1.2. Systemic toxicity and other limitations of tumor immunotherapy

While there are many forms of tumor immunotherapy that have proven highly effective in pre-clinical models, the clinical usage of immunotherapies for cancer treatment remains limited. Cell-based therapies, such as the adoptive transfer of autologous tumor antigen-specific T cells for the treatment of melanoma, are expensive procedures that are labor-intensive and require highly specialized technical expertise. Despite promising results in clinical trials for metastatic melanoma patients, adoptive T-cell therapies have yet to demonstrate sufficient improvements in efficacy (compared to currently established cancer therapies) in order to achieve market approval in the US.[10,11] Additional complexities such as the genetic engineering of T cells (for increased proliferation and resistance to apoptosis, or improved effector function) prior to adoptive transfer can enhance the overall efficacy of therapy, but require even greater levels of labor, cost and technical expertise. Presently, the only FDA-approved cell-based cancer therapy is Sipileucel-T for the treatment of advanced prostate cancer, in which autologous leukocytes are isolated from a patient, cultured and activated in the presence of a prostate cancer antigen and the immune-

stimulatory cytokine GM-CSF, and then re-infused into the patient. The overall cost of Sipileucel-T reaches nearly $100,000 per patient, and provides an average increase in survival time of only 4.1 months.[11,15]

Non-cell-based biologic immunotherapies have also been tested in a vast array of pre-clinical tumor models and clinical cancers. Such immunotherapies, although considerably more expensive than traditional regimens of chemotherapy, are nevertheless far more affordable than cell-based therapies. However, the primary limitation of many immunotherapeutic agents, despite extensive records of potent efficacy in small-animal models, is that these agents can elicit serious (potentially fatal) side effects following systemic infusion, due to nonspecific systemic activation of leukocytes.[16-21] Thus, the clinical effectiveness of many immunostimulants has remained limited by the lack of a strategy to achieve therapeutic efficacy while avoiding excessive systemic exposure.

Dose-limiting toxicities of anti-tumor immunotherapies have been observed in multiple pre-clinical animal studies and human clinical trials.[18,21-25] For example, the co-administration of the immunostimulatory cytokines interleukin-12 (IL-12) and IL-18 causes a fatal inflammatory response in mice, characterized by high levels of systemic inflammatory cytokines such as interferon-gamma (IFN-γ) and tumor necrosis factor-alpha (TNF-α) released into the serum ("cytokine storm").[21] IL-2 cytokine therapy, though already approved for the treatments of advanced metastatic melanoma and renal cancer, requires in-patient monitoring and administration due to its potentially fatal side effects, and in particular "vascular leak syndrome", in which leakage from blood vessels and capillaries can cause a dangerous loss of blood pressure and significant fluid accumulation in the lungs.[16] Similarly, immuno-agonistic monoclonal antibodies such as anti-CD40 and anti-CTLA-4 have demonstrated anti-tumor efficacy

simultaneous with similar dose-limiting systemic side effects in both mice and humans.[17,23-25] Systemic or off-target inflammatory toxicities observed in human patients have included liver damage, transient depletions or abnormalities in circulating hematologic cell populations, inflammatory ocular damage, symptoms of severe autoimmunity, and serum cytokine release, which causes fatigue, nausea, fever, and muscular aches.[22,25,26] In the most severe case, a phase I safety study of the T-cell stimulatory antibody anti-CD28 resulted in near-lethal inflammatory shock and multi-organ failure in human patients, despite having shown no signs of lethal inflammatory toxicity in pre-clinical animal testing.[27,28] These examples illustrate the challenge in finding an appropriate dosing regimen for immunomodulatory agonists that can balance between stimulating an anti-tumor immune response and avoiding nonspecific inflammatory effects. Given the well-established potency of such immunotherapeutics, developing a strategy to mitigate the toxicity of these compounds while maintaining their therapeutic efficacy could substantially improve their prospects for clinical translation.

1.3. Strategies to limit systemic toxicity of immunostimulatory therapies

Previous studies have attempted to address the issue of minimizing systemic side effects of immunostimulatory therapy. In one recent study, Ahonen et al found paradoxically that the hepatotoxic effects of intravenous anti-CD40 therapy could be greatly reduced or even eliminated by the systemic co-adminstration of a TLR7 agonist.[29] However, the authors were not able to determine specific cellular or molecular mechanisms by which the combination therapy resulted in reduced toxicity; nor did they examine whether or not this reduction in toxicity is universal to all combinations of TLR ligands with anti-CD40 therapy.

The use of targeting motifs to enhance the specific localization of immunostimulatory ligands at tumor sites represents another possible strategy for reducing the off-target inflammatory effects of systemically administered immunotherapy. In two separate studies, Hamzah et al described the use of fusion peptide-targeted anti-CD40 + IL-2, or surface peptide-targeted liposomes encapsulating CpG.[30,31] Although both methods succeeded in increasing the localization of therapy to the tumor site, and thus greatly improved the anti-tumor response relative to non-targeted therapy, neither strategy was able to eliminate systemic exposure to the immunostimulatory agonists. Targeted delivery of anti-CD40 + IL-2 still resulted in elevated serum levels of hepatic ALT enzyme and the inflammatory cytokine TNF-α, while targeted delivery of CpG-liposomes could not prevent non-specific scavenging by the reticulo-endothelial system (RES), as indicated by substantial particle uptake in the spleen. Similarly, Johnson et al studied the intravenous administration of a tumor antigen-targeted antibody-IL-2 fusion protein, and found that less than 5% of the injected dose actually reached the tumor following i.v. delivery.[32] These results confirmed that the use of tumor-specific antibody targeting is not sufficient to abrogate systemic circulation and exposure.

1.4. Local immunotherapy and the priming of a systemic anti-tumor immune response

In light of the dangers of systemic immunostimulatory therapy, intratumoral or peritumoral treatments have also been tested in an attempt to reduce the level of systemic exposure to potent immuno-agonists. In the clinical setting, local immunotherapy has so far been proposed primarily for the treatment of unresectable tumors or for post-surgical adjuvant therapy to prevent local recurrence.[33-36] Pre-clinical studies in animal models have shown that the generation of a local anti-tumor immune response can drive systemic/distal tumor inhibition.

Hypothetically, this could occur either by the systemic dissemination of locally stimulated tumor-specific T cells (or other immune effectors), or by the migration of locally activated APCs bearing tumor-specific antigens that enable T cell priming at distal lymphoid organs and other tumor sites. For example, local therapies applied at a single tumor site using anti-CD40,[37] CpG,[38] target antibody-cytokine (IL-2) fusion proteins,[32] and other immunostimulants have successfully inhibited the growth of distal untreated tumors.[9,39-42] Notably in these studies, when an unrelated tumor model was implanted at the distal site, no distal tumor inhibition could be observed, confirming the antigen-specific nature of the locally primed anti-tumor response. Such an adaptive immune response is highly desirable in the clinical setting since it could enable immunological targeting of unknown tumor metastases or disseminated malignancies, following locally delivered immunotherapy at a known tumor site. Indeed, the intratumoral injection of CpG has recently been tested in a phase I clinical trial against B-cell lymphoma in humans, and some patients exhibited anti-lymphoma clinical responses at distant, untreated tumor sites.[43]

Induction of an adaptive, tumor antigen-specific immune response has also been reported in pre-clinical studies to confer immunological anti-tumor memory, as evidenced by the ability of treated mice to reject subsequent tumor challenges, following the immune-mediated elimination of a primary treated tumor.[41,44,45] In the context of human cancer patients, such an adaptive memory response would theoretically enable the immunological rejection of a recurrent tumor growth at a later time (without requiring additional regimens of therapy), whether at a local or distant anatomical tissue/organ.

Despite such therapeutic benefits, pre-clinical and clinical studies have established that the local injection of soluble agonists[46-50] or controlled release of drugs from a local injection site[51-53] does not necessarily prevent such agonists from entering the systemic circulation and dispersing

to distal lymphoid organs. This could occur either by drainage through lymphatics to the thoracic duct or via direct entry into the bloodstream from leaky tumor vessels. In mice, subcutaneous or intratumoral administrations of the immunotherapeutic cytokines IL-2 or IL-12/GM-CSF resulted in rapid clearance from the local injection site and detection in other peripheral organs within minutes after injection.[49,52] Similarly, in human patients, high circulating levels of IL-12 or IL-2 were observed within 30 minutes or 3 hours (respectively) after intratumoral/subcutaneous injection.[46,54] Such observations have necessitated the use of isolated organ perfusion in order to avoid the systemic toxicity of some local recombinant cytokine therapies. For example, the use of TNFα therapy to treat unresectable soft-tissue malignancies in the limbs (currently approved in Europe) requires isolated limb perfusion, a procedure in which major blood vessels are clamped or ligated in order to eliminate the spread of locally administered TNFα into systemic circulation.[55-57] This clearly illustrates that the maximum tolerated dose in locally administered immunotherapy may still be restricted by the need to limit undesired widespread exposure and off-target inflammatory symptoms.

Motivated by the practical and biological limitations of highly potent anti-tumor immunotherapies as described above, we therefore sought to develop a biomaterial-based delivery strategy for immune-stimulatory factors that could physically retain injected therapeutics at a local tumor site and limit their tissue drainage. The primary goals of such a strategy are to demonstrate that the therapeutic efficacy of these agents is not compromised following biomaterial-based delivery, activating a potent anti-tumor immune response while eliminating symptoms of systemic inflammatory toxicity.

1.5. Biomaterial vehicles for the delivery of cancer therapy

Biomaterial delivery vehicles have previously been developed for a wide range of therapeutic and prophylactic applications, from vaccine delivery to small-molecule and biologic drug delivery. Biomaterial-based systems can take the form of microspheres, nanoparticles, micelles, or macroscopic gel-like matrices, and can be developed from a variety of synthetic or naturally occurring polymer and lipid compositions. In the specific context of cancer therapy, the use of drug delivery systems can confer a number of advantages compared to the administration of free drugs alone, including: 1) the ability to shield the active drug from non-specific uptake, clearance, or degradation, thereby prolonging *in vivo* half-life of the drug; 2) the ability to shield the host/patient from drug activity in undesired tissues and organs, thus reducing toxicity and unwanted side effects; and 3) the addition of passive and active targeting strategies to improve the selectivity of drug delivery, either to the tumor or to the desired tumor-associated cell populations.[58,59]

Historically, the majority of research in the use of biomaterial vehicles or particle systems for cancer therapy has focused on the encapsulation and delivery of small-molecule anti-cancer drugs. This has been motivated in part by the poor solubility of many small-molecule drugs in aqueous buffers, necessitating development of novel delivery strategies to allow such drugs to be injected in a fluid-phase formulation. Currently, the most well-known application of drug delivery systems in clinical cancer therapy is the formulation of the chemotherapeutic drug doxorubicin into liposomes, known as Doxil. Doxil consists of the encapsulation of doxorubicin into the core of liposomal nanoparticles, which include polyethylene glycol-modified ("PEGylated") lipids on their surface. This provides distinct advantages over free doxorubicin in several indications of cancer, including enhanced *in vivo* stability and circulation time, and

improved specificity of uptake in tumors, leading to reduced toxicity in off-target organs such as the heart and other cardiovascular tissues.[58]

1.6. Current limitations in particle-based delivery of biologic anti-tumor therapeutics

In comparison to small-molecule drugs and inhibitors, biologic anti-cancer drugs such as immunostimulatory cytokines, antibodies, siRNA, and DNA frequently demonstrate very low efficiencies of encapsulation or loading into microparticle or nanoparticle systems. This can be attributed to a variety of factors including macromolecular size, charge, hydrophilicity, and conformational stability in the presence of harsh environments such as extreme pH or osmolarity. In addition, the release kinetics of proteins and other biologic drugs following loading into particle delivery systems frequently remains sub-optimal, with a rapid burst release of the protein drug commonly observed. Even in the case of locally injected therapies, the biologic agent would be free to drain into systemic circulation once released from its delivery vehicle, thus re-introducing the risk of systemic toxicity due to non-specific uptake or binding of the highly immunostimulatory therapeutic agent. Although there have been multiple reports of pre-clinical therapeutic efficacy in murine tumor models, following the particle-encapsulated delivery of immunomodulatory cytokines (such as IL-2, IL-12, and GM-CSF)[49,52,60-65] or TLR ligands (such as CpG DNA),[31] the systemic circulating levels of these agents following particle-mediated delivery and the symptoms of systemic inflammatory toxicity have not been explicitly evaluated in these studies. In fact, soluble drugs or immuno-agonists released from locally-injected carriers were reported to reach the systemic circulation as early as 6 hr post-injection.[51,52] In all, the controlled release of immunotherapeutic biologics from micro- or nano-particle systems has not yet achieved clinical success and approval.

An alternative to the micro- or nanoparticle encapsulation of anti-tumor immunotherapies is the formulation of viscous, injectable macroscopic hydrogels, emulsions, or matrices (composed of either natural or synthetic polymers), into which biologics can be entrapped. In such systems, the diffusion rate of the entrapped therapeutic can be controlled by modifying the macroscopic porosity of the gel or emulsion, enabling prolonged release of cytokines and antibodies such as IL-15, IL-2, or anti-CD40 following local injection at a tumor site.[51,66,67] Theoretically, the kinetics of local release can be optimized in these systems, in order to allow high local concentrations of immunostimulatory agents to accumulate for maximal anti-tumor efficacy, while maintaining a sufficiently low level of systemic exposure to prevent toxic side effects. This strategy was successfully demonstrated in a pre-clinical mouse model by Fransen et al using anti-CD40 mixed into a slow-release Montanide (water-in-oil) emulsion.[67] However, it is evident that any release of the therapeutic agent can still drain into systemic circulation via the lymphatics or vasculature, raising the question of whether this optimal therapeutic dosing window can truly be translated from mice to humans, to fully ensure that inflammatory toxic effects in off-target tissues will not be induced in treated patients.

Another alternative strategy to reduce the level of systemic draining following particle-mediated delivery is to physically anchor the immunotherapeutic agent to the micro- or nanoparticle surface, via covalent conjugation. In this manner, release of the immunostimulatory agonist becomes dependent solely on the degradation of the particle vehicle, instead of allowing free diffusion of the agonist out of the particle core. Previous studies using this technique of covalent surface conjugation have primarily been performed in the context of targeting the delivery of particles to cell types expressing specific surface receptors. For example, a frequently studied strategy for cancer therapy is to deliver chemotherapy-loaded particles

preferentially to tumor cells, by modifying the particle surface with the addition of targeting peptides or antibodies specific to proteins over-expressed on malignant cells (including HER2, EGFR, CD19, CD20, EPCAM, and many others).[58,59,68-70] The goal of this strategy is to increase specific binding and uptake of drug-loaded particles by cancerous cells relative to healthy cells, thus focusing the cytotoxic effects of the loaded chemotherapy. Similarly, this approach can be used to enhance the specificity of delivery of other cytotoxic agents such as radioisotopes, as well as imaging or contrast agents.[71] However, there have been few published reports describing the use of covalent conjugation onto a nanoparticle surface as a method to deliver locally restricted, high doses of an immunotherapeutic cargo (such as an immunostimulatory antibody or protein) for local cancer therapy.

One previous study performed by Dominguez et al. described the use of polylactide (PLA) nanoparticles bearing covalent surface-coupled anti-CD40 and anti-neu antibodies.[72] The anti-neu antibody provided targeting to tumor cells (in a murine tumor model) that express the neu peptide, while anti-CD40 is an immunomodulatory agonist that potently stimulates APCs expressing the co-stimulatory surface receptor CD40. Significant anti-tumor therapeutic responses were observed following either the intra-tumoral (local) or systemic (intravenous) injection of anti-neu/anti-CD40 nanoparticles, although a direct examination of the severity and breadth of anti-CD40-induced systemic toxicity was not described, nor was the systemic level of anti-CD40 measured following nanoparticle delivery. In addition, quantitation of the conjugated therapeutic antibody on the PLA nanoparticles was not reported. A well-characterized and generalizable platform that combines the efficient delivery of immunostimulatory agonists to a local tumor site, with the simultaneous elimination of systemic toxicities commonly associated with such immunotherapies, remains an unmet need.

In the present studies, we have sought to overcome the challenges described above by developing and fully characterizing a nanoparticle platform for the delivery of immunostimulatory agents. An ideal platform for local tumor therapy should enable the physical, spatial sequestration of immunomodulatory agonists at the tumor site in order to minimize systemic exposure and toxicity; induce a potent anti-tumor response at the treated tumor site; stimulate long-lasting and systemic anti-tumor immunity to protect against recurrent or distal tumors; and demonstrate the versatility to provide consistent delivery of a variety of immunotherapeutic agents for tumor treatment (Figure 1.1).

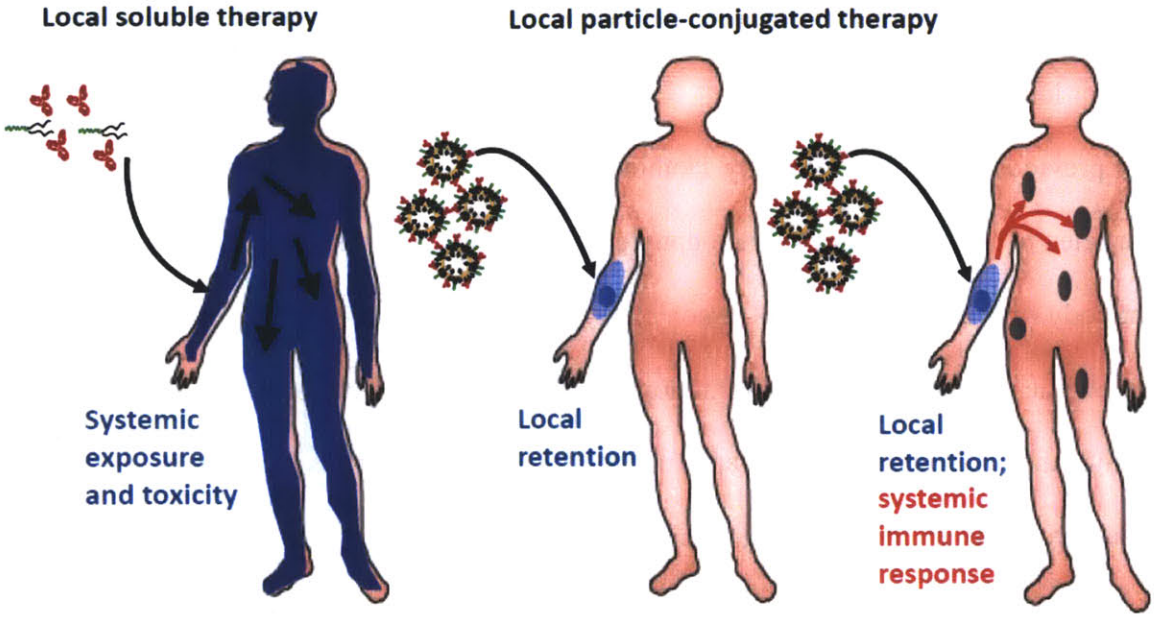

Figure 1.1. The ideal response to a locally restricted cancer immunotherapy. Soluble agonists can drain systemically and cause widespread exposure and toxicity even after local injection (left), while a nanoparticle-conjugated therapy is locally sequestered to prevent systemic exposure (middle). The locally primed immune response can subsequently disseminate to target multiple distal or metastatic tumors (right).

CHAPTER 2: Scope and Aims of Current Thesis

Based upon the motivations and research background described previously, the following specific aims were formulated for this thesis:

I) Develop a strategy for nanoparticle-coupled local delivery of immunostimulatory therapy, for the treatment of solid tumors. The goals of this specific aim were to develop, optimize, and characterize formulations of polymeric or liposomal nanoparticles, for the ability to bind and deliver an immunostimulatory agent for tumor treatment. This study focused on the delivery of anti-CD40, which carries a well-established record of therapeutic anti-tumor efficacy (primarily via the stimulation of APCs) along with severe systemic inflammatory effects, in both pre-clinical and clinical studies. The evaluation of different nanoparticle formulations was accomplished by measuring the efficiency and stability (*in vitro* and *in vivo*) of antibody coupling; quantitating systemic levels of antibody draining into serum circulation *in vivo* following local administration; confirming local sequestration and retention of the therapeutic antibody in the injected tumor tissue; and demonstrating proof-of-concept anti-tumor responses to ensure that nanoparticle conjugation did not abrogate the potency of antibody therapy. The optimal nanoparticle formulation satisfying these criteria was then used for the delivery of various immunotherapeutic cargoes, in the subsequent aims of the thesis.

II) Demonstrate the local anti-tumor efficacy of nanoparticle-mediated immunotherapy against a subcutaneous B16 melanoma tumor model, while reducing systemic exposure and inflammatory toxicity. The goals of this specific aim were to use the nanoparticle system developed in Aim I for the delivery of efficacious immunotherapies against a subcutaneously

implanted B16 murine melanoma model. The nanoparticle-conjugated delivery of multiple immunostimulatory agents, such as the addition of a TLR ligand or an immunostimulatory cytokine with an agonistic antibody, were tested for local anti-tumor efficacy and systemic toxicity *in vivo*. An effective therapeutic regimen of local (intra-tumoral) injections of nanoparticles was established along with detailed characterization of the bio-distribution of the combined immunotherapy, and the ability to induce memory and/or systemic anti-tumor immunity were assayed using secondary or simultaneous distal tumor challenges. Mechanistic experiments were performed to gain an understanding of how the anti-tumor immune response was primed following intra-tumoral nanoparticle-conjugated therapy.

III) Optimize the therapeutic potency and versatility of nanoparticle-coupled immunostimulatory agonist therapy. The final objective of this study was to maximize the clinical relevance of the nanoparticle-anchored strategy of immunotherapy developed in the previous two aims. To accomplish this, additional candidates of immunostimulatory agents were screened for the greatest therapeutic potency of local, systemic, and memory anti-tumor immune responses. In particular, immunomodulatory factors capable of directly activating tumor-resident cytotoxic T cells were investigated, as such a strategy could hypothetically stimulate the most robust adaptive anti-tumor response. This served to demonstrate the versatile applicability of the nanoparticle-coupled delivery strategy to multiple immuno-agonists. As before, measurements of systemic exposure and toxicity were performed to confirm the local retention of immunotherapeutics, and biologically-oriented mechanistic experiments were carried out to determine the immunological cell populations responsible for mediating the therapeutic response.

CHAPTER 3

Local nanoparticle-conjugated delivery of immunomodulatory agents for tumor therapy: proof-of-concept using anti-CD40 antibody

3.1. Abstract

This chapter describes the initial development of anti-CD40-coupled nanoparticles for the treatment of subcutaneously implanted murine B16 tumors. Preliminary experiments were conducted using phospholipid-coated PLGA nanoparticles, synthesized by a double emulsion technique. Maleimide-functionalized lipids were included in the nanoparticle coating layer, providing a reactive group for two different coupling schemes. In the first scheme, anti-CD40 was mixed with SAT(PEG)4, a crosslinking reagent that binds to exposed primary amines on one end while bearing a thiol group on the opposite end; "thiol-functionalized" anti-CD40 was then added to PLGA nanoparticles for maleimide-thiol conjugation. In the second scheme, anti-CD40 was incubated under mild reducing conditions to expose thiols from hinge-region disulfide bonds, then mixed with PLGA nanoparticles for maleimide-thiol conjugation. Nanoparticle coupling under either scheme yielded stable binding of anti-CD40, but this delivery strategy achieved only moderate levels of anti-tumor efficacy following local injection into established subcutaneous tumors. Bio-distribution analysis of nanoparticles following intra-tumoral injection showed the considerable aggregation of nanoparticles *in vivo*, which could account for the slight loss of efficacy when equivalent doses of nanoparticle-conjugated anti-CD40 were compared to free soluble anti-CD40. This motivated a switch from polymeric nanoparticles to maleimide-functionalized liposomes as the delivery vehicle, with antibody coupling carried out via a similar conjugation protocol. *In vivo* experiments demonstrated modest improvements in therapeutic

efficacy using anti-CD40-coupled liposomes, while maintaining minimal levels of systemic toxicity. The results described here formed the basis for the subsequent aims of this thesis.

3.2. Introduction

3.2.1. Anti-CD40 as a cancer immunotherapy

Previous studies have conclusively established the therapeutic efficacy of immunomodulatory agents for inducing potent anti-tumor responses. For example, cytokines such as IFNα, IL-2, IL-12 and IL-15, antibodies such as anti-CTLA-4 and anti-PD1, and TLR agonists such as CpG DNA and Imiquimod have all demonstrated potent immune-stimulatory activity in a wide variety of pre-clinical tumor models and clinical trials with human cancer patients.[6,9,12,41,43,46,73,74] Of these, anti-CTLA-4 (Ipilimumab) has been approved for the treatment of metastatic melanoma, while IL-2 (Aldesleukin) has been approved for metastatic melanoma and metastatic renal cancer, and IFNα is used in the treatment of certain leukemias.

The surface receptor CD40, expressed on antigen-presenting cells such as DCs, B cells, and macrophages, represents another common target of anti-tumor immunotherapy. CD40 is the cognate receptor for CD40 ligand (CD40L), which is expressed by T cells, and is involved in co-stimulatory interactions during T cell priming by APCs. Agonistic immunostimulatory antibodies against CD40 act by directly triggering the CD40 receptor and circumventing the need for CD40L binding.[19] The ligation of CD40 and subsequent activation of DCs and other APCs has been reported in a variety of tumor models to prime a potent cytotoxic $CD8^+$ T cell (CTL)-mediated response.[44,45,75-77] Therapeutic responses have been demonstrated against both CD40-expressing tumor lines (such as B cell lymphoma) and non-expressing tumors (such as renal cell carcinoma).[37,78,79] Additionally, in some reported studies (in both mice and humans), anti-tumor

responses have been observed via the activation of macrophages, NK cells, or B cells, which can then exert tumor-inhibitory effects in a T-cell independent manner.[80-85] However, despite a substantial record of pre-clinical success, and recent promising clinical responses in human patients bearing non-Hodgkins lymphoma, multiple myeloma, or other solid malignancies, anti-CD40 antibodies have yet to gain FDA approval.[19,22-24]

A primary concern that has significantly limited the clinical success of anti-CD40 therapy is the well-established inflammatory toxicity that occurs following the systemic (intravenous) infusion of anti-CD40 in human patients.[23-25] Dose-limiting toxicities have been observed in a large fraction of patients, including symptoms of liver and ocular inflammatory damage, elevated levels of inflammatory cytokines in serum, hematologic abnormalities (T-cell depletions or other lymphopenias), and various patient discomforts (chills, fatigue, nausea, and fever). Similarly, inflammatory toxicities in the liver, lungs, and gut have previously been observed in mouse models following intravenous soluble anti-CD40 therapy.[86-90] While these symptoms are reversible and can be treated in human patients using anti-inflammatory agents such as steroid pre-medications, these dose limitations have hindered the ability to achieve a clinically effective therapeutic window between significant efficacy and the onset of toxicity. Moreover, although the aforementioned side effects were mostly transient in nature, two recent studies in mice unexpectedly observed long-term immuno-suppression following anti-CD40 therapy as well, possibly relating to the activation-induced apoptosis of $CD4^+$ or $CD8^+$ T cells.[91,92] Therefore, we considered that anti-CD40 would be an ideal candidate therapy to test with our proposed strategy of nanoparticle-anchored local delivery.

3.2.2. Strategies for protein and antibody delivery via nanoparticle vehicles

The local delivery of anti-CD40 and other immunomodulatory factors encapsulated into biomaterial vehicles has previously been reported in various studies, ranging from the use of liposomes and nanoparticles (diameter <1μm) to larger microspheres (diameter >1μm) and macroscopic hydrogels. Examples include the delivery of cytokines and Toll-like Receptor (TLR) ligands in microspheres, liposomes, or crosslinked hydrogel matrices.[49,51,52,62,63,93] In each of these studies, which were carried out in therapeutic tumor challenge models, significant anti-tumor effects were observed, although the systemic inflammatory effects of such potent immunostimulatory treatments were not directly examined. Liposomes and gelatin nanoparticles have also been used to deliver encapsulated anti-CD40 or CpG in the setting of prophylactic vaccinations or pre-tumor challenge.[50,53,94] Disparate and conflicting levels of systemic side effects have been reported in these studies, perhaps reflecting differences in the stability of agonist entrapment in these various carriers. Since soluble factors released from particle carriers are known to spread into systemic circulation,[51,52] this motivates our proposed strategy of physically anchoring immunomodulatory compounds to locally retained particle carriers for the purpose of minimizing systemic toxicity, instead of the more commonly used encapsulation/release strategies cited above.

For lipid-based particles such as liposomes or lipid-coated polymeric nanoparticles, a frequently reported strategy for attaching targeting moieties to the particle surface is via a "post-insertion" technique.[95-97] This strategy consists of first attaching the targeting peptides or antibodies to lipid micelles or a dispersed mixture of phospholipids, via a range of possible chemical coupling reactions, such as maleimide-thiol or ester-amine conjugations. Subsequently, the targeting micelles can be mixed with previously prepared liposomes or lipid-

coated particles, under conditions in which the spontaneous insertion of micelles into the lipid bilayer is thermodynamically favored. While the insertion of micelles into liposomes has been reported to be highly efficient, the initial reaction of the biologic agent (whether antibodies, proteins, peptides, or other biologics) to lipid molecules remains the principal limitation in overall efficiency. Therefore, for the present study, we decided to forego the post-insertion approach for the conjugation of immunotherapeutic antibodies, and instead used direct conjugation to maleimide-functionalized lipids on the surface of prepared nanoparticles or liposomes. The use of spontaneous micelle insertion will be further discussed in subsequent chapters, for the addition of a synthetic CpG DNA-lipid conjugate to previously coupled antibody-bound liposomes.

3.3. Methods

3.3.1. Synthesis of anti-CD40-coupled PLGA nanoparticles

Phospholipid-coated poly-lactide-co-glycolide (PLGA) nanoparticles were first prepared by a double emulsion/solvent evaporation technique, as previously established in our lab.[98] PLGA was dissolved in dichloromethane along with a mixture of phospholipids (DOPC, DOPG, and maleimide-PEG(2000)-DSPE in a 70 : 17.5 : 12.5 molar ratio), and emulsified by sonication with a fractional volume of water. The resulting emulsion was added into an excess volume of dichloromethane and sonicated again, creating a non-uniform dispersion of phospholipid-coated PLGA-core nanoparticles and microparticles. Nanoparticles were separated by sucrose gradient centrifugation, then washed and re-suspended in phosphate-buffered saline (PBS) in preparation for antibody conjugation. Nanoparticle size was measured using either dynamic light scattering or static laser diffraction.

Anti-CD40 (clone FGK4.5, rat IgG2a isotype, from Bio-X-Cell) was coupled to maleimide-functionalized nanoparticles using one of the following reaction schemes: 1) conjugation via SAT (N-Succinimidyl S-acetyl(thiotetraethylene glycol)) linker; or 2) conjugation via DTT (dithiothreitol) reduction (Figure 3.1). For conjugation via SAT, anti-CD40 was incubated for 2h with a molar excess of the SAT(PEG)$_4$ bifunctional crosslinker (Pierce), which binds to reactive amines (on anti-CD40) on one end and carries a sulfhydryl group on the other end, separated by a short PEG (polyethylene glycol) spacer. Effectively, this resulted in the addition of multiple reactive thiol groups to the antibody. Brief incubation with hydroxylamine induced the deprotection of these reactive thiol groups, and following passage through a desalting column to remove excess reagents, anti-CD40 was immediately mixed with previously prepared lipid-coated nanoparticles in the presence of a reducing buffer (TCEP) to allow for maleimide-thiol coupling to the nanoparticle surface. Antibody-nanoparticle coupling was allowed to proceed overnight (at least 8 hours) at room temperature.

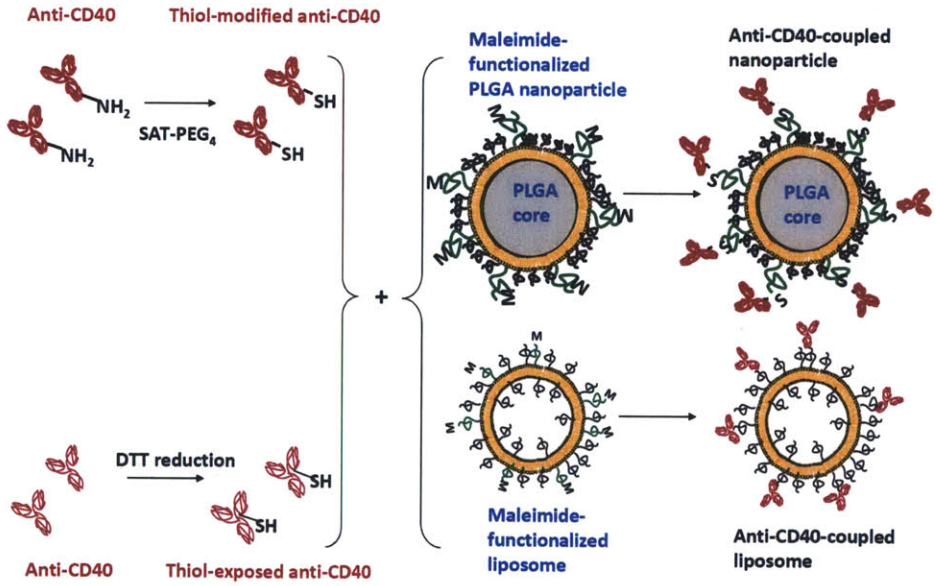

Figure 3.1. Methods for anti-CD40 coupling to PLGA nanoparticles or liposomes. Reactive thiols are prepared by addition of a SAT-PEG$_4$ linker to amines, or by DTT reduction, allowing the conjugation of the antibody to maleimide-bearing particles.

For conjugation via DTT reduction, anti-CD40 was briefly incubated with a 10x molar excess of DTT (approximately 1-2mM) for 20-25min in the presence of EDTA. This concentration of DTT constitutes mild reducing conditions, causing cleavage of accessible disulfide bonds on the antibody into exposed reactive thiol groups, primarily in the hinge region of the antibody. Following passage through a desalting column to remove DTT, the reduced (thiol-exposed) anti-CD40 was immediately mixed with lipid-coated nanoparticles for maleimide-thiol coupling, which was allowed to proceed overnight at room temperature.

3.3.2. Synthesis of anti-CD40-coupled liposomes

Maleimide-functionalized liposomes were synthesized by the re-hydration of a dried phospholipid film and subsequent sonication/extrusion to form small unilamellar vesicles. Phospholipid lipid films (DOPC, cholesterol, methoxy-PEG(2000)-DSPE, and maleimide-PEG(2000)-DSPE in a 50:35:10:5 molar ratio) were first vacuum-dried, then re-suspended and vortexed in PBS. The suspensions were sonicated for 4-5min, followed by syringe extrusions through various membrane sizes as required (50nm, 100nm, or 200nm). Anti-CD40 was then coupled to liposomes using either of the conjugation protocols that had previously been used for coupling to lipid-coated PLGA nanoparticles: via a SAT crosslinker or DTT reduction and maleimide-thiol reaction (Chapter 3.3.1, Figure 3.1). Various lipid compositions were tested for optimal efficiency of antibody binding to liposomes, including the presence or absence of cholesterol, the presence of DOPG, and a titration of the maleimide-PEG(2000)-DSPE content.

3.3.3. Quantification of anti-CD40 coupling and release

Following coupling to either PLGA-core nanoparticles or liposomes, the quantity of conjugated anti-CD40 was measured by first incubating particles briefly in aqueous buffer containing the surfactant Tween 20 (0.5%). This causes the disruption of the antibody-coupled lipid coating on nanoparticles, or the complete dissolution of antibody-coupled liposomes, thus solubilizing lipid-conjugated antibody for quantitation assays. Absorbance at 280nm was used to determine total protein content, while an ELISA was performed to quantitate "functional" levels of anti-CD40. The functional ELISA was designed as follows: 96-well plates were coated with an anti-human IgG antibody, followed by the addition of a recombinant mouse CD40/human Fc fusion protein, which acts as a specific capture agent for anti-CD40 (a rat IgG2a isotype). The level of captured antibody was then measured using an HRP-conjugated anti-rat IgG as the detection antibody, followed by an HRP-sensitive substrate for colorimetric measurement.

In vitro release studies of anti-CD40-coupled PLGA nanoparticles or liposomes were performed at 37 deg C, in either RPMI complete medium or PBS, with or without the addition of 10% fetal calf serum. PLGA nanoparticles were simply incubated and pelleted at the desired timepoints, and supernatants removed for quantitation of released antibody. Liposomes were incubated in membrane dialysis cassettes with a 300kD MWCO (permeable to any released antibody, but not to intact liposomes), and samples and dialysis buffers were collected at the desired timepoints to measure anti-CD40 levels.

3.3.4. *In vitro* confirmation of anti-CD40 activity after conjugation to PLGA nanoparticles

To confirm that the conjugation of anti-CD40 to nanoparticles does not hinder its ability to potently stimulate CD40-expressing APCs, anti-CD40-coupled nanoparticles were added to

murine bone marrow-derived dendritic cell (BMDC) cultures (on day 5 or 6 of culture, in immature state). After 24 or 48 hours, cells were harvested, stained, and analyzed by flow cytometry for the upregulation of CD70 surface expression, a previously reported marker of CD40-induced activation. Soluble (unconjugated) anti-CD40 and isotype IgG-coupled nanoparticles were used as positive and negative controls for CD70 upregulation, respectively.

3.3.5. B16F10 tumor therapy using anti-CD40-coupled liposomes and nanoparticles

As a model of tumor therapy, and for characterizing the *in vivo* bio-distribution of anti-CD40-coupled particles, B16F10 tumors were implanted subcutaneously into the hind flanks of female C57BL/6 wild-type mice (6-8 weeks old). The parental line of B16F10 (no foreign antigen expression) was used to ensure a weakly immunogenic, aggressively progressing tumor growth. 5×10^4 B16F10 tumor cells, washed and suspended in Hank's Balanced Salt Solution (HBSS), were implanted on one or both flanks, and tumors were allowed to establish for 8 or 9 days prior to the start of therapy, by which time tumors had an average area of ~$12mm^2$. For anti-tumor therapy experiments, mice received intra-tumoral (local) injections on the indicated days as described in Chapter 3.4 below (for example, days 8/10/12/14 as a representative dosing regimen). Body mass of treated mice was measured daily to monitor overall systemic toxicity, and serum was collected at various timepoints during the course of treatment, in order to systemically circulating levels of anti-CD40 and markers of inflammatory toxicity. Serum levels of the pro-inflammatory cytokines TNFα and IL-6 were measured by ELISA, while the serum level of alanine transaminase (ALT), a hepatic enzyme that correlates with liver inflammatory damage, was measured by standard biochemical assay (Infinity ALT kit, Thermo Fisher).

3.3.6. Biodistribution analysis following locally injected anti-CD40 therapy

For bio-distribution analyses, single or multiple intra-tumoral injections of anti-CD40-coupled nanoparticles or liposomes were administered into established subcutaneous B16 tumors. Fluorescent rhodamine-labeled DOPE phospholipid or a hydrophobic fluorescent dye (DiD or DiI) was incorporated (<0.5%) into nanoparticles or liposomes to facilitate *in vivo* detection of the injected particles. Tumors, tumor-proximal lymph nodes, distal lymph nodes, and spleens were excised at the desired timepoints, and either immediately snap-frozen using liquid nitrogen for histological analysis, or physically dissociated into single-cell suspensions for flow cytometric analysis. Histological analysis was performed on cryosectioned tissue samples, with the direct imaging (via confocal microscope) of unstained sections for detection of fluorescently labeled particles, or the processing of immuno-stained sections (acetone-fixed) for detection of specific immunological cell populations and the secondary detection of locally retained anti-CD40. Flow cytometry analysis was performed by staining the recovered cell suspensions with fluorescent antibodies against the surface markers of interest, including the use of CD45 expression as a gating marker for tumor-infiltrating leukocytes.

3.3.7. Statistical analysis

Data are shown as mean ± SEM, unless indicated otherwise. Comparisons of Kaplan-Meier survival curves were performed using a log-rank test. For all other data, comparisons of two experimental groups were performed using two-tailed unpaired t-tests unless indicated otherwise. Statistical analysis for all data contained in this thesis was performed using GraphPad Prism software.

3.4. Results and Discussion

3.4.1. Development and characterization of anti-CD40-coupled nanoparticles

Immunostimulatory agents such as anti-CD40 are known to induce potent anti-tumor responses, but can result in inflammatory toxic effects upon systemic exposure. We sought to develop a generalizable strategy for the nanoparticle-coupled delivery of immuno-agonists, to locally sequester the therapeutic agent following a local injection. Our initial attempts at the development of biomaterial delivery vehicles included the use of crosslinked alginate microspheres for the encapsulation and controlled release of Toll-like Receptor (TLR) ligands, including a TLR9 agonist (CpG DNA) and synthetic TLR7/8 agonists (Imiquimod and Resiquimod, from Invivogen). However, the loading efficiency of such compounds was below the expected threshold for therapeutic efficacy of loaded particles *in vivo*, and the sustained release of these agonists for >1-2 days could not be achieved. Therefore, we proposed a strategy for the covalent conjugation of anti-CD40, a potent immunostimulatory antibody, to the surface of lipid-coated polylactide-*co*-glycolide (PLGA) nanoparticles.

PLGA nanoparticles have previously been used in a wide variety of applications, such as drug delivery vehicles and vaccine adjuvants, and have an established record of bio-degradability and safety. Previous work in the Irvine Lab performed by Bershteyn et al had established a protocol for the synthesis of maleimide-functionalized lipid-coated nanoparticles.[98] Using this protocol (described in Methods above), PLGA nanoparticles were generated with a mean diameter of 320nm, bearing a 12.5% molar ratio of reactive maleimide groups incorporated into the phosopholipid coating on the particle surface. In parallel, anti-CD40 was prepared by modifying reactive amines with the bifunctional SAT(PEG)$_4$ crosslinker, yielding reactive thiol groups capable of coupling to maleimide-functionalized nanoparticles (Figure 3.1). Using this

coupling strategy, approximately 30-50 μg of anti-CD40 was bound per mg of PLGA nanoparticles. Staining of anti-CD40-coupled nanoparticles with a fluorescent secondary anti-rat IgG antibody confirmed the presence of conjugated antibody on the particles (Figure 3.2a). Notably, PLGA nanoparticles displayed a tendency to aggregate following antibody conjugation, resulting in an effective mean diameter of 800-1000nm (Figure 3.2b), as measured by static laser diffraction. The loss in colloidal stability occurred irrespective of whether anti-CD40 or a control rat IgG2a isotype antibody was conjugated, and was likely caused by the antibody-mediated crosslinking of nanoparticles, via the presence of multiple reactive thiols on each antibody.

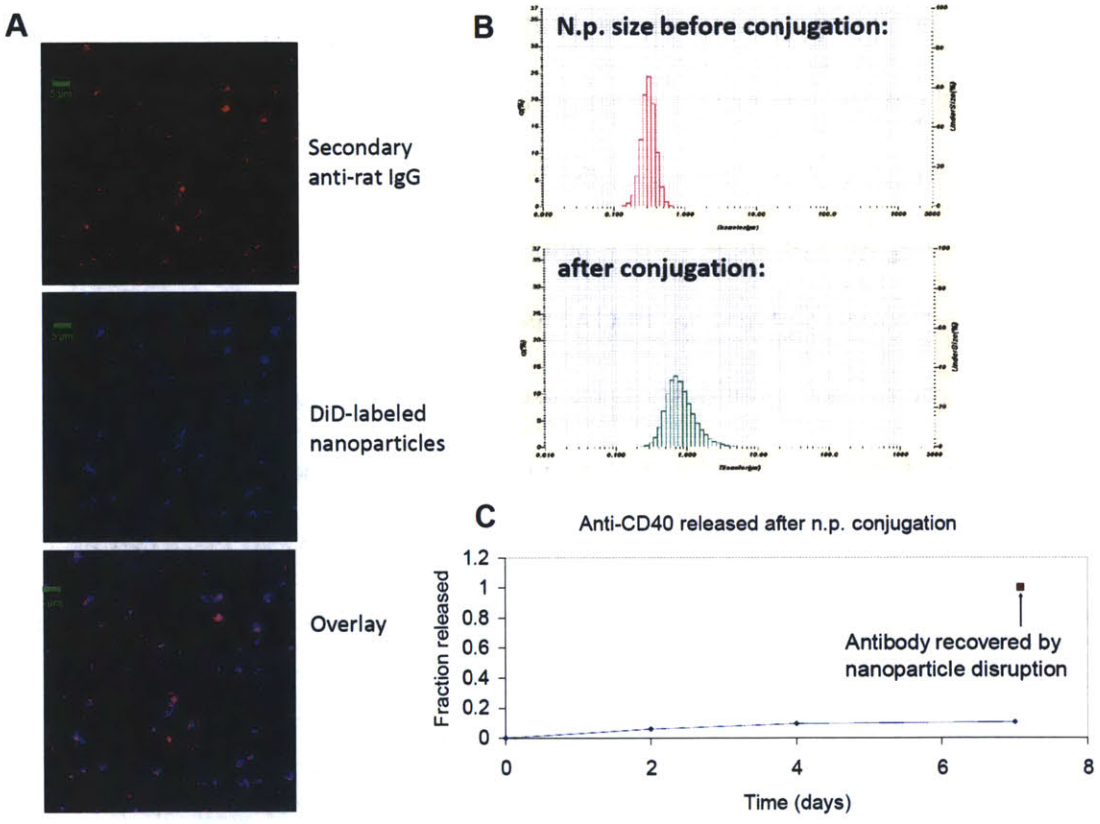

Figure 3.2. Characterization of anti-CD40-coupled PLGA-core nanoparticles, conjugated via a SAT(PEG)$_4$ crosslinker. A) Confocal imaging showing co-localization of secondary staining against anti-CD40 (red) with fluorescently labeled nanoparticles (blue). Scale bar = 5μm. B) Aggregation of PLGA nanoparticles (n.p.) following anti-CD40 conjugation; size distributions were measured by static laser diffraction. C) Stability of anti-CD40 binding to PLGA n.p.

Anti-CD40-coupled nanoparticles were incubated at 37°C in PBS for up to 7 days, to examine the stability of antibody binding to the nanoparticle surface. Figure 3.2c shows that minimal release of the antibody occurred over a 7-day period, as expected given the covalent reaction scheme used for antibody coupling. Disruption of the lipid surface coating after 7 days, using Tween20 as a surfactant, allowed the antibody to be re-solubilized and recovered. Quantitation of the recovered antibody revealed nearly 100% recovery, confirming that this nanoparticle conjugation strategy did not disrupt or denature the conformational integrity and structure of anti-CD40.

To ensure that nanoparticle conjugation did not hinder the stimulatory activity of anti-CD40, antibody-coupled nanoparticles were added to *in vitro* cultures (day 5 or 6) of murine bone marrow-derived dendritic cells (BMDCs), for 24 or 48 hours. Following incubation, cells were harvested, fluorescently stained for CD70 expression, and analyzed by flow cytometry. The upregulation of CD70 expression has previously been used both *in vitro* and *in vivo* as a marker of DC activation through the co-stimulatory CD40 pathway.[99] Figure 3.3 shows the results of CD70 staining on DCs incubated for 24hr with anti-CD40-coupled nanoparticles, control IgG-coupled nanoparticles, or soluble unconjugated anti-CD40, or left untreated. Similar levels of CD70 upregulation were observed in the presence of anti-CD40-coupled nanoparticles or soluble anti-CD40, compared to IgG-nanoparticle or untreated controls, confirming that the stimulatory activity of anti-CD40 was maintained after binding to the nanoparticle surface.

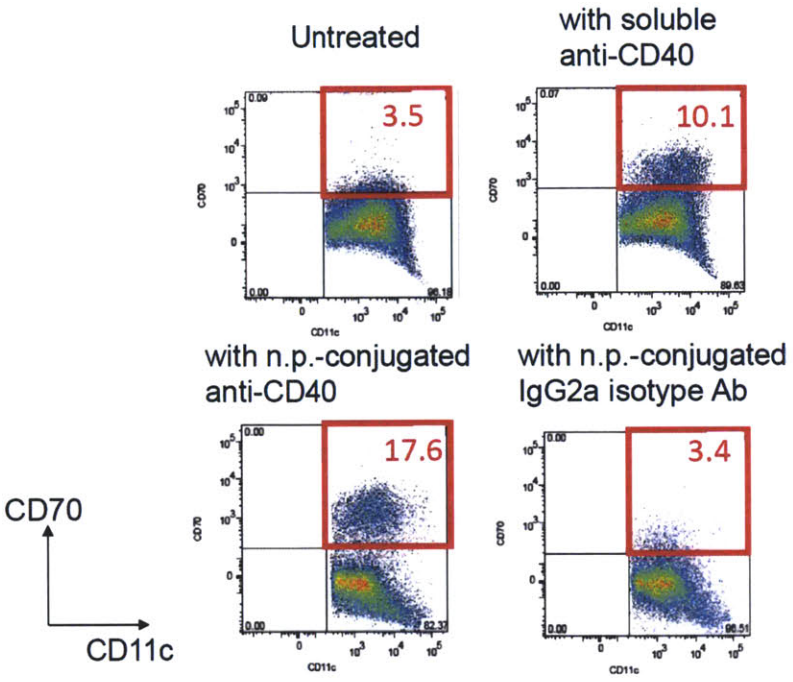

Figure 3.3. CD70 expression following the *in vitro* incubation of bone marrow-derived DCs with anti-CD40-coupled nanoparticles or soluble anti-CD40, as a marker of DC activation.

3.4.2. B16F10 tumor therapy via local injection of anti-CD40-coupled PLGA nanoparticles: therapeutic efficacy and systemic toxicity

Having established a preliminary method for anti-CD40 conjugation to nanoparticles, we next tested whether local nanoparticle-mediated delivery could induce anti-tumor immune responses comparable to the local injection of free soluble anti-CD40. 50,000 B16F10 murine melanoma cells were implanted subcutaneously into the hind flanks of wild-type C57BL/6 mice, and allowed to establish a solid tumor for 8-9 days prior to treatment. Beginning on day 8 or 9, mice received 3-4 doses of anti-CD40 in soluble or nanoparticle-conjugated form, injected intra-tumorally, up to a cumulative dose of 20 mg/kg (approximately 100-125μg per dose). Figure 3.4a shows the average tumor growths measured in two separate experiments, using a dosing regimen of days 8/13/17 or days 9/11/14/16. Anti-CD40-nanoparticles significantly inhibited

B16 tumor growth compared to saline-treated controls, but were less effective than equivalent doses of soluble anti-CD40, under either dosing regimen.

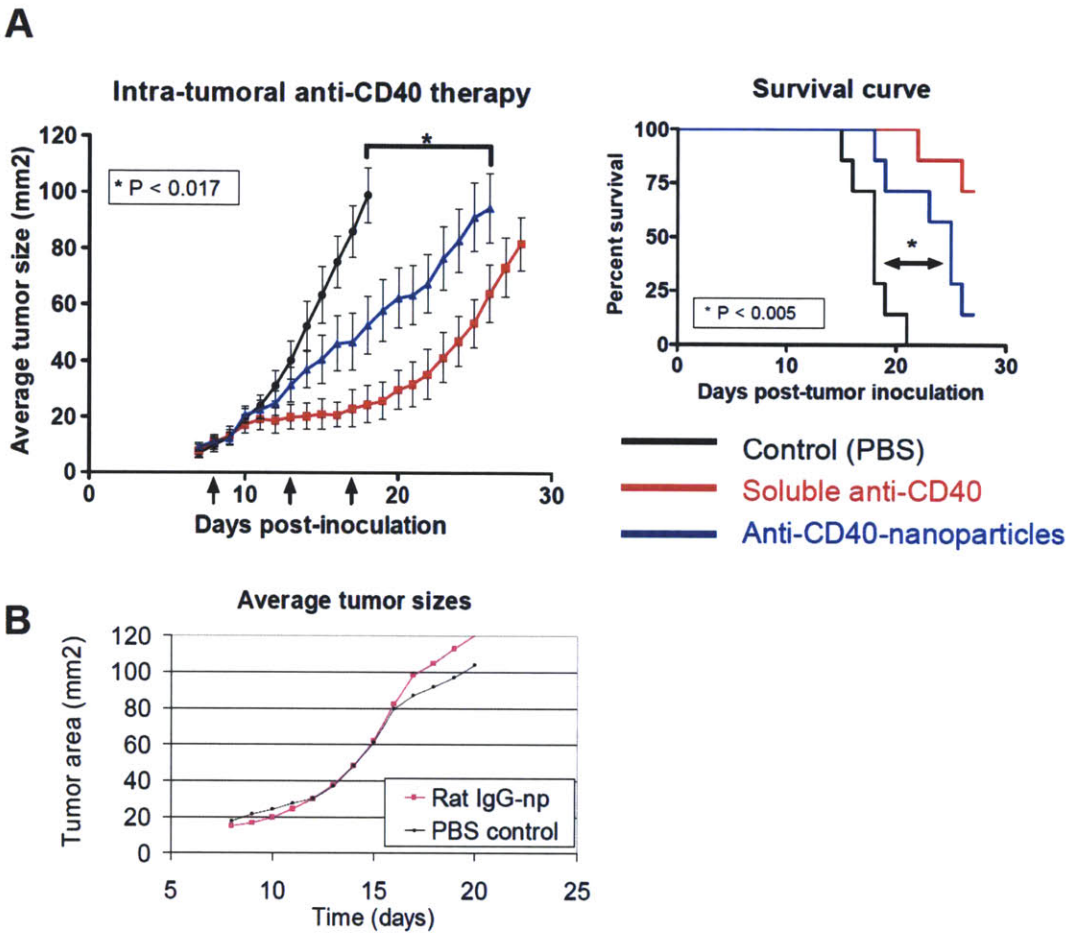

Figure 3.4. Therapeutic efficacy of anti-CD40-coupled PLGA-core nanoparticles vs. soluble anti-CD40 in the treatment of subcutaneous B16F10 tumors. A) Average tumor growths and overall survival following anti-CD40 therapy. Arrows indicate days of treatment. B) Average tumor growths following control therapy using a rat IgG2a isotype antibody.

The same trend was observed when analyzing the overall survival of mice (euthanized when tumor burden reached $100mm^2$), with anti-CD40-nanoparticles providing a modest but statistically significant benefit over untreated mice, while remaining less effective than soluble antibody. Importantly, the intra-tumoral injection of IgG isotype-conjugated nanoparticles had negligible effect on the progression of B16 tumors and overall mouse survival (Fig 3.4b). These

preliminary results demonstrated a proof-of-principle that the nanoparticle-coupled delivery of immunostimulatory agonists could induce an anti-tumor therapeutic response.

Since a primary objective of nanoparticle-coupled delivery was to enable the priming of anti-tumor responses while minimizing systemic toxicity, we evaluated several measures of systemic inflammatory effects over the course of the anti-CD40 treatment regimen described above. Given the stability of anti-CD40 binding and low level of release from the nanoparticle surface *in vitro* (Fig 3.2), it was expected that our strategy of intra-tumorally injected, nanoparticle-coupled delivery would be able to physically sequester the agonistic antibody at the local tumor site, and thus minimize systemic toxicity. As shown in Figure 3.5a, this hypothesis was confirmed by tracking the weight changes of treated mice over the duration of therapy, as an overall measure of body condition. Mice that received soluble doses of anti-CD40, despite being locally injected, showed significant weight loss immediately after the start of therapy. Weight loss peaked at ~10% on day 3 post-injection, comparable to the loss experienced by mice in an inflammatory lipopolysaccharide (LPS)-induced acute phase response.[100,101] This result is consistent with the expectation that soluble anti-CD40 can drain rapidly from the injection site, enter the systemic circulation, and cause widespread inflammatory effects. The transient nature of the systemic response to soluble anti-CD40 has been previously observed and may reflect systemic tolerization to the antibody's effects on repeated treatment.[29,86] On the other hand, mice that received nanoparticle-coupled anti-CD40 did not experience any significant weight changes compared to untreated control mice.

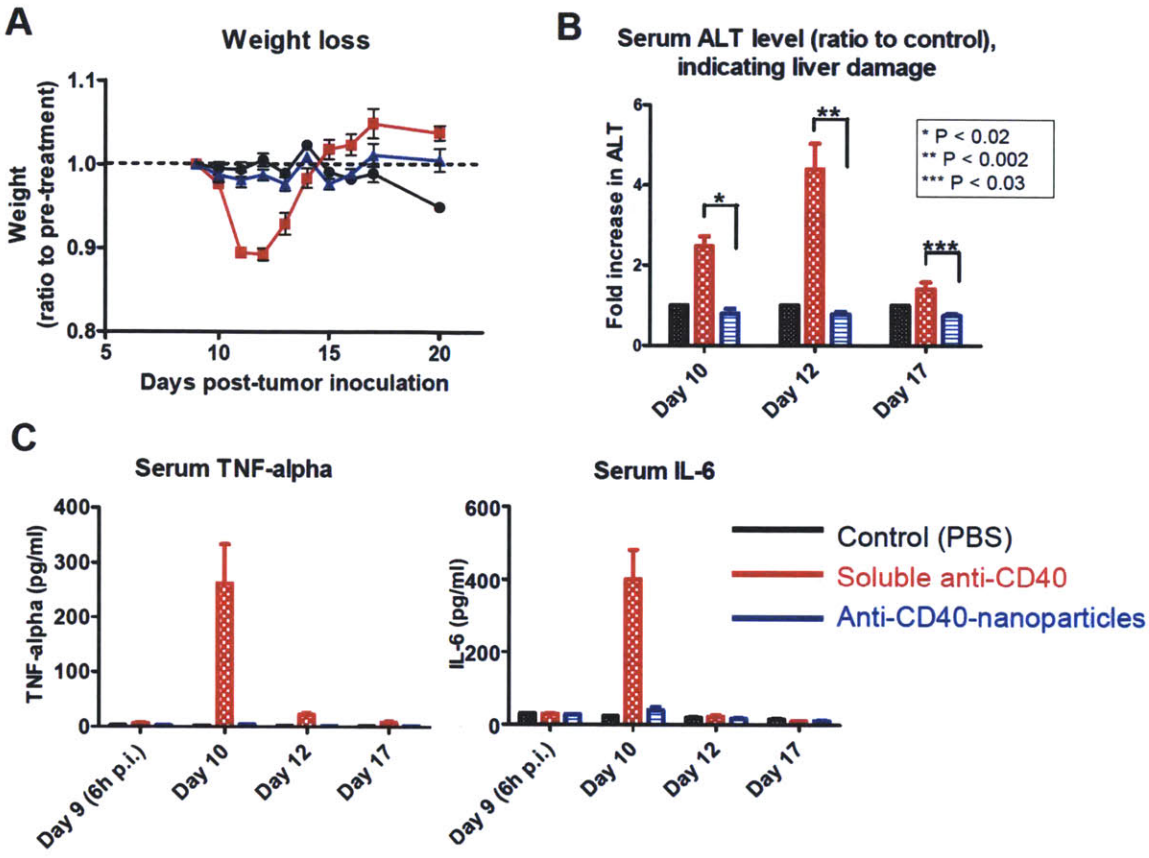

Figure 3.5. Elimination of systemic inflammatory symptoms by the nanoparticle-coupled delivery of anti-CD40, compared to soluble anti-CD40. A) Average changes in weight as an overall measure of body condition over the course of therapy. B) Serum ALT levels, indicative of hepatic inflammatory damage. C) Serum levels of pro-inflammatory cytokines, indicative of systemic inflammatory toxicity.

Serum levels of alanine transaminase (ALT), a hepatic enzyme used as a clinical marker of liver inflammatory damage, were also significantly elevated in soluble anti-CD40 treated mice, but not in anti-CD40-nanoparticle treated mice (Figure 3.5b). This result is consistent with multiple previous reports of liver inflammatory damage in both pre-clinical mouse models and clinical human patient trials following systemic anti-CD40 infusion.[23,25,86] Furthermore, serum levels of the pro-inflammatory cytokines TNFα and IL-6 were increased following soluble anti-CD40 therapy, but not with nanoparticle therapy (Figure 3.5c). Overall, these results clearly

demonstrate that the use of locally injected, nanoparticle-conjugated delivery is able to minimize the systemic toxicity of potent immunostimulatory therapeutics such as anti-CD40.

3.4.3. Local retention and biodistribution analysis of anti-CD40-coupled PLGA nanoparticles

We had hypothesized that nanoparticle-coupled delivery of anti-CD40 would reduce the systemic inflammatory effects commonly associated with soluble therapy, by minimizing systemic draining and exposure to the agonist following a local injection. To confirm this, serum was collected from treated mice and circulating levels of anti-CD40 were measured by ELISA, after single or multiple intra-tumoral injections of soluble or PLGA nanoparticle-conjugated antibody. Figure 3.6a shows that nanoparticle-coupled delivery significantly decreased systemic exposure to anti-CD40, compared to the levels of anti-CD40 that leaked into systemic circulation following soluble injection. The detection of anti-CD40 at the latter stages of the treatment regimen may have been hampered by the presence of anti-rat isotype titers (not shown). For additional confirmation of the local sequestration of anti-CD40, tumors were excised after the end of therapy (multiple doses), dissociated into single-cell suspensions, and the fluid supernatants removed in order to quantitate (by ELISA) the remaining level of anti-CD40 in the local tissue. As shown in Figure 3.6b, significantly higher levels of antibody were recovered from mice treated with nanoparticles, relative to mice that had received soluble anti-CD40. While the absolute level of recovered anti-CD40 was lower than expected (across all groups), this may have been caused by destruction of antibody during the processing of tissues for analysis, or the gradual uptake and degradation of anti-CD40-nanoparticles by APCs in the tumor and surrounding tissues.

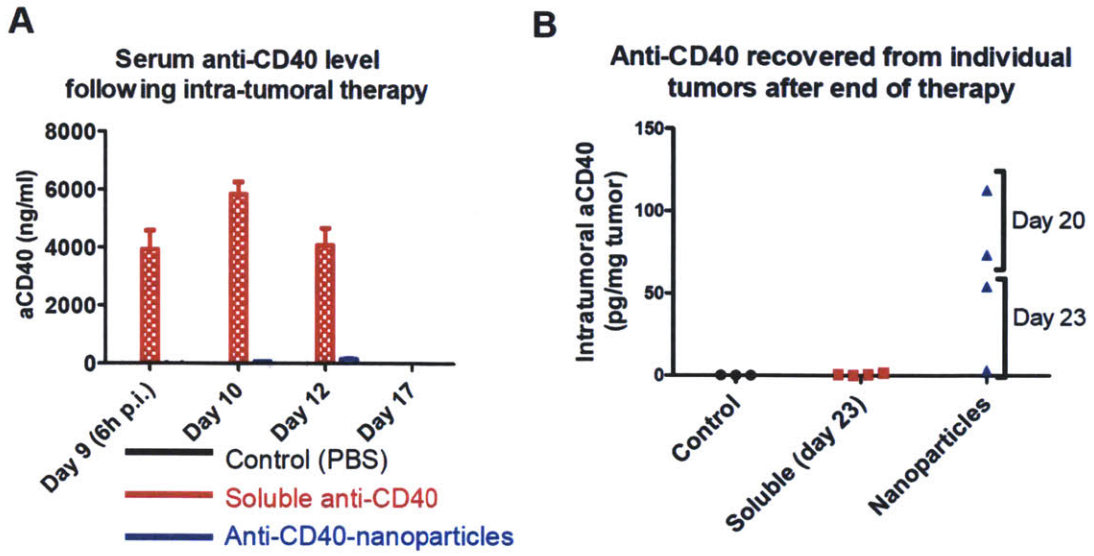

Figure 3.6. Local retention of anti-CD40 following intra-tumoral injections of anti-CD40-nanoparticles. A) Systemically circulating levels of anti-CD40 following soluble or nanoparticle-conjugated delivery. B) Local recovery of anti-CD40 from individual tumors, following soluble or nanoparticle-conjugated treatments.

Given the prolonged persistence of anti-CD40 in the injected tumor and surrounding tissues following PLGA nanoparticle-coupled delivery, we had expected that therapeutic efficacy would be enhanced compared to equivalent doses of locally injected soluble anti-CD40. However, as shown above in Figure 3.4, soluble anti-CD40 consistently induced stronger inhibition of tumor growth than nanoparticle-conjugated antibody. In hopes of gaining a better understanding of how the anti-tumor response was being primed, we sought to examine in greater detail the bio-distribution of anti-CD40-coupled PLGA nanoparticles following intra-tumoral injection. Histological analysis was performed on tumors that had been treated with fluorescently labeled anti-CD40-nanoparticles; tumors were excised, cryosectioned, and then directly imaged via confocal microscopy for the local distribution of particles. Figure 3.7 shows representative images of whole tumor cross-sections, showing that anti-CD40-coupled PLGA nanoparticles were poorly or inconsistently dispersed within the local tissue. This could result in large areas

within a given tumor that effectively do not receive any immunotherapy, whereas intra-tumoral injections of soluble anti-CD40 would be expected to diffuse rapidly throughout the tumor and local tissue. We considered that the poor dispersion of PLGA nanoparticles could be attributed to the aggregation of particles following antibody coupling, which resulted in a mean diameter of >800nm in diameter, as shown in Figure 3.2. However, reducing the dose of anti-CD40-nanoparticles to an equivalence of 40μg/dose, in an attempt to reduce particle aggregation effects, only resulted in further decreases in therapeutic efficacy (not shown). This led to the consideration of alternative strategies and particle vehicles for the conjugated delivery of anti-CD40, with the goal of achieving a more uniform local distribution of antibody, and in doing so, enhancing the anti-tumor efficacy of nanoparticle-delivered anti-CD40 therapy.

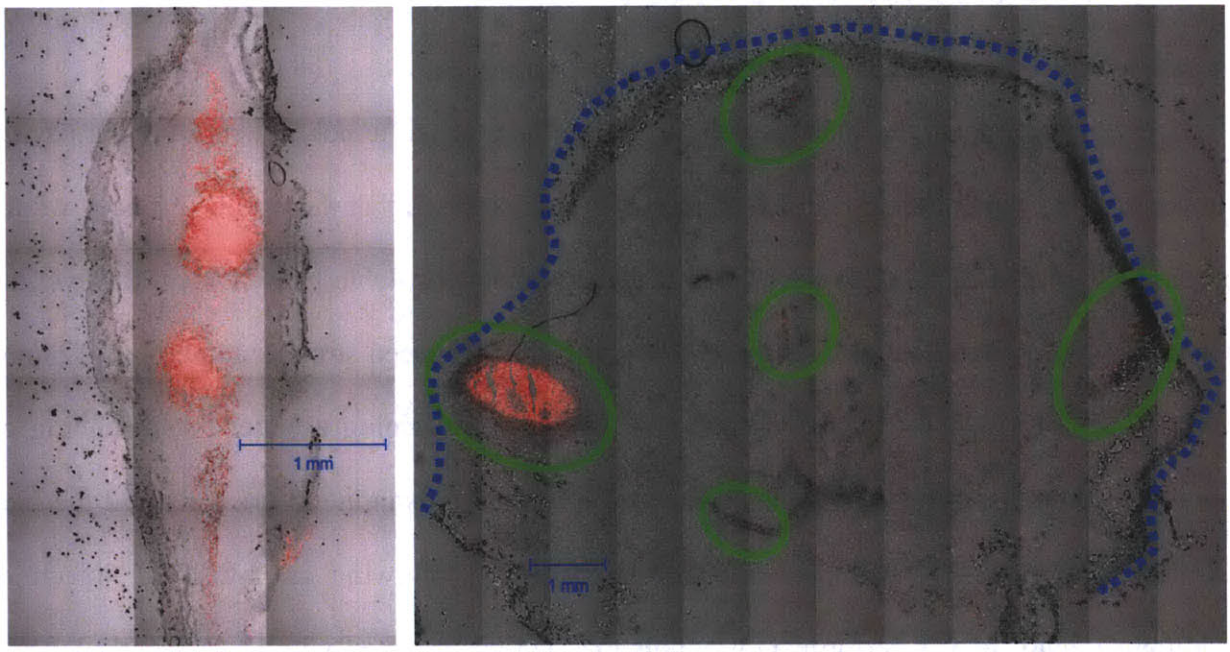

Figure 3.7. Poor dispersion of anti-CD40-coupled PLGA nanoparticles in tumors and the surrounding tissue, following intra-tumoral injection. Representative images of excised tumor cryosections, showing the distribution of labeled anti-CD40-nanoparticles (red), highlighted in green circles. Blue dotted line marks the periphery of the solid tumor mass. Scale bar = 1mm.

3.4.4. Improving strategies for anti-CD40 delivery: development of anti-CD40-coupled liposomes and conjugation via DTT reduction

Since we had hypothesized that a greater dispersion of locally injected particles throughout the tumor would improve therapeutic efficacy, we investigated the use of liposomes as an alternative to lipid-coated PLGA nanoparticles for the delivery of anti-CD40. The use of liposomes was motivated by two primary factors: 1) the size of liposomes can be easily tuned to a range of 100-200nm in diameter, considerably smaller than the PLGA nanoparticles used to date in this study; and 2) liposomes have a higher fluidity and deformability, consisting simply of a lipid bilayer without the relatively stiffer polymeric core. Either or both of these factors could allow liposomes to disperse more readily than PLGA nanoparticles throughout the tumor immediately following injection, given the spatial restrictions of an established solid tumor densely filled with cells, vasculature, and associated stroma. In addition, since an essential goal was to maintain the ability to prevent systemic inflammatory toxicity following local injection, liposomes were an attractive candidate for an alternative delivery vehicle, given the ability to control their size using sonication or extrusion techniques.

To begin, we synthesized liposomes composed to DOPC, DOPG, and maleimide-PEG(2000)-DSPE in a 70 : 17.5 : 12.5 molar ratio (refer to Chapter 3.3.2 methods). Anti-CD40 was coupled to the surface of liposomes using the same SAT crosslinking protocol as previously described for PLGA nanoparticle conjugation (Figure 3.1), and anti-CD40-liposomes were extruded to a mean diameter of ~200nm post-conjugation. The quantity of liposome-coupled anti-CD40 was determined using functional ELISA as described in Chapter 3.3.3, including the use of Tween20 surfactant (0.5% in PBS) to disrupt liposomes after antibody conjugation. A direct comparison between anti-CD40-nanoparticles and anti-CD40-liposomes was conducted, to

evaluate their therapeutic efficacies against subcutaneously implanted B16 tumors (Figure 3.8). Mice were treated with 4 intra-tumoral injections, at 50μg of antibody per dose, on days 9/11/13/16 of tumor growth. Although anti-CD40-liposomes were able to eliminate symptoms of systemic toxicity (weight loss, serum ALT levels, and serum TNFα levels) equally as well as PLGA nanoparticles, no apparent improvement in tumor inhibition was observed (Figure 3.8).

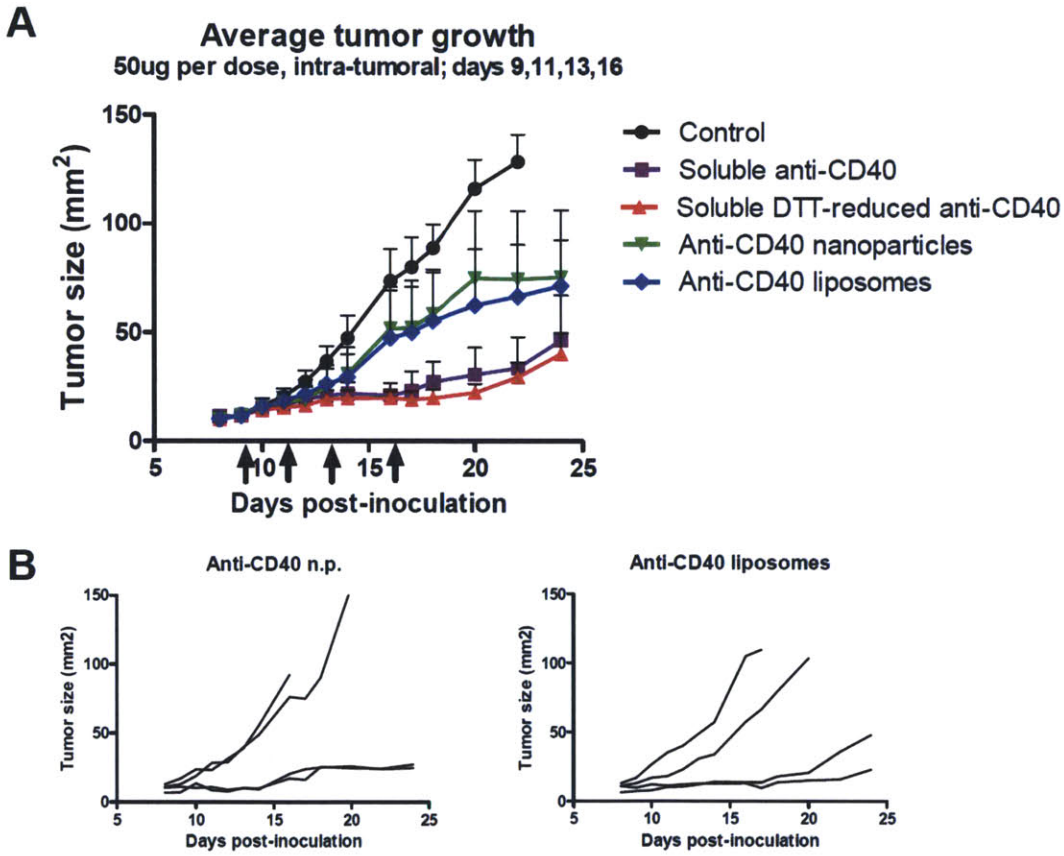

Figure 3.8. Moderate therapeutic efficacy of the initial formulation of anti-CD40-coupled liposomes. A) Average tumor growths following therapy with soluble anti-CD40, anti-CD40-nanoparticles, or newly developed anti-CD40-liposomes. Arrows indicate days of treatment. B) Comparison of individual tumor growths (n=4) following nanoparticle-coupled and liposome-coupled anti-CD40 therapies.

Histological and flow cytometric analysis of tumors immediately following injection, or 24hr and 48hr post-injection, revealed the poor *in vivo* persistence of this initial formulation of anti-CD40-coupled liposomes. As shown in Figure 3.9a with the imaging of tumor cryosections,

rhodamine-labeled anti-CD40-liposomes were dispersed throughout the tumor immediately following injection, but were then rapidly cleared from the local tissue in 24 to 48 hours. Figure 3.9b contains representative flow cytometry results demonstrating that a significantly lower level of rhodamine fluorescence could be detected at the tumor at 24 and 48hr following liposome injection, compared to the injection of rhodamine-labeled PLGA nanoparticles (anti-CD40-coupled). This indicated that although anti-CD40-coupled liposomes displayed a more uniform local dispersion as expected, some degree of optimization would still be required to achieve a maximal level of immunostimulatory efficacy.

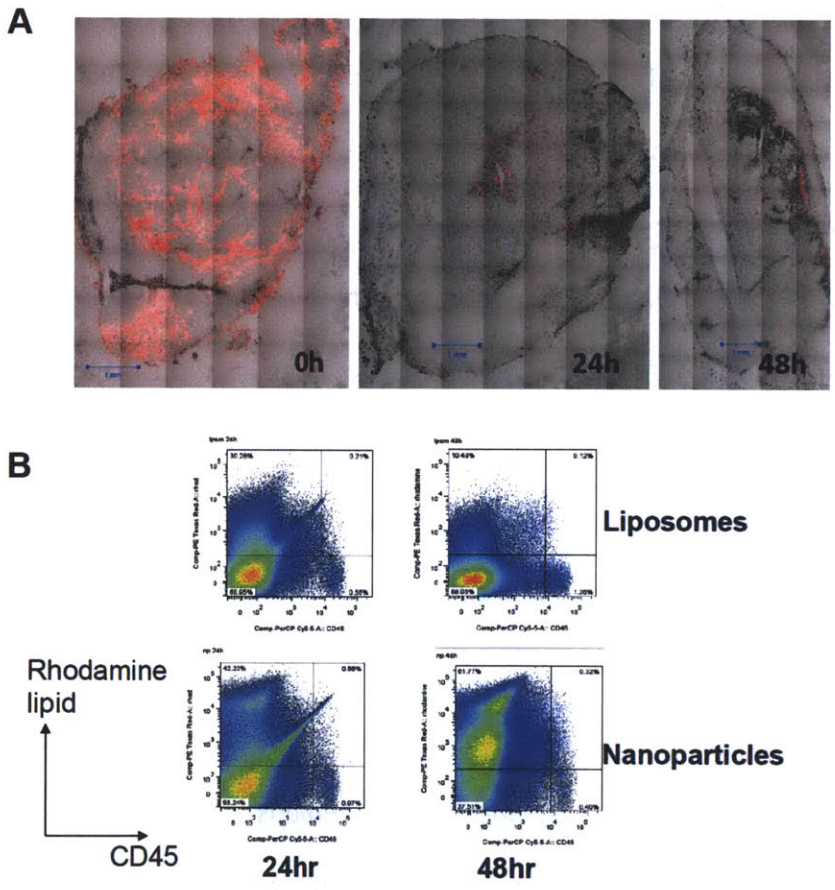

Figure 3.9. Poor *in vivo* persistence of the initial formulation of anti-CD40-coupled liposomes, despite rapid local dispersion following intra-tumoral injection. A) Representative images of tumor cryosections at 0h, 24hr, or 48hr following an intra-tumoral injection of labeled anti-CD40-liposomes (red). B) Flow cytometry analysis of tumor samples at 24hr or 48hr following injections of rhodamine-labeled anti-CD40-liposomes or anti-CD40-nanoparticles.

Over the course of these initial investigations into the use of liposomes as a delivery vehicle for local anti-CD40 therapy, a new protocol was developed for the maleimide-thiol conjugation of anti-CD40 and other antibodies. One concern regarding the previous technique of SAT-mediated conjugation was whether or not the non-specific reaction of the $SAT(PEG)_4$ bifunctional crosslinker to exposed amine groups was hindering the therapeutic activity of anti-CD40. As an alternative method to yield reactive thiol groups on anti-CD40, we considered the use of a mild reducing agent to preferentially cleave disulfide bonds in the antibody's hinge region, resulting in exposed thiols that could be used for reaction with maleimide-functionalized liposomes (refer to Figure 3.1). Previous groups have demonstrated that under mild reducing conditions, hinge-region disulfide bonds in antibodies are selectively cleaved prior to other less accessible disulfides.[102] Therefore, by titrating to a minimal dose or incubation time of the reducing agent, this technique can select hinge disulfides as the specific residues to be exposed and subsequently used for maleimide-thiol conjugation to particle carriers.

We first compared a number of reducing agents of varying potency, including beta-mercaptoethanol, dithiothreitol (DTT), and tris(2-carboxyethyl)phosphine (TCEP). The incubation of anti-CD40 with 1-2mM of DTT (equivalent of a 25x molar excess to antibody) at room temperature for 20-25 minutes was determined to induce sufficient disulfide cleavage to enable antibody coupling with maleimide-functionalized liposomes or PLGA nanoparticles (refer to Chapter 3.3.2 methods). Unmodified and DTT-treated stocks of anti-CD40 were measured by functional ELISA (as described in Chapter 3.3.3 methods), and it was confirmed that DTT reduction did not abrogate the ability of anti-CD40 to bind to a recombinant CD40 receptor. Furthermore, intra-tumoral injections of unmodified or DTT-reduced anti-CD40 in soluble form induced comparable levels of tumor growth inhibition, confirming that there was no loss of *in*

vivo functionality (Figure 3.8). Therefore, for the remainder of the present study, this DTT reduction protocol was used for the covalent coupling of anti-CD40 and all other antibodies to maleimide-functionalized liposomal carriers.

3.4.5. Optimization of anti-CD40-coupled liposomes for enhanced *in vivo* persistence and therapeutic efficacy.

As shown in Figures 3.8-3.9, the initial formulation of anti-CD40-liposome therapy resulted in rapid *in vivo* clearance and sub-optimal anti-tumor efficacy, with a lack of complete cures and lower overall potency compared to soluble antibody. Thus, we attempted to optimize the formulation of liposomes in order to increase *in vivo* persistence and efficacy. While the initial formulation of liposomes had contained DOPC / DOPG / maleimide-PEG(2000)-DSPE in a 70 : 17.5 : 12.5 ratio, we investigated the conjugation efficiency of DTT-reduced anti-CD40 on newly synthesized liposomes without any DOPG content, with the addition of cholesterol, and with titrating levels of maleimide-functionalized lipid. Firstly, the removal of DOPG was motivated by corroborating data produced in the Irvine Lab, suggesting that the strongly negative charge carried by DOPG might potentiate the nonspecific uptake, clearance, or degradation of liposomes *in vivo*. Secondly, the presence of cholesterol is well-known to improve the stability of small unilamellar liposomes that contain unsaturated lipids such as DOPC. Since cholesterol is a relatively small molecule compared to the phospholipid chains, it is capable of "packing" into free spaces in the lipid bilayer, thereby decreasing its fluidity and potentially increasing its resistance to degradation. Thirdly, the maleimide-PEG content in the lipid composition was titrated down in order to minimize partitioning of the PEGylated phosopholipid chains into small micellar structures distinct from the liposomes, a process which occurs more favorably with a

large excess of the highly hydrophilic PEGylated phospholipid. Since the maleimide reactive group is attached to the PEGylated DSPE phospholipid, such partitioning would likely have resulted in a significant level of anti-CD40 coupling to micelles, which would be more rapidly cleared than intact liposomes *in vivo* due to their sub-100nm size.

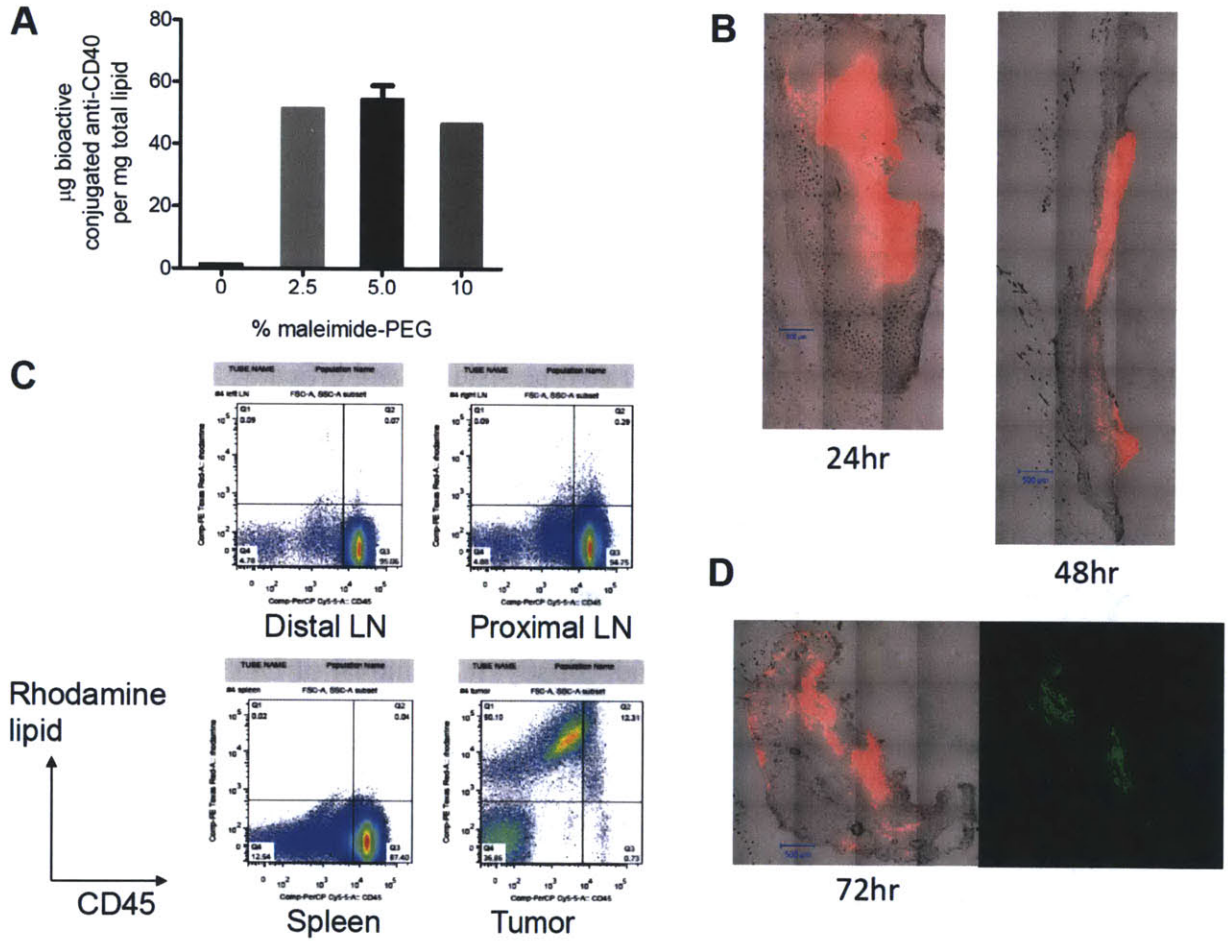

Figure 3.10. Optimization of liposome formulation for highest antibody conjugation efficiency and prolonged *in vivo* persistence. A) Optimizing the lipid composition of liposomes for maximal efficiency of anti-CD40 coupling. B,C) Increased levels of rhodamine-labeled modified liposomes (red) remaining at the tumor site, at 24hr and 48hr post-injection, detected by cryosection imaging or histology. D) Secondary staining (green) against anti-CD40 showing durable co-localization with liposomes (red) at the tumor site, in cryosection images.

Figure 3.10a contains a representative plot from the various optimizations of the liposome composition, demonstrating that a 2.5 to 10% (by mole) range of maleimide-PEG(2000)-DSPE

content resulted in roughly equivalent levels of anti-CD40 conjugation: approximately 55μg of anti-CD40 per total mg of lipid. Omitting the maleimide-PEG phospholipid from liposomes completely abrogated the ability to bind DTT-reduced anti-CD40. For the titration shown here, cholesterol was included at 35% by mole, in addition to DOPC at 50% and methoxy-PEG(2000)-DSPE for the remaining %. A 5% maleimide content was chosen for all subsequent experiments involving anti-CD40-coupled liposomes in this study, based on the observation of slightly enhanced colloidal stability following anti-CD40 conjugation compared to the other formulations. Furthermore, the pre-concentration of anti-CD40 to at least 5mg/ml via centrifugal spin column, prior to DTT reduction and liposome conjugation, was found to greatly improve the overall efficiency of antibody-liposome coupling.

Following the optimization of antibody coupling efficiency, anti-CD40-liposomes were injected intra-tumorally for the histological analysis of *in vivo* persistence. Figure 3.10b shows cryosections of subcutaneous tumors excised at 24hr and 48hr post-injection, displaying high levels of rhodamine-labeled lipid still visible within or surrounding the injected tumor, while Figure 3.10c shows flow cytometry analysis of excised tumors at 24hr. This constituted a substantial improvement over the low level of fluorescence observed using previous formulations of liposomes in this study (Figure 3.9a). Moreover, secondary staining of cryosections using an anti-rat isotype antibody confirmed the co-localization of anti-CD40 antibody (at the injected tumor) with rhodamine-labeled lipid fluorescence, for over 72 hours (Figure 3.10d). Importantly, rhodamine fluorescence was not observed in the spleens or distal lymph nodes of treated mice, indicating that injected liposomes did not enter the systemic circulation to any significant degree (Figure 3.10c). Note that the detection of a directly fluorescently labeled anti-CD40 (tagged using Alexa Fluor 555 antibody labeling kit, Molecular

Probes) proved not to be feasible for *in vivo* experiments, by either histological analysis or flow cytometry, due to an insufficient degree of labeling.

Having characterized and optimized the newly modified anti-CD40-liposomes, we next measured their overall anti-tumor efficacy in a B16 tumor therapy experiment. B16F10 tumors were implanted subcutaneously in C57BL/6 mice and allowed to establish for 9 days prior to the start of therapy. Mice were then treated intra-tumorally on days 9/11/13/15, with 75μg of anti-CD40 per dose in either soluble or liposome-coupled form. Figure 3.11a-b shows the average tumor progression and individual tumor growth curves of treated and control untreated mice.

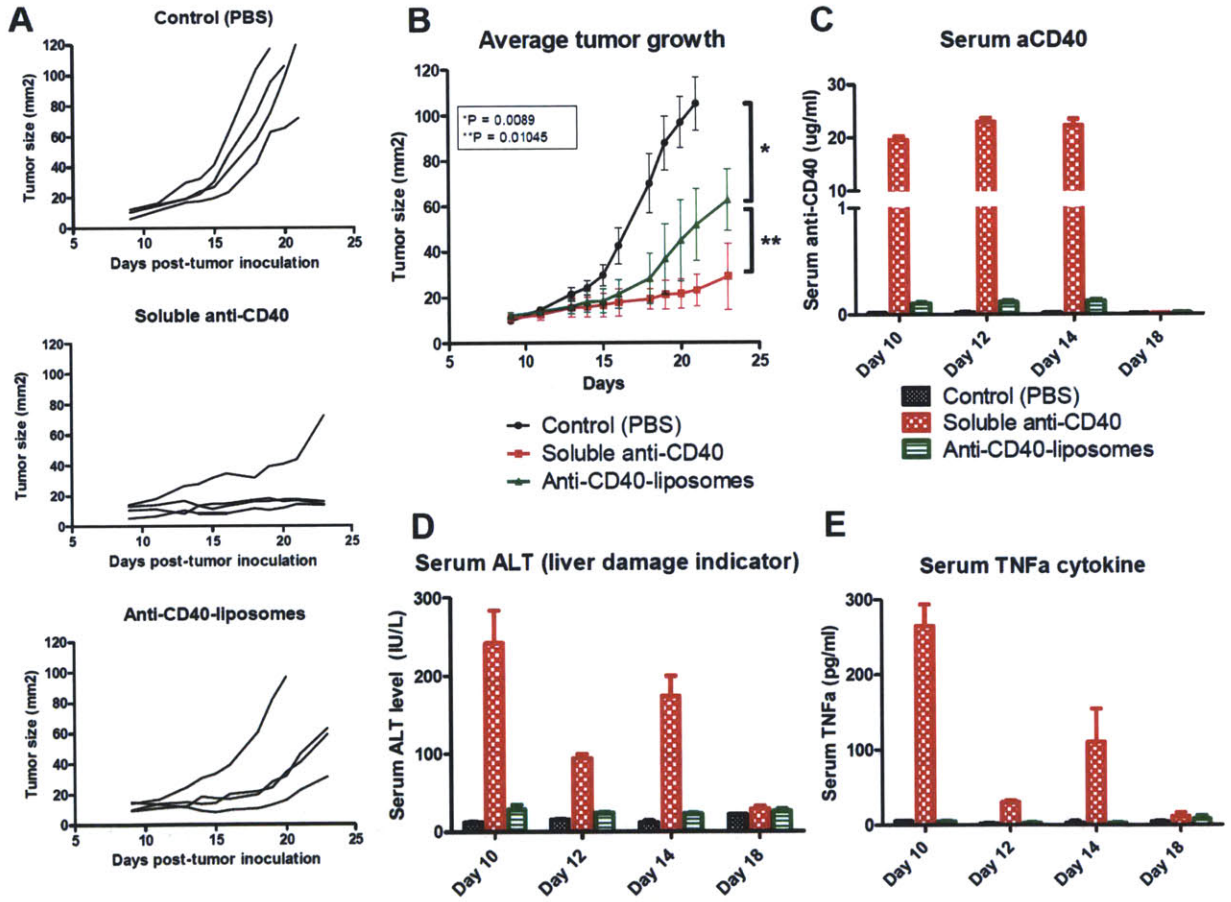

Figure 3.11. Successful inhibition of tumor growth and simultaneous elimination of systemic toxicity by intra-tumorally injected anti-CD40-liposomes. A) Individual tumor growths (n=4) in mice receiving control, soluble anti-CD40, or anti-CD40-liposome therapy on days 9/11/13/15. B) Average tumor growths showing moderate inhibition by liposome therapy and potent

inhibition by soluble therapy. C) Systemically circulating levels of anti-CD40 at indicated timepoints throughout the treatment course. D,E) Serum levels of ALT enzyme and TNF-alpha, indicative of systemic inflammatory toxicity induced by soluble anti-CD40.

Although anti-CD40-liposomes successfully inhibited tumor progression compared to control mice ($p=0.0089$ by paired t-test), liposome therapy still performed significantly worse than soluble anti-CD40 therapy. However, measurements of systemic exposure and inflammatory toxicity demonstrated that the strategy of liposome-coupled delivery provided an enormous benefit compared to soluble therapy, consistent with all the previous toxicity data in this study. For example, circulating levels of anti-CD40 were dramatically reduced by liposome-coupled delivery (Figure 3.11c), correlating with the elimination of inflammatory markers such as serum ALT (Figure 3.11d) and the pro-inflammatory cytokine TNFα (Figure 3.11e) throughout the course of therapy. Overall, these therapeutic results confirmed the ability of locally injected, nanoparticle-conjugated immunostimulatory agents to induce anti-tumor responses while minimizing systemic side effects.

3.5. Summary and Conclusions

In the first part of this study, we developed a conceptual strategy for the local immunotherapy of established solid tumors while avoiding systemic toxicity. By covalently anchoring a highly potent immunostimulatory agonist to a nanoparticle carrier, followed by local intra-tumoral injection, the immunotherapeutic agent was restricted from draining into systemic circulation while maintaining the ability to stimulate a local anti-tumor immune response. Using liposomes or lipid-coated PLGA nanoparticles, anti-CD40 was conjugated via maleimide-thiol reaction and delivered for the treatment of subcutaneously implanted B16F10 tumors in mice. Statistically significant inhibition of tumor growth was achieved in the absence of side effects

such as weight loss, systemic inflammatory cytokine release, and liver inflammatory damage. Bio-distribution analyses confirmed both the local retention of particle-delivered anti-CD40, and a dramatic reduction in the systemic exposure to the antibody.

In spite of the preliminary therapeutic success and optimization of the particle carrier, there were clear limitations to anti-CD40-liposome therapy that remained to be addressed. Although modest delays in tumor progression were consistently achieved, no completely curative responses had yet been attained. Attempts to increase the dosage per injection of nanoparticle- or liposome-coupled anti-CD40 did not yield significant improvements in therapeutic efficacy, most likely due to the aggregation of particles when administered intra-tumorally in a highly concentrated form. Moreover, local soluble injections of anti-CD40 consistently inhibited tumor growth for a more prolonged period than either anti-CD40-coupled liposomes or PLGA nanoparticles (although measurements of systemic exposure and toxicity were consistently elevated with soluble therapy). Given the extended persistence of liposome-coupled anti-CD40 at the injected tumor, compared to the extremely rapid clearance of soluble anti-CD40, it was surprising that soluble therapy induced a more potent anti-tumor response. Soluble therapy was also more efficacious than particle-coupled therapy for the treatment of larger tumors (if the start of therapy was delayed beyond day 10 post-inoculation), an important consideration for the clinical relevance and translatability of this therapeutic strategy.

With these limitations in mind, the subsequent aims of this study were directed towards two overall objectives: 1) the investigation of additional immunotherapeutics that could be combined with anti-CD40 into this nanoparticle/liposome-coupled delivery strategy; and 2) gaining a better mechanistic understanding of how anti-tumor immunity was primed following particle-coupled delivery in comparison to soluble therapy. In addressing these objectives, the ultimate goal

remained to achieve a curative anti-tumor immune response, in the absence of systemic exposure and inflammatory toxicity.

CHAPTER 4

Induction of potent local anti-tumor immune responses by intra-tumoral injection of liposome-anchored anti-CD40/CpG therapy

4.1. Abstract

In this portion of the study, we sought to improve the overall therapeutic efficacy of the nanoparticle-coupled delivery strategy developed in Aim I of this thesis. While liposome-anchored anti-CD40 monotherapy induced significant anti-tumor responses locally in the absence of systemic toxicity, complete cures were not achieved, and liposome therapy remained less potent than soluble therapy. CpG oligonucleotides, a ligand for Toll-Like Receptor 9 (TLR9), have previously demonstrated potent anti-tumor effects, as well as potential synergy when combined with anti-CD40 and other immune-stimulatory agents. However, the clinical use of CpG DNA has similarly been hampered by dose-limiting inflammatory toxicity provoked upon systemic exposure. We hypothesized that by adding CpG DNA to anti-CD40-coupled liposomes, we could retain the bio-activity of both therapeutics in the local tumor tissue and tumor-draining lymph node, while limiting systemic exposure to these potent molecules. Combinatorial anti-CD40/CpG liposomes were prepared, and their therapeutic efficacy, systemic toxicity, and *in vivo* bio-distribution were assessed following intra-tumoral injections into established B16F10 tumors. Anti-CD40/CpG liposomes successfully inhibited tumor growth and induced a survival benefit similar to locally injected soluble anti-CD40+CpG. Biodistribution analyses following local delivery showed that the liposomal carriers successfully sequestered both anti-CD40 and CpG *in vivo*, and did not elicit off-target inflammatory effects such as significant increases in serum ALT levels, systemic inflammatory cytokines, or overall

weight loss. Therefore, combinatorial anti-CD40/CpG liposomes provided a substantial therapeutic improvement over anti-CD40-liposomes alone. The majority of this work was published in a first-author publication, *Biomaterials 32(2011): 5134-5147.*[103]

To increase our understanding of the relative contributions of innate and adaptive immunity to the observed primary anti-tumor responses, preliminary mechanistic experiments were also performed, including the depletion of CD8+ T cells and the use of intra-lymph node injections of anti-CD40/CpG liposomes. Both innate and adaptive responses were found to contribute to the anti-tumor response, which was not surprising given the direct stimulation of APCs such as macrophages and DCs via both CD40 and TLR9. However, despite the highly potent local anti-tumor responses stimulated by anti-CD40/CpG liposome therapy, anti-tumor memory was not consistently primed, as only a small fraction of the surviving mice after primary tumor therapy were able to reject a secondary tumor re-challenge.

4.2. Introduction

4.2.1. Motivation for anti-CD40/CpG combination therapy

Agonists against CD40, a co-stimulatory receptor expressed on the surface of APCs, are known to elicit potent anti-tumor immune responses, but they can also cause severe inflammatory side effects following systemic infusion (as reviewed in Chapter 3.2.1). Pre-clinical studies have shown the efficacy of anti-CD40 therapy against a wide variety of tumor models, either as a mono-therapy,[37,45,77] in combination with chemotherapy,[104] or in combination with other immunostimulants such as IL-2 and IL-15.[30,73,79,105] As described in the previous chapter, we successfully developed a strategy to deliver anti-CD40 therapy via coupling to nanoparticle or liposomal carriers, to enable the local sequestration of potent anti-CD40 therapy

at an injected tumor site, thus minimizing systemic exposure and toxicity. However, liposome-coupled anti-CD40 monotherapy was not sufficient to provide complete curative responses against the B16 tumor model in mice. Therefore, we sought to investigate the combination of anti-CD40 therapy with additional liposome-coupled immunostimulatory agents, in order to improve the anti-tumor response.

CpG oligonucleotides, ligands for Toll-like receptor 9 (TLR9) expressed by APCs, represent another class of potent immunostimulatory factors. Stimulation of the TLR9 receptor directs APCs towards priming potent, T_H1-dominated T-cell responses, by increasing the production of pro-inflammatory cytokines and the presentation of co-stimulatory molecules to T cells.[106,107] Like anti-CD40, CpG therapy has been tested against a wide variety of tumor models in mice, and has consistently been shown to promote tumor inhibition or regression.[8,38,108-113] However, recent studies have also suggested that systemic over-exposure to CpG can have potentially dangerous side effects, including lymphoid follicle destruction and the suppression of adaptive T-cell immunity via indoleamine 2,3-dioxygenase (IDO) induction in the spleen.[114-117] Thus, both anti-CD40 and CpG show substantial anti-tumor potency concurrent with issues of systemic toxicity.

Several previous studies have investigated the combination of anti-CD40 with additional immunostimulatory agonists. In particular, synergy between anti-CD40 and TLR ligands has been demonstrated in a variety of murine tumor models including B16 melanoma, resulting in highly potent anti-tumor responses *in vivo*.[29,82,118-121] Furthermore, it has been proposed that in the absence of co-activation such as TLR stimulation or other microbial priming ("danger") signals, anti-CD40 therapy alone can actually lead to the impairment of CD8+ T cell-mediated anti-tumor responses, possibly by activation-induced apoptosis. For example, Berner et al

reported the suppression of secondary anti-tumor responses following successful primary immunotherapy using anti-CD40 + IL-2; Kedl et al observed the accelerated deletion of tumor antigen-specific CTLs following anti-CD40 monotherapy; and Mauri et al observed immuno-suppressive effects following the administration of anti-CD40 monotherapy in a murine model of chronic autoimmunity.[92,122-124] Furthermore, Schulz et al showed that microbial stimuli are required for the full activation of DCs stimulated with CD40 ligation, as measured by production of the stimulatory cytokine IL-12.[125] Therefore, the addition of the TLR9 agonist CpG DNA to anti-CD40-coupled liposomes was well-motivated with the potential to provide a significant improvement to the anti-tumor responses previously attained.

4.2.2. Novel synthetic CpG DNA-lipid conjugates for incorporation into liposome carriers

Since one of the principal objectives of this study was to eliminate the systemic toxicity of immunotherapy, the addition of CpG to anti-CD40 liposome-coupled delivery required a strategy for anchoring CpG to liposomal carriers. In order to accomplish this, we considered the ability of lipid-based micelles to insert spontaneously into lipid bilayers, such as the outer surface of pre-formed liposomes.[95,96] Within the Irvine Lab, a novel DNA-phospholipid conjugate had recently been developed by Liu et al.[126,127] This synthetic conjugate, composed of a DNA oligonucleotide sequence linked by a short polyethylene glycol (PEG) spacer to two hydrocarbon chains, is an amphiphilic compound that self-assembles into stable micelles when suspended in aqueous buffers (chemical structure shown in Figure 4.1). Previous work by Liu had already demonstrated that these DNA-lipid micelles could be stably incorporated into phospholipid membranes. Therefore, a DNA-lipid conjugate was synthesized containing a frequently reported

immunostimulatory CpG oligonucleotide sequence (CpG 1826), and tested in combination with the anti-CD40-liposomes described in Chapter 3.

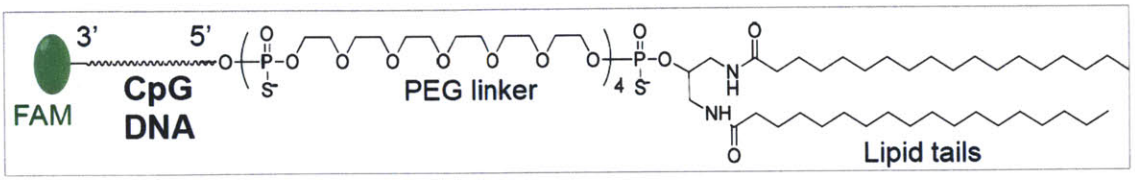

Figure 4.1. Structure of synthetic CpG DNA-lipid conjugate, for incorporation into anti-CD40-coupled liposomes. Synthesized and characterized by Haipeng Liu (Irvine Lab).[125,126]

4.3. Methods

4.3.1. Synthesis of combinatorial anti-CD40/CpG-coupled liposomes

Cholesterol-stabilized liposomes were synthesized as described in Chapter 3, with a composition of cholesterol / DOPC / maleimide-PEG(2000)-DSPE / methoxy-PEG(2000)-DSPE 35/50/5/10 by mol%; 0.5 mol% of rhodamine-labeled DOPE was incorporated for biodistribution experiments. Anti-CD40 (at ~12-15mg/ml) was prepared by DTT reduction, then mixed with maleimide-functionalized liposomes at a ratio of 3 mg Ab:1 μmol liposomes for covalent coupling. The maleimide-thiol reaction was allowed to proceed for at least 10 hr at 25°C, followed by centrifugation of the resulting aggregated liposomes and multiple washes with PBS, to remove unbound antibody. Prior to use, anti-CD40-liposomes were syringe-extruded 25X through 200nm polycarbonate filter membranes.

CpG-lipid conjugates were prepared as previously described.[126,127] To create combination liposomes simultaneously bearing anti-CD40 + CpG, a post-insertion approach[97] was used to insert the purified CpG-lipid conjugate onto the surface of anti-CD40-conjugated liposomes: ~3nmol CpG-lipid was mixed with previously prepared anti-CD40-liposomes (1μmol) for 2hr at 25°C. The resulting combination liposomes were again centrifuged and washed multiple times

with PBS, to remove unimer or micellar CpG-lipid, then syringe-extruded 25X through 200nm filter membranes prior to use. Final liposome size distributions were characterized by dynamic light scattering. An overall schematic describing the synthesis of anti-CD40/CpG combinatorial liposomes is presented in Figure 4.2.

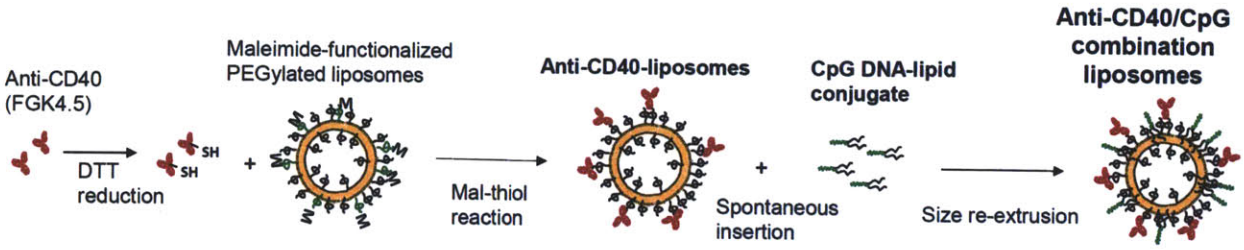

Figure 4.2. Overall schematic of anti-CD40/CpG combination liposome synthesis. Anti-CD40-liposomes are prepared first as previously described (Chapter 3), then combined with a CpG DNA-lipid conjugate, to obtain combinatorial anti-CD40/CpG liposomes.

4.3.2. Characterization of anti-CD40/CpG combination liposomes

Bioactive anti-CD40 conjugated to liposomes was quantified by a functional ELISA assay as described in Chapter 3.3.3. Free CpG and CpG-lipid were both tracked using a fluorescent FAM label on the 3' end, with ex/em wavelengths at 480/520nm. To measure the *in vitro* release of anti-CD40 or CpG-lipid from combination liposomes, dialysis cassettes with a 300kD MWCO membrane were used. 400µl samples were dialyzed against 20ml PBS containing 10% fetal calf serum, with gentle agitation, at 37°C. Samples and dialysis buffers were collected at each indicated timepoint; anti-CD40 was measured by sandwich ELISA and CpG was measured by its fluorescent label FAM. All samples were mixed with 0.5% Tween 20 to disrupt intact liposomes prior to quantitation

4.3.3. B16 tumor therapy using anti-CD40/CpG combination liposomes

For *in vivo* tumor experiments, C57BL/6 mice were anaesthetized and inoculated subcutaneously on the right hind flank with $5x10^4$ B16F10 cells in Hank's Balanced Salt Solution (HBSS). Tumors were allowed to establish for 8 days before the start of therapy, by which time they had reached an average area of ~12 mm^2. Mice then received intra-tumoral injections on days 8/10/12/14 (unless otherwise noted) using PBS, soluble anti-CD40 only, soluble CpG only, anti-CD40-liposomes, soluble anti-CD40 + CpG, or anti-CD40/CpG combination liposomes. Each dose, whether in soluble or liposomal form, consisted of 40 μg of anti-CD40, with or without 20 μg of CpG (unless otherwise noted). The weight change of treated mice was monitored as an indication of overall body condition, and serum was collected from mice at the indicated time points via retro-orbital bleeding, for the measurement of circulating inflammatory markers. Mice were euthanized when tumor areas exceeded 100 mm^2, per institutional guidelines.

Intra-lymph node injections of anti-CD40/CpG liposomes were performed using a non-surgical technique previously reported by Jewell et al.[128] Mice were inoculated subcutaneously with B16 tumor cells as described above. For non-invasive injection of therapy into tumor-proximal lymph nodes, a tracer dye was first injected subcutaneously at the tail base, 24hr prior to the start of therapy. Draining of the tracer dye into the inguinal lymph nodes enabled the nodes to be visualized through the mouse skin. Rhodamine-labeled combination liposomes were then administered on days 8/10/12/14/16, at an effective dose of 8μg anti-CD40 + 4μg CpG in a 20μl volume per injection (1/5 of the dose administered in intra-tumoral therapy). Flow cytometry analysis was performed on day 18 to confirm the presence of rhodamine-labeled

liposomes and FAM-labeled CpG-lipid in the directly injected lymph nodes, at significantly higher levels than in mice that had received intra-tumoral therapy.

To investigate whether cytotoxic T cells were essential for the therapeutic efficacy of anti-CD40/CpG liposomes, antibody depletion of CD8+ cells was performed. Anti-CD8a (clone 2.43, Bio-X-Cell) was injected intra-peritoneally into tumor-bearing on days 6/11/14/17, at a dose of 300μg per injection, and mice received liposomal or soluble therapy as described above. Flow cytometry was used to validate that this dosing regimen eliminated >98% of CD8+ T cells from the tumor, lymph nodes, spleen, and systemic circulation prior to the start of anti-CD40/CpG therapy and continuing throughout the duration of treatment.

To test the anti-tumor memory response of soluble- or liposome-treated mice, B16-bearing mice received anti-CD40/CpG combination therapy as described above, on days 9/11/13/15. Three days following the last dose of therapy, PBS-treated, soluble anti-CD40+CpG treated, or anti-CD40/CpG liposome-treated mice were inoculated subcutaneously on the distal flank with a secondary challenge of $5x10^4$ B16F10 cells. Naïve mice (that had not received primary tumors) were also inoculated to ensure the viability and progression of the particular batch of tumor cells. Long-term surviving mice that were able to reject both the primary tumor and secondary challenge were subsequently re-challenged on day 90, to evaluate the persistence of the memory response.

4.3.4. Analysis of systemic toxicity following intra-tumoral anti-CD40/CpG therapy

Blood was collected from mice at the indicated time points and centrifuged to remove the cellular fraction. Circulating serum levels of TNF-alpha and IL-6 were measured by ELISA, while the serum level of free anti-CD40 was measured by sandwich ELISA using recombinant

CD40 receptor (as described in Chapter 3.3.3). Systemic circulating levels of CpG were detected via its fluorescent FAM label (ex/em at 480/520nm). Serum levels of the hepatic enzyme ALT (alanine transaminase) were measured using a standard biochemical assay (Infinity ALT reagent kit, Thermo Fisher), according to the manufacturer's instructions.

4.3.5. Analysis of *in vivo* biodistribution of anti-CD40/CpG liposome therapy

For biodistribution experiments, a single intratumoral injection of soluble or liposomal formulations was given at a dose of 40 μg anti-CD40 ± 20 μg CpG between days 8-10 post-inoculation, when tumors were at a size of 12-15 mm^2, and mice were euthanized 24hr or 48hr later. Tumors, tumor-proximal or distal lymph nodes, and spleens were harvested and either immediately snap-frozen using liquid nitrogen (for cryosectioning) or digested with 100μg/ml Liberase Blendzyme III (Roche) for 15min at 37°C, followed by mechanical dissoctiation and rinsing through 40 μm nylon mesh cell strainers to obtain cell suspensions. Cryosections were imaged directly without any further processing for the optimal detection of fluorescent FAM-labeled CpG, FAM-labeled CpG-lipid, and rhodamine-labeled liposomes. For secondary immunostaining against anti-CD40, cryosections were acetone-fixed and stained using a DyLight649-labeled anti-rat IgG, with minimal cross-reactivity against mouse IgG (Jackson Immuno). For flow cytometry analysis, recovered cells were re-suspended in PBS + 1% BSA and stained with fluorescent antibodies against CD45, CD11c, and F4/80. Cellular events were gated based on forward and side scatter, and tumor-infiltrating leukocytes were gated from other cell populations based on CD45 expression.

4.4. Results and Discussion

4.4.1. Synthesis and characterization of anti-CD40/CpG combination liposomes

In the previous part of this study (Chapter 3), we developed anti-CD40-coupled liposomes capable of eliciting local anti-tumor immune responses while minimizing systemic toxicity following intra-tumoral injection. In an effort to increase the efficacy of this therapy, we next incorporated CpG DNA (a TLR9 agonist) onto the surface of these liposomes. Anti-CD40 was first coupled onto maleimide-functionalized liposomes as previously described (Chapter 3). Aggregation of liposomes occurred during the coupling reaction, consistent with the availability of multiple thiol groups per antibody, which could mediate crosslinking between liposomes. The aggregated anti-CD40-liposomes were pelleted by centrifugation and washed to remove unbound antibody, then mixed with CpG-PEG-lipid conjugates, enabling the lipophilic tails of the CpG-lipid to spontaneously insert into the liposomal bilayer surface. After washing again to remove unbound CpG, the anti-CD40/CpG-coupled liposomes were membrane-extruded to a mean diameter of approximately 150nm, with a std. dev. of 18nm (Figure 4.3a). Mixing fluorescently-tagged CpG-lipid (130μg/ml) with anti-CD40-liposomes (14.4mg lipid/mL) gave CpG insertion with ~90% efficiency, resulting in 20 ± 2.2μg CpG oligonucleotides (~3 nmol) per total mg liposomes. The high efficiency of CpG-lipid association with liposomes and high level of CpG loading per lipid mass contrasted with the low efficiency of soluble non-lipidated CpG entrapment we could achieve by traditional liposomal encapsulation in PEGylated liposomes, where only 2μg of CpG was encapsulated per mg lipid. The mean sizes of anti-CD40-liposomes or combination liposomes were stable for at least 7 days in storage at 4°C.

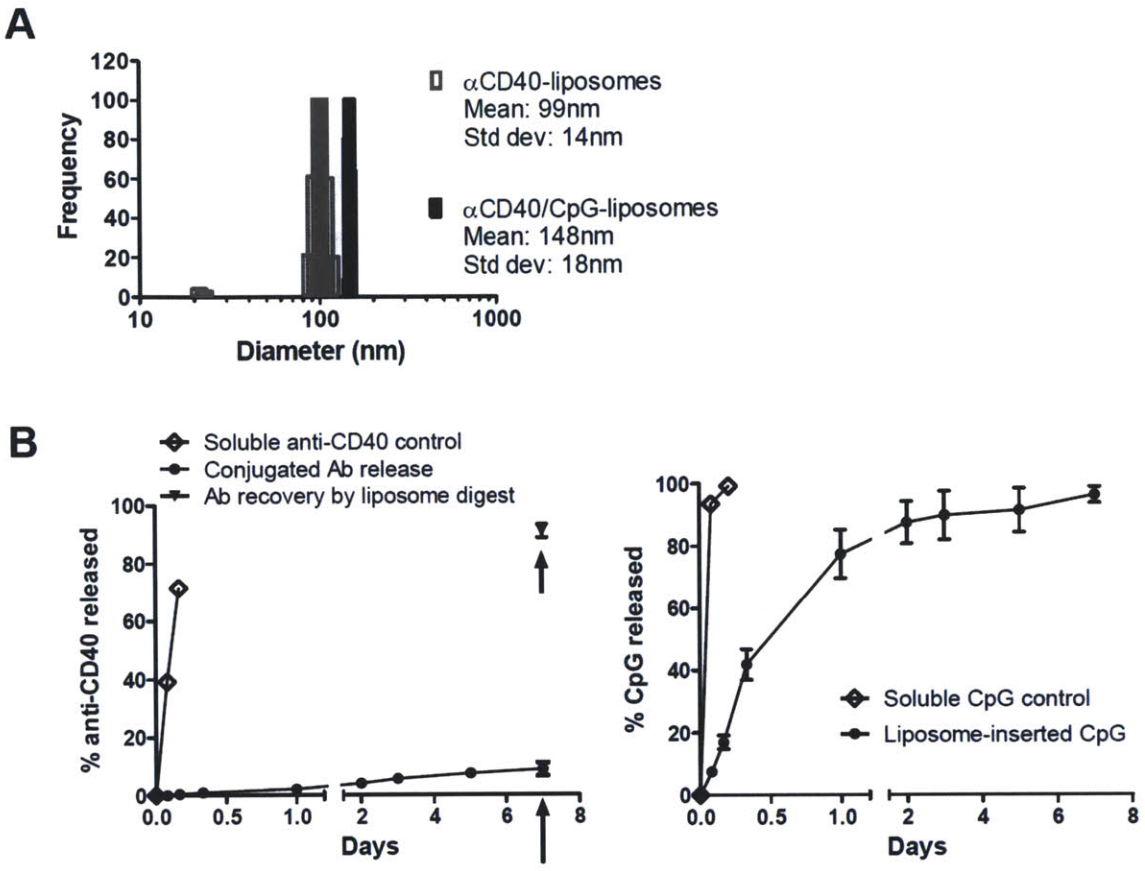

Figure 4.3. *In vitro* characterization of anti-CD40/CpG combination liposomes. A) Size distributions of anti-CD40-liposomes and anti-CD40/CpG liposomes following membrane re-extrusion, as measured by dynamic light scattering. B) Controlled release of anti-CD40 and CpG from combination liposomes (filled symbols), by dialysis against serum-containing PBS, versus the dialysis of freely soluble agonists (open symbols). Arrow indicates day 7 disruption of liposomes via Tween 20 surfactant, to measure total remaining amount of bound anti-CD40.

To test the stability of anti-CD40 and CpG association with PEGylated liposomes, the release of the immunostimulatory ligands from vesicles was measured *in vitro* in the presence of serum: combination liposomes carrying anti-CD40 and CpG were dialyzed (300kD MWCO membrane) against PBS pH 7.4 containing 10% fetal calf serum at 37°C, and release of the ligands into the dialysis buffer was monitored over time. Soluble anti-CD40 and CpG both diffused freely through the membrane with substantial release from the dialysis cassette in <5hr (Figure 4.3b). By contrast, lipid-coupled anti-CD40 effectively tethered the antibody to the liposome surfaces,

with <10% of the initial loading released over 7 days (Figure 4.3b), consistent with previous data in the absence of added CpG-lipid. After 7 days, the liposomes were disrupted by adding 0.5% Tween 20 surfactant, and >90% of the coupled anti-CD40 was immediately recovered. CpG-lipid inserted into combination liposomes was retained by the vesicles less efficiently; nearly 80% of the oligo was released by 24 hr and release was complete by ~7 days (Figure 4.3b). CpG release may reflect the ability of oligo-lipids to self-assemble favorably into highly stable micelles in aqueous buffers.[127] Gel electrophoresis of released samples confirmed that the fluorescent measurements of labeled CpG represented fully intact FAM-labeled CpG-lipid, with only a low level of degradation of these phosphorotioate backbone-stabilized oligos (or cleavage of the FAM label) by serum nucleases over 24 hr (not shown). Thus, the vesicles efficiently retain anti-CD40 but release CpG over approximately one week under strong sink conditions. Combination liposomes stored in PBS at 4°C showed negligible loss of either anti-CD40 or CpG over at least 2 weeks (not shown).

4.4.2 Inhibition of B16 tumor growth and evaluation of systemic exposure and toxicity following intra-tumoral anti-CD40/CpG liposome therapy

Combination therapies of anti-CD40 mixed with TLR agonists such as CpG oligonucleotides have previously been shown to provide substantially enhanced anti-tumor immune responses compared to anti-CD40 monotherapy.[29,82,121,122] We reasoned that the enhanced potency of anti-CD40 + CpG signaling combined with the controlled release of CpG-lipid from liposomes (as indicated by *in vitro* data) might allow the liposome-delivered combination therapy to achieve potency comparable to soluble anti-CD40+CpG therapy, while still avoiding systemic inflammation that might be augmented by the addition of soluble CpG. Therefore, we tested the

anti-tumor efficacy of soluble or liposomal combination anti-CD40/CpG in the B16 tumor model. Mice received 4 intratumoral injections, given every other day starting on day 8 post-tumor inoculation, of either soluble agent alone, soluble anti-CD40 + CpG, anti-CD40-only liposomes, or anti-CD40/CpG liposomes, at equivalent doses of 40 μg anti-CD40 and 20 μg CpG per injection. As shown in Figure 4.4a, 3/13 mice treated with soluble anti-CD40+CpG exhibited "complete responses", defined as apparent cures of the animals and lack of tumor progression or new tumor nodule formation over 45 days. The remaining mice showed a delay in tumor growth compared to untreated animals but eventually all succumbed (Figure 4.4b); we quantified this delay in tumor growth as a time to progression (time to tripling of initial tumor size from the start of therapy) (Figure 4.4c). Such a mixture of complete and partial responses to immunotherapy has previously been reported and has been correlated with the tumor size at the start of treatment.[9] In the current study, however, the initial tumor burden of the three mice showing the strongest anti-tumor responses was only slightly smaller than that of the remaining mice. The addition of soluble CpG to soluble anti-CD40 provided only a modest enhancement over soluble anti-CD40 alone, which induced 1/8 complete responses and showed a slightly more rapid time to progression for the remaining tumors (Figure 4.4b).

In comparison, liposomal anti-CD40/CpG elicited no complete responses (0/13), but instead showed a significant increase in the time to progression for partial responders compared to the equivalent soluble therapy ($p = 0.04$), from a mean of 27.8 ± 1.4 days for soluble treatment to 33.4 ± 1.8 days for liposomal anti-CD40/CpG (Figure 4.4a-c). Anti-CD40/CpG liposome therapy significantly prolonged the survival of tumor-bearing mice compared to PBS-treated controls (Figure 4.4b, $p<0.0001$ by log-rank test), and induced a mean survival benefit comparable to soluble immunotherapy regimens ($p>0.05$, not significant). Furthermore,

combinatorial liposome therapy demonstrated a substantial increase in potency over liposomal anti-CD40 alone (Figure 4.4a-b), suggesting a synergistic effect in the particle-mediated co-delivery of both immunostimulants.

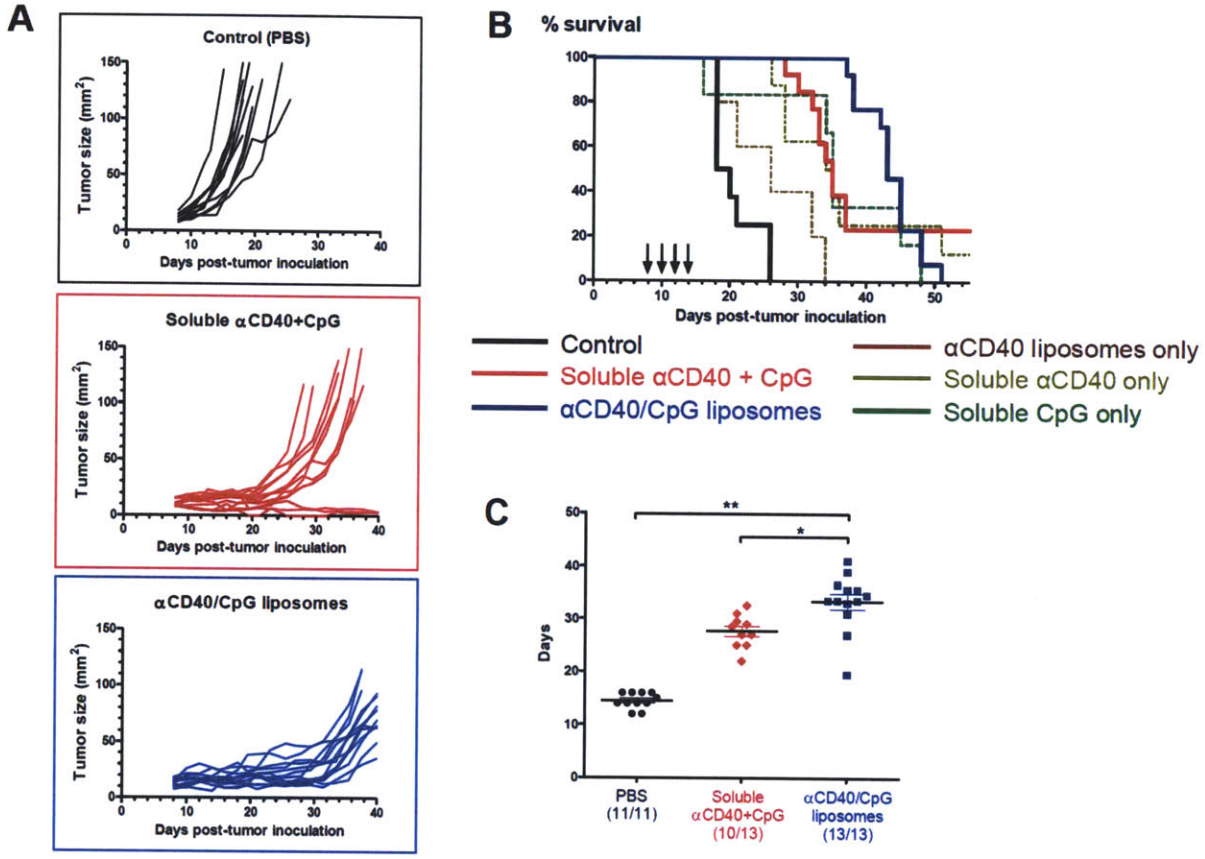

Figure 4.4. Potent inhibition of B16 subcutaneous tumors by anti-CD40/CpG combination liposomes. A) Individual tumor growth curves (n=11 to 13 per group), combined from three independent experiments. Mice were treated intra-tumorally on days 8/10/12/14 with 40μg anti-CD40 and 20μg CpG per injection, either in soluble (red) or liposome-coupled formulations (blue). B) Overall survival of B16 tumor-bearing mice; arrows indicate days of therapy. Mice were euthanized when tumor burden exceeded 100mm^2. C) Time to tumor progression for partial responders to therapy, defined as the day at which tumor burden reached 3x the initial tumor size at the start of therapy. Complete responders that received soluble therapy were omitted in this analysis. *p=0.04, **p=0.004

Thus, though liposomal therapy showed the loss of a minority of complete responses seen with soluble immunostimulatory ligands, the majority of animals actually exhibited longer times to

progression following liposomal therapy compared to the soluble treatment regimens. Further understanding of the change in therapeutic outcome obtained with liposomal delivery compared to soluble therapy (loss of a minor complete response population but gain in overall time to progression) represents a key area for future study and improvement of this approach. Notably, modifying the liposome-coupled treatment regimen so that eight injections were administered (every 2d from day 9 to day 23), each at half the dosage of the originally described four-injection regimen, yielded no significant improvements in therapeutic efficacy or overall survival benefit (not shown).

To determine whether the therapeutic effect of anti-CD40/CpG liposomes was still achieved with minimized systemic side effects, overall weight loss and circulating serum inflammatory markers were monitored following locally-administered therapy. The addition of soluble CpG to soluble anti-CD40 intratumoral therapy greatly exacerbated the weight loss of animals through the entire course of treatment (Figure 4.5a vs. Figure 3.5a), showing statistically significant differences versus PBS-treated animals from day 9 through day 16 ($p \leq 0.04$). In contrast, anti-CD40/CpG-liposomes showed a mild, transient effect that reached statistical significance only on day 10 (mean 4% weight loss at this time point, $p=0.04$) (Figure 4.5a). Serum levels of hepatic ALT enzyme were significantly elevated in mice at 24 hr after the first injection of soluble anti-CD40 + CpG, indicative of inflammatory hepatic damage (Figure 4.5b), while mice treated with anti-CD40/CpG liposomes showed a barely detectable increase above background levels that did not reach significance ($p=0.07$, n.s.). Similarly, serum levels of the pro-inflammatory cytokines IL-6 and TNF-α were greatly increased in mice that received soluble anti-CD40/CpG, but not in mice that received liposome-anchored agonists (Figure 4.5c). Taken together, these data demonstrate that dual-agonist immunotherapy employing liposomal delivery was capable of

stimulating a potent local anti-tumor immune response, without inducing the systemic toxicity elicited by an equivalent dose of locally-administered soluble agonists.

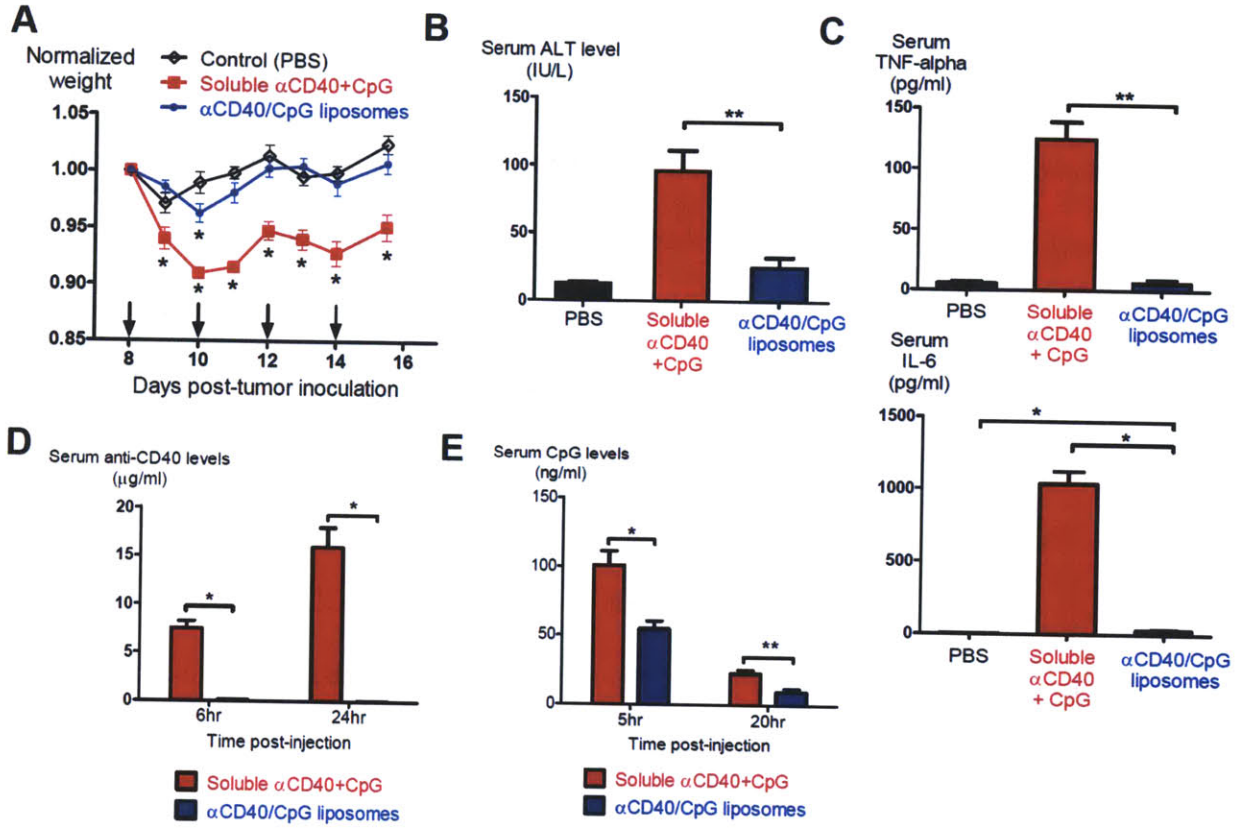

Figure 4.5. Minimal systemic toxicity induced by locally injected anti-CD40/CpG liposomes in comparison to soluble anti-CD40 + CpG. A) Weight loss following intra-tumoral soluble (red) or liposome-coupled (blue) anti-CD40/CpG therapy. Statistical significance was calculated relative to PBS controls by unpaired t-test at each time oint: *p≤0.04. B) Serum level of hepatic ALT enzyme at 24hr following first dose of soluble of liposome-coupled therapy. **p=0.004. C) Serum circulating levels of inflammatory cytokines at 24hr following first dose of soluble of liposome-coupled therapy. *p<0.0001, **p<0.0001. D,E) Systemic exposures to anti-CD40 and CpG at timepoints following an intra-tumoral dose of soluble or liposome-coupled therapy. *p<0.001, **p=0.002.

To determine whether the lack of systemic inflammation following liposome-anchored αCD40/CpG delivery was achieved as a result of lowered systemic exposure to both of these agents, we collected blood serum at various time points following intratumoral injections. Consistent with the *in vitro* release data, negligible levels of anti-CD40 could be detected in

serum at 6 or 24 hr after local liposome-anchored αCD40/CpG therapy (Figure 4.5d, or later times, not shown), indicating that lipid anchoring effectively prevented dissemination of the antibody to the systemic circulation. In contrast, locally-administered soluble anti-CD40+CpG or anti-CD40 alone resulted in high levels of circulating antibody within 6 hr post-injection (Figure 4.5d and data not shown). The release of liposome-inserted CpG-lipid from combination liposomes occurred much more rapidly than the release of lipid-anchored anti-CD40 *in vitro* (Fig. 4.3b), so a similar trend was expected *in vivo*. Figure 4.5e shows that fluorescently-labeled CpG from combination liposome delivery could be detected in serum at 5 hr following intra-tumoral injection, and also remains present at a measurable level in serum up to 20 hr post-injection. However, the level of circulating CpG following liposomal delivery was approximately half that attained following intratumoral soluble anti-CD40+CpG therapy at both time points ($p=0.0008$ and $p=0.002$, respectively, Figure 4.5e). Thus, liposome-anchored CpG delivery lowered the systemic exposure to this agent as well.

4.4.3. Local and systemic biodistribution analyses of anti-CD40 and CpG following liposome-coupled intra-tumoral delivery

Low levels of anti-CD40 and CpG in the serum following liposomal delivery could either reflect preferential retention of the nanoparticle-anchored agonists in the tumor site/tumor draining lymph nodes or more rapid clearance/degradation of the particle-delivered agonists. We thus performed histological analysis on cryosections of tumors and tumor-draining lymph nodes, to directly visualize the local retention and proximal draining of intratumorally-injected immunostimulatory ligands. Established B16 tumors were given a single intratumoral injection of PBS, soluble unlabeled anti-CD40 + FAM-labeled CpG, or rhodamine-tagged liposomes

conjugated with anti-CD40 and FAM-labeled CpG-lipid. Figure 4.6 shows representative cryosections of tumors excised at 48hr following soluble or combination liposome therapy. Liposomes (red) were retained at a high level at the tumor for over 48 hr post-injection, while secondary anti-rat IgG staining (yellow) against anti-CD40 co-localized closely with the liposomes, confirming that anti-CD40 remained coupled to the liposome carrier *in vivo*. FAM-labeled CpG-lipid (green) was also highly retained at the tumor site for at least 48hr following liposomal delivery, but was more dispersed through the local dermal and subcutaneous tissue. This was consistent with the release of CpG-lipid from liposomes that had been observed in the presence of serum *in vitro*.

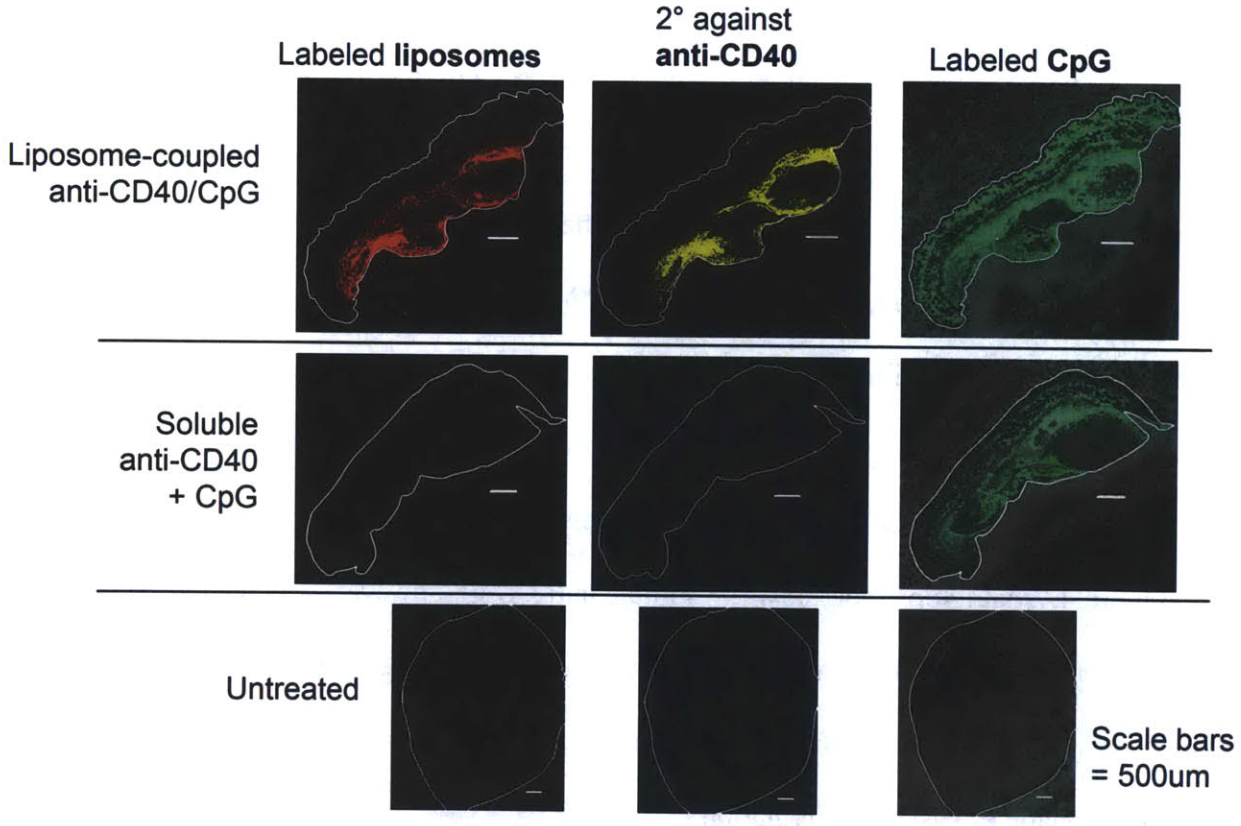

Figure 4.6. Histological analysis of anti-CD40/CpG biodistribution at the injected tumor, following soluble or liposome-coupled therapy. Immunofluorescent staining of tissue cryosections shows rhodamine-labeled liposomes (left panels, red); anti-CD40 (middle, yellow); and CpG (right, green overlaid with brightfield). Edges of tumor sections are outlined in white. Tissues were excised 48hr following a single intra-tumoral injection.

Tumors that received soluble anti-CD40+CpG therapy also showed significant levels of CpG remaining in the tumor site at 24 and 48hr, consistent with earlier reports of the nonspecific interactions of phosphorothioate-backbone CpG with tissue matrix proteins.[129,130] However, significantly lower amounts of anti-CD40 remained within the tumor mass following soluble therapy, (Figure 4.6), indicating rapid draining away from the injection site.

The initiation of antigen-specific anti-tumor responses requires the interactions of activated APCs and T-cells in the tumor-proximal lymph node. Since this is also the collection site for lymphatic draining from the tumor, we examined whether anti-CD40 and CpG reached the tumor-proximal LN following soluble or liposomal delivery. At 24 hr following treatment with anti-CD40/CpG liposomes, a low level of rhodamine-labeled lipid (Figure 4.7) was observed, primarily at the subcapsular and intermediate sinus areas, co-localized with secondary staining for anti-CD40 (yellow). As with the tumor cryosections, FAM-labeled CpG-lipid (green) appeared to be distributed in a more dispersed pattern than the liposomes/anti-CD40. By 48hr, fluorescent signals from rhodamine-liposomes, FAM-CpG, or secondary anti-CD40 staining in the tumor-proximal LN of liposome-treated mice were greatly diminished, though still detectable above PBS-treated background levels. By comparison, mice that received soluble anti-CD40+CpG therapy showed surprisingly low levels of CpG in the tumor-draining LN, at both 24hr (Figure 4.7) and 48hr (not shown). Soluble anti-CD40, however, was readily detected in a diffuse pattern in the tumor-proximal LN at both timepoints, consistent with the tumor-site and serum observations that locally-administered soluble anti-CD40 drains rapidly from the injection site into lymphatic or systemic circulation.

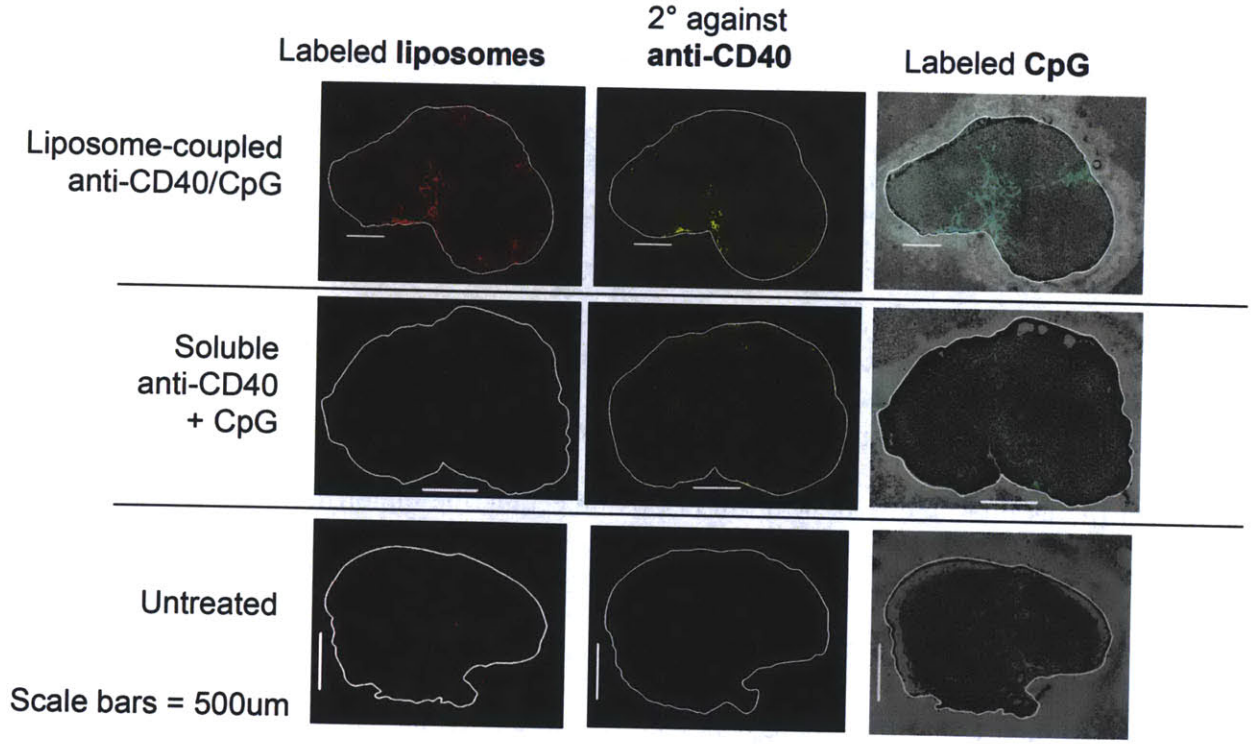

Figure 4.7. Histological analysis of anti-CD40/CpG biodistribution at the tumor-proximal lymph node. Immunofluorescent staining of tissue cryosections shows rhodamine-labeled liposomes (left panels, red); anti-CD40 (middle, yellow); and CpG (right, green overlaid with brightfield). Tissues were excised 24hr following a single intra-tumoral injection.

Given the persistence of liposomal anti-CD40/CpG in the tumors and draining lymph node, and the observed colocalization of anti-CD40 with liposomes but dispersion of CpG-lipid, we used flow cytometry to separately trace the binding/uptake of CpG and liposomes by cells at these sites following local therapy. A variety of leukocytic cell populations have previously been implicated in mediating the anti-tumor effects of anti-CD40 and CpG therapies. TLR9 expression is found predominantly in APCs such as dendritic cells, macrophages, and B cells, and the activation of any of these cells by TLR9 stimulation is known to potentiate antigen cross-priming, the production of T_H1-skewed cytokines, and the induction of potent CTL and NK-cell responses.[131] Although the mechanisms of anti-CD40 tumor inhibition are currently less well defined, various studies[78,80,132] have implicated DCs, macrophages, B cells, or combinations

thereof as the primary cells responsible for priming potent CTL or NK-cell activity or T-cell independent immune responses.[44,45,75,84,133-135] Therefore, we examined the ability of liposome-coupled anti-CD40 and CpG to contact and bind to APCs present in the local tumor environment, as well as APCs in the tumor-draining lymph node, where the adaptive immune response is primed.

Established B16 tumors were injected once intratumorally with PBS, soluble anti-CD40 + FAM-labeled CpG, or combination liposomes carrying anti-CD40 + FAM-labeled CpG-lipid + fluorescent rhodamine-lipid. At 24 or 48 hr post-injection, the tumor tissues, distal and tumor-proximal lymph nodes, and spleens were harvested and processed into cell suspensions for analysis. Cells were gated on CD45 expression (common leukocyte marker), CD11c (marker for dendritic cells), and F4/80 (macrophages), since these antigen-presenting cells express both the CD40 receptor and the TLR9 receptor for CpG, and represent primary targets of this immunotherapy. Figure 4.8a shows representative flow cytometry histograms of excised tumor samples at 48 hr post-injection, illustrating that the majority of tumor-infiltrating DCs ($CD45^+CD11c^+$) and macrophages ($CD45^+F4/80^+$) were positive for rhodamine-labeled liposomes (with their coupled anti-CD40 cargo) and FAM-labeled CpG. As summarized in Figure 4.8b, this high level of uptake by tumor-infiltrating APCs was consistently observed at both 24 and 48 hr post-injection, indicating that liposomally delivered anti-CD40/CpG therapy had reached its intended targets for local immunomodulation.

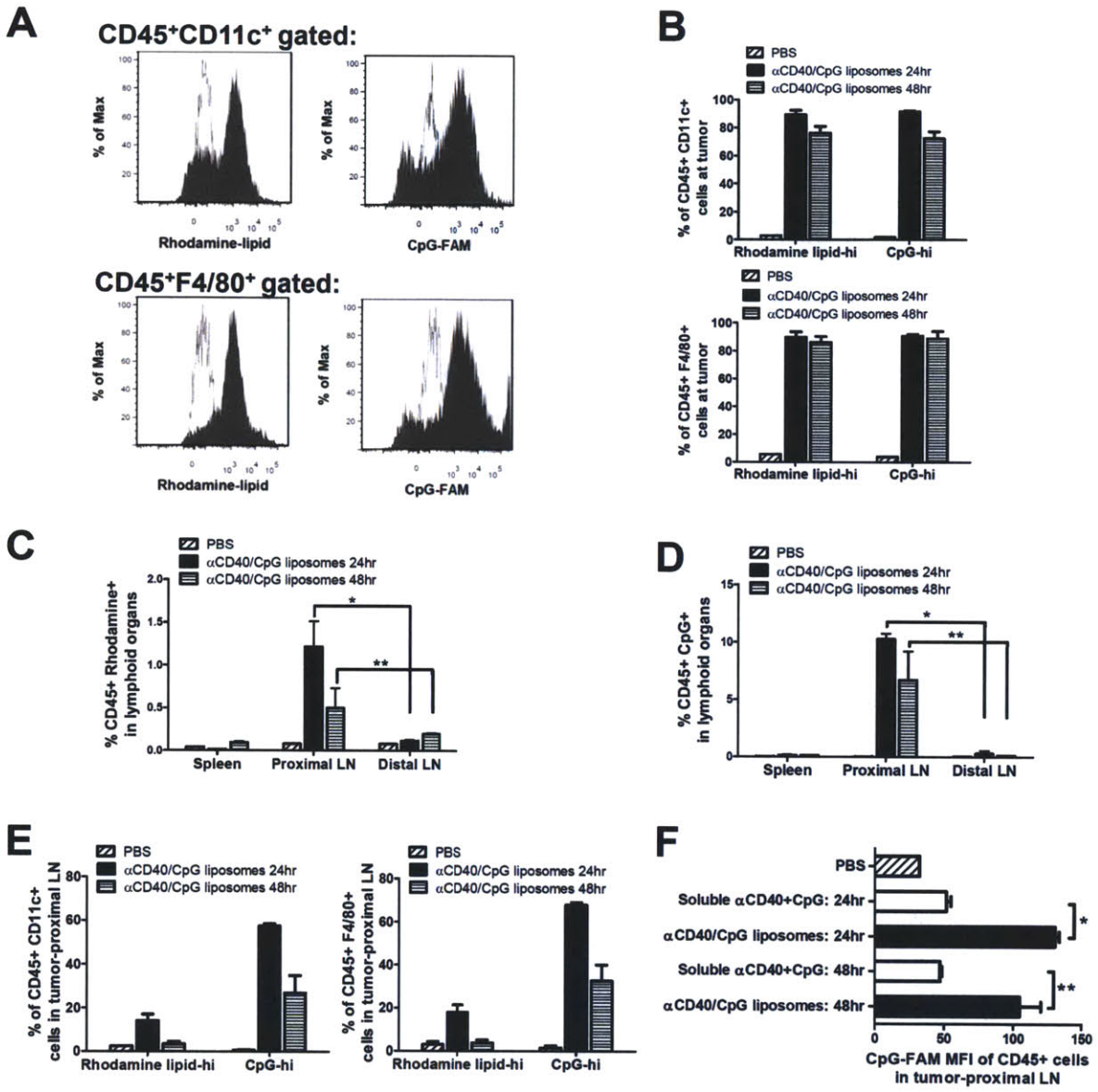

Figure 4.8. Flow cytometry analysis of anti-CD40/CpG biodistribution following intra-tumoral soluble or liposome-coupled therapy. A) Representative histograms of excised tumor tissues at 48 hr following a single intratumoral injection of anti-CD40/CpG liposomes, showing the uptake of rhodamine-labeled liposomes (left) and FAM-labeled CpG (right) by the majority of dendritic cells (top, CD45+CD11c+ staining) or macrophages (bottom, CD45+F4/80+ staining). Filled histograms = liposomal therapy; open histograms = background controls. B) Bar graph summary of the flow cytometry analysis depicted in (A), showing the percentage of dendritic cells (top) or macrophages (bottom) positive for rhodamine-liposomes or FAM-CpG in excised tumor tissues. C) Flow cytometry analysis of distal and tumor-proximal lymphoid organs following a single dose of liposomal anti-CD40/CpG therapy, indicating preferential drainage of rhodamine-labeled liposomes to the tumor-proximal lymph node, with minimal leakage to distal lymph nodes or the spleen. P-values determined by unpaired t-test: *p=0.03, **p=0.14(N.S.). D) Flow cytometry analysis showing preferential local drainage of FAM-labeled CpG, analogous to part (c);

*p<0.0001, **p=0.03. E) Co-staining of rhodamine-labeled liposomes or FAM-labeled CpG with dendritic cells (left, CD45+CD11c+) and macrophages (right, $CD45^{+}F4/80^{+}$) in the tumor-proximal lymph node, following a single intra-tumoral liposomal injection. (F) Mean fluorescent intensity (MFI) of FAM-labeled CpG in $CD45^{+}$ leukocytes in the tumor-proximal lymph node following intra-tumoral soluble or liposomal anti-CD40/CpG treatment. *p<0.0001, **p=0.02.

Consistent with the histological data, flow cytometry analysis of proximal and distal lymphoid organs following intratumoral injection confirmed that a small fraction of leukocytes in the tumor-proximal LN took up liposomes (Figure 4.8c) and ~10% of these cells took up CpG-lipid (Figure 4.8d). As expected, barely detectable levels of either component were observed in spleens or contralateral lymph nodes, consistent with the elimination of systemic toxicity via liposomal coupling and local retention. $CD11c^{+}$ dendritic cells and $F4/80^{+}$ macrophages in the tumor-draining LN both took up rhodamine-labeled liposomes and FAM-labeled CpG by 24hr post-injection (Figure 4.8e), suggesting the successful delivery to APCs in the draining LN, and fluorescent CpG could still be detected at 48 hr post-injection. Whether the co-localization of fluorescent signals with these APCs resulted from the direct draining of therapeutics to the proximal LN, or the lymphatic migration of tumor-resident APCs that had bound or taken up therapeutics, was not explicitly investigated.

In addition, higher overall levels of FAM-labeled CpG were observed in the proximal LN following combination liposome delivery than following soluble delivery, as quantified by mean fluorescent intensity in cells at both time points (Figure 4.8f). This suggests that the CpG-PEG-lipid conjugate achieved enhanced draining to the proximal lymph node compared to free soluble CpG, although the diminished level of co-localizing rhodamine-lipid fluorescence suggests that this did not occur via the draining of intact liposomes, but rather by the draining of released CpG-lipid micelles. Whether the enhanced draining relative to free CpG was mediated by the

micellar nature of the released CpG-lipid, and/or the presence of the PEG linker in the CpG-lipid conjugate, was not investigated in this thesis.

4.4.4. Elucidating the mechanisms of the anti-tumor response mediated by anti-CD40/CpG combination liposome therapy

The previous experiments demonstrated that anti-CD40/CpG therapy could induce the potent inhibition of B16 tumor growth. However, in a large majority of mice, tumors eventually progressed (with some delay) following the cessation of therapy. To improve on these therapeutic results, we first attempted to gain a more complete understanding of the mechanisms responsible for the observed anti-tumor responses. Previous studies in a variety of mouse models have reported that anti-CD40 and CpG therapy inhibit tumor growth via the priming of tumor-specific cytotoxic $CD8^+$ T-cells.[37,38,44,67,76,78,111,133] Additionally, $CD8^+$ T cell-mediated responses have also been shown to be essential in the induction of anti-tumor immunity specifically in the B16 tumor model, following a variety of immunotherapeutic treatments.[136-141] Therefore, we evaluated the efficacy of soluble or liposome-coupled anti-CD40/CpG therapy in CD8-depleted mice.

Subcutaneous tumor-bearing mice were depleted of CD8-expressing cells by intra-peritoneal injection of an anti-CD8a antibody (clone 2.43) on days 6/11/14/17. Flow cytometry analysis confirmed the >98% elimination of $CD8^+$ T cells in tumors, lymph nodes, spleen, and circulation. Mice then received intra-tumoral therapy with either soluble or liposome-coupled anti-CD40 + CpG, on days 8/10/12/14 as previously described.

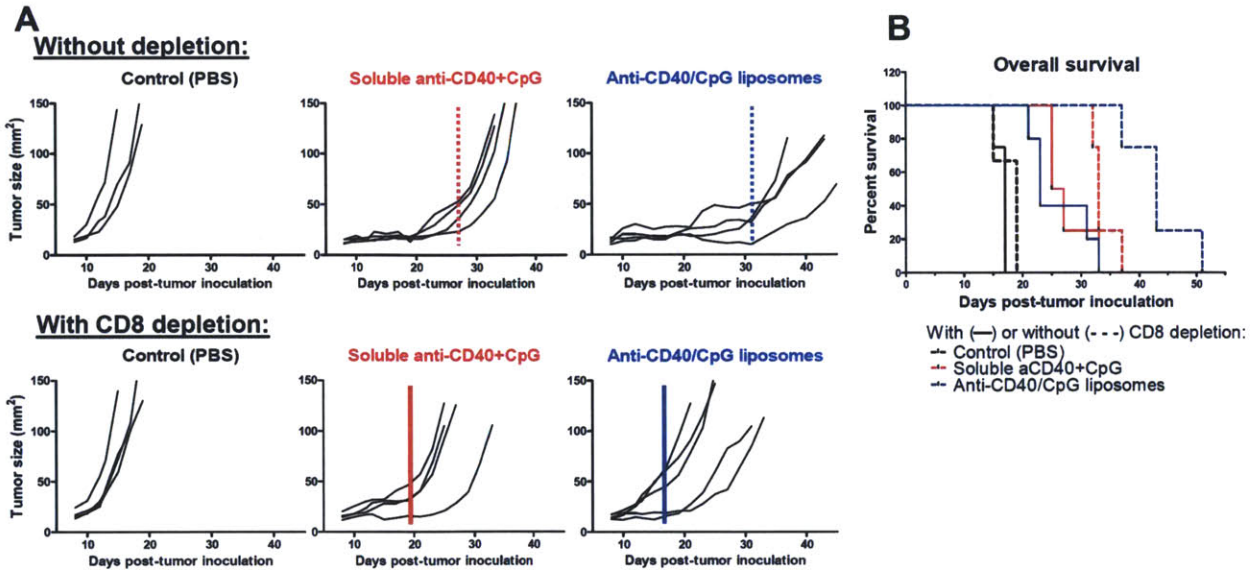

Figure 4.9. Anti-tumor efficacy of anti-CD40/CpG therapy in mice depleted of $CD8^+$ T cells. A) Individual tumor growths (n=3 to 5 per group) in mice treated with soluble (red) or liposome-coupled (blue) anti-CD40/CpG combination therapy, without depletion (top row) or with $CD8^+$ CTL depletion (bottom row). Mice received intra-tumoral therapy on days 8/10/12/14, as previously described. Solid vertical lines represent average times at which tumors escaped immune inhibition and began to rapidly progress. B) Overall survivals of treated mice with the depletion of $CD8^+$ CTLs (solid lines), compared to undepleted mice (dashed lines). Mice were euthanized when tumor burden exceeded $100mm^2$.

As shown in Figure 4.9, CD8 depletion had no effect on tumor growths in control untreated mice. As expected, the efficacy of anti-CD40/CpG therapy (either soluble or liposome-conjugated) was significantly reduced in the absence of $CD8^+$ cells, demonstrating the importance of the CTL-mediated immune response in this model. Nevertheless, CD8-depleted mice that received anti-CD40/CpG treatment also showed a modest delay in tumor growth and a moderate benefit in overall survival time compared to control mice, indicating the presence of a CTL-independent response in addition to CTL-mediated anti-tumor effects. These results suggested that besides the expected adaptive $CD8^+$ T cell response, innate immune effectors such as directly stimulated macrophages or NK cells may have contributed significantly to the anti-tumor response induced by anti-CD40/CpG therapy. The apparent importance of innate

effectors observed in this study is consistent with previous reports by Buhtoiarov et al and Rakhmilevich et al that illustrated the ability of anti-CD40 and CpG combination therapy to potently stimulate macrophages and induce T cell-independent anti-tumor effects.[82,118,135]

Since the primary site of adaptive immune priming is expected to be the tumor-proximal lymph node, we next examined whether intra-lymph node injections of anti-CD40/CpG therapy could prime an effective anti-tumor response. It is generally believed that constitutive priming of tumor-specific T cells occurs in the draining lymph node as a result of either direct draining of tumor antigens, or the trafficking of APCs from the tumor site that have endocytosed tumor-specific antigens.[133] In the absence of immunotherapy, this constitutive priming may be insufficient for anti-tumor immunity due to local immunosuppression at the tumor site and/or the elicitation of tolerized tumor-specific T cells by tolerogenic APCs. We hypothesized that intra-lymph node stimulation of tumor antigen-bearing APCs via anti-CD40/CpG therapy might enable the priming of non-tolerized CTLs and subsequent CTL homing to the tumor to effect tumor cell killing.

Using a non-surgical, non-invasive technique developed by Jewell et al[128] in the Irvine Lab, we compared the efficacy of intra-nodal versus intra-tumoral injections of anti-CD40/CpG liposomes. Mice were inoculated with subcutaneous B16 tumors and treated with intra-tumoral therapy on days 8/10/12/14 as previously described (Chapter 4.3.3), or with intra-nodal therapy on days 8/10/12/14/16. Due to the volume limitation of intra-lymph node injections, the dose per intra-nodal injection was restricted to 1/5 of the dose per intra-tumoral injection (8μg anti-CD40 + 4μg CpG, compared to 40μg anti-CD40 + 20μg CpG). Nevertheless, flow cytometry analysis performed on day 18 (2 days following final injection) confirmed significantly increased levels of fluorescently labeled liposomes and CpG-lipid in the tumor-proximal lymph node following

intra-nodal injection, compared to the low levels detected following intra-tumoral injection and subsequent lymphatic draining (not shown). Despite the potent stimulation of APCs in directly injected lymph nodes (including observations of lymphomegaly), the overall therapeutic response to intra-nodal therapy was markedly weaker in comparison to intra-tumoral therapy, as indicated by the individual tumor growth curves and overall survival (Figure 4.10). Therefore, it was concluded that lymph node priming alone is not sufficient for effective anti-tumor immunity, and that the stimulation of local (tumor-resident) innate effectors is likely required for the full therapeutic benefit of anti-CD40/CpG liposomes.

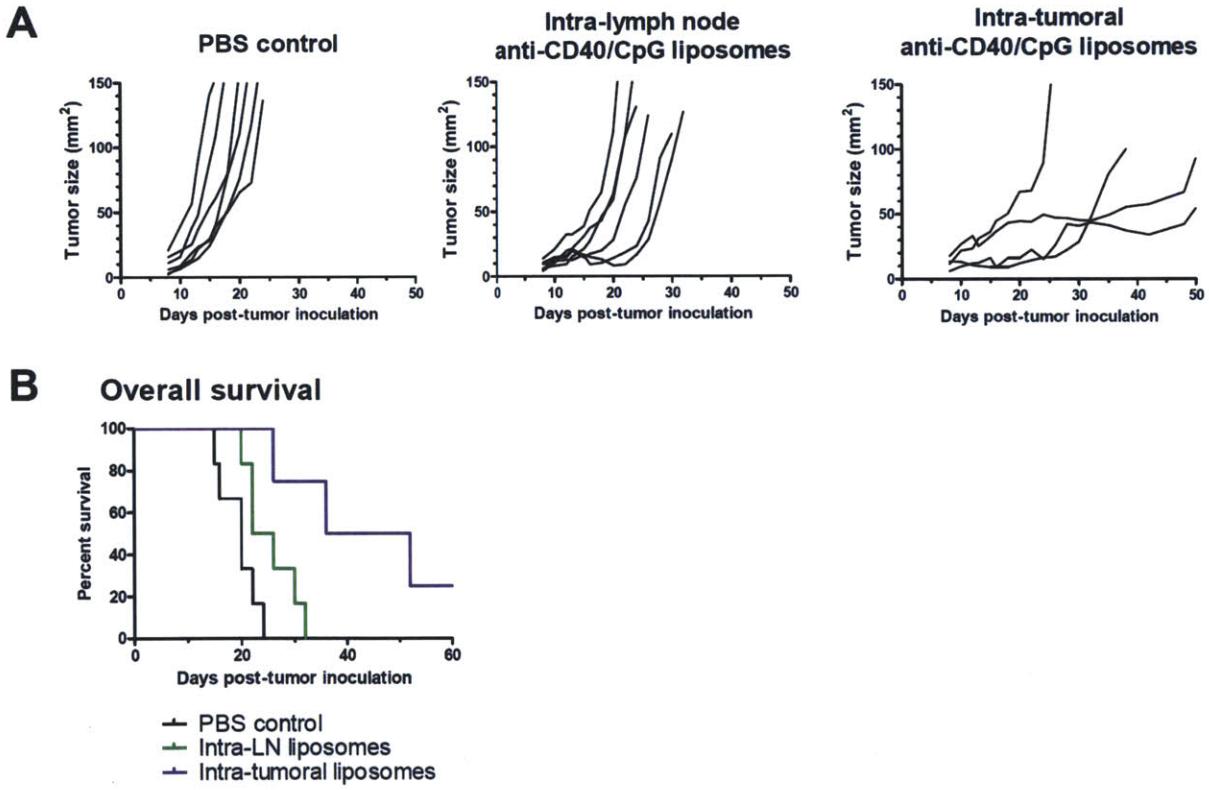

Figure 4.10. Therapeutic efficacy of intra-lymph node injections versus intra-tumoral injections of anti-CD40/CpG liposomes. A) Individual tumor growths (n=4 or 6 per group) in mice receiving saline control, intra-lymph node, or intra-tumoral injections of liposome-coupled anti-CD40/CpG therapy. Mice received 5 doses, on days 8/10/12/14/16, at the same dose as previously described. B) Overall survival of mice receiving intra-lymph node or intra-tumoral administration of combination therapy.

4.4.5. Assessing the induction of systemic and memory anti-tumor immunity by primary anti-CD40/CpG liposome therapy

The above experiments performed with CD8 depletion or with the intra-lymph node injection of therapy suggested that the anti-tumor response to anti-CD40/CpG liposomes was mediated by a combination of both innate and adaptive immune effectors. We hypothesized that if an adaptive, tumor-specific immune response had been successfully primed, the systemic dissemination of tumor-specific CTL effectors should enable the inhibition or rejection of a distal, identical tumor inoculation. Importantly, the parental B16F10 tumor line is considered to be weakly immunogenic due to the absence of exogenous or foreign transfected antigens. As a result, control mice that did not receive primary immunotherapy would not be expected to develop effective, tumor-specific adaptive immunity. Therefore, to test for the development of tumor-specific adaptive immunity, we performed a secondary re-challenge experiment, in which primary B16 tumor-bearing mice were treated locally with anti-CD40/CpG therapy in soluble or liposome-conjugated formulation, and then subsequently inoculated with fresh B16 tumor cells on the opposite flank.

As shown in Figure 4.11a, the weak immunogenicity of B16 tumors was confirmed by 100% progression of the secondary tumor inoculation in untreated, primary tumor-bearing mice (administered on day 18 of primary tumor growth). In contrast, secondary distal inoculations (day 18 post-primary tumor, equal to 3 days after the final therapeutic dose) in mice treated with either soluble or liposome-coupled anti-CD40/CpG resulted in complete rejection of the secondary tumor in 2 of 6 mice in each group (Figure 4.11c). The rejection of the secondary tumor was durable in these mice, with no observable tumor growth from the secondary challenge for over 10 weeks post-inoculation. Simultaneously, naïve mice that received primary tumor

inoculations displayed 100% tumor progression in the absence of immunotherapy, confirming the viability of the particular batch of tumor cells used in this challenge (Figure 4.11a). Furthermore, ELISA analysis of serum collected immediately prior to the secondary inoculation confirmed that there were no detectable levels of anti-CD40 or CpG remaining in circulation, which might have impacted the ability of the secondary tumor to establish (not shown). Interestingly, the two mice in each therapy group exhibiting secondary tumor rejection correlated with the strongest inhibition of the primary treated tumor growths (Figure 4.11b). The ability to resist a secondary tumor challenge is an extremely promising result for the demonstration of clinical relevance and applicability, as it indicates that the anti-tumor immune response primed by local anti-CD40/CpG therapy may be able to prevent tumor recurrence or to potentially target metastatic outgrowths.

Conversely, the remaining 4 mice in both treated groups (soluble or liposome-coupled) showed rapid tumor progression without any evidence of immune-mediated inhibition; the average growth kinetics of these progressing tumors was statistically indistinguishable from control untreated tumors (Figure 4.11d). This all-or-nothing response to the secondary tumor challenge suggests that only a small fraction of mice developed a B16-specific adaptive immune response, enabling secondary tumor rejection. In the remainder of the treated mice, local innate effectors such as macrophages might have been primarily responsible for the inhibition of the primary tumor, while lacking the homing or targeting specificity to act on the distal secondary tumor inoculation.

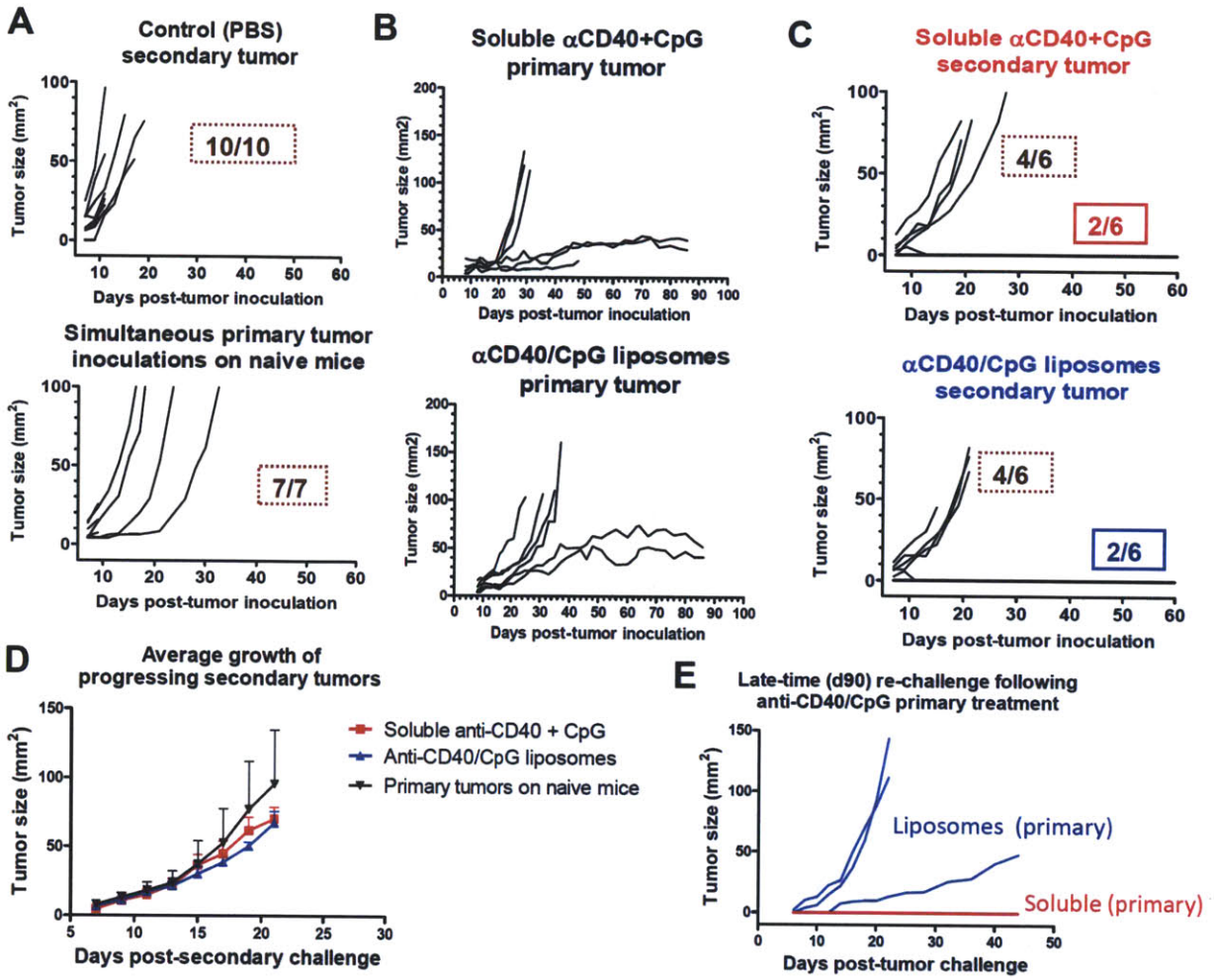

Figure 4.11. Secondary challenge of primary tumor-bearing mice on the distal flank, to assess systemic and memory anti-tumor immunity following primary anti-CD40/CpG therapy. A) Individual tumor growths in control mice: secondary tumor challenge in untreated tumor-bearing mice (top), and simultaneous primary tumor inoculations in naïve mice (bottom). Highlighted numbers indicate fraction of progressing tumors in each group. B) Primary tumor growths in mice receiving soluble (top) or liposome-coupled anti-CD40/CpG therapy, according to the treatment regimen previously described. C) Secondary tumor growths in mice treated with anti-CD40/CpG therapy at their primary tumors only (same mice as shown in part b). Highlighted numbers indicate fractions of progressing or rejected tumors in each group. Secondary challenges were inoculated on day 18 of primary tumor growth. D) Average growths of the progressing secondary tumors shown in part c, following primary soluble or liposome-coupled therapy. E) Day 90 re-challenge of the mice that had rejected the day 18 secondary challenge (fraction shown in part c), following primary anti-CD40/CpG therapies. n=3 for initial liposome-coupled therapy at primary tumor (blue); n=2 for initial soluble therapy (red).

To assess the long-term memory response of mice treated with anti-CD40/CpG therapy, the survivors of the previously described secondary challenge experiment were *re*-challenged by an additional tumor inoculation on day 90. By this timepoint, only mice that had completely rejected the day 18 secondary challenge remained alive; the anti-tumor responses in this limited number of mice had also successfully controlled the growth of all initial primary tumors. Surprisingly, all 3 out of 3 mice that had initially received liposome-coupled therapy (2 mice primary tumor + d18 challenge, 1 mouse primary only) were unable to reject the day 90 secondary re-challenge (Figure 4.11e). This indicated that even in the fraction of liposome-treated mice that had initially developed effective tumor-specific responses, an effective level of anti-tumor adaptive immunity could not be maintained long-term. On the other hand, 2 out of 2 mice that had initially received soluble anti-CD40/CpG therapy retained the ability to reject the late-time secondary re-challenge (Figure 4.11e). Given the clear superiority of soluble therapy in this challenge model, it was apparent that further optimization of local liposome-delivered therapy would be necessary in order to elicit long-lasting and systemically protective anti-tumor immunity.

As a potential alternative to using local intra-tumoral therapy for the priming of systemic immunity, we tested in a separate experiment whether intravenously injected anti-CD40/CpG liposomes could accumulate in established subcutaneous B16 tumors, via the enhanced permeability and retention (EPR) effect of tumors. If successful, a systemic injection would enable the targeting of therapy to multiple distant tumors, allowing a local immune response to be primed at each site of tumor growth and removing the need for the systemic dissemination of local anti-tumor immunity. Therefore, fluorescently labeled anti-CD40/CpG liposomes were injected intravenously via tail-vein, and whole-animal imaging was performed at 24 hours post-

injection. The majority of intravenously injected liposomes were shown to accumulate in the liver, spleen, and lungs, with minimal fluorescence detectable in the subcutaneous tumor (Figure 4.12). This clearly indicated that the anti-CD40/CpG liposomes developed in this study would not be amenable to systemic delivery, thus confirming the need to improve the systemic potency of intra-tumorally delivered liposome therapy.

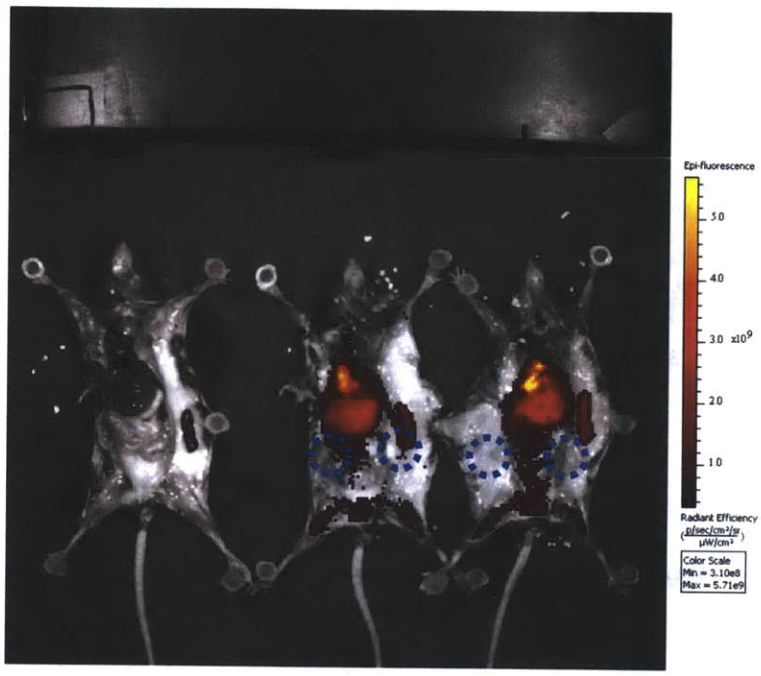

Figure 4.12. Distributions of intravenously injected anti-CD40/CpG liposomes. Pseudo-color images showing fluorescently labeled liposomes accumulating mainly in the liver, lungs, and spleen, and not in subcutaneous flank tumors (middle and right mice). Minimal background fluorescence was observed in uninjected mice (left). Dashed blue circles denote approximate locations of subcutaneously implanted tumors.

4.5. Summary and Conclusions

In this section of the thesis, we successfully coupled CpG DNA to anti-CD40-liposomes by spontaneous membrane insertion. Liposomal surface coupling of both ligands caused local retention at a high level in the tumor and surrounding tissue following intra-tumoral injection,

allowing them to be presented to APCs at the tumor and the tumor-draining lymph node while restricting them from entering systemic circulation or reaching distal lymphoid organs. As a result, liposome-coupled anti-CD40/CpG therapy induced potent local anti-tumor responses against subcutaneous B16 tumors, comparable to those elicited by soluble combination therapy and with significantly greater efficacy than anti-CD40-liposomes alone, but without any observable evidence of systemic toxicity. Future studies will be needed to elucidate the underlying mechanisms governing differences in the therapeutic outcome of liposomal vs. soluble therapy. Nevertheless, the results described here suggest that nanoparticle anchoring can used to block systemic toxicity while maintaining anti-tumor effects for two distinct immunostimulatory agonists, and underscore the versatility and combinatorial capacity of the liposome-coupled delivery strategy developed in this study.

The ultimate objective of locally delivered anti-tumor immunotherapy is to prime an effective, long-lasting, systemic immune response that is capable of the disseminated targeting of multiple lesions, tumor recurrences, and/or metastases. Preliminary experiments to assay for the development of systemic or memory anti-tumor immunity following intra-tumoral anti-CD40/CpG liposome therapy proved only moderately successful: the majority of treated mice were unable to reject a secondary B16 tumor challenge only 3 days after the cessation of therapy, and the few long-term survivors of the initial secondary challenge were unable to maintain effective anti-tumor immunity when re-challenged at a later time (day 90). A CD8 depletion study and a trial therapy using intra-lymph node injections of anti-CD40/CpG liposomes suggested that a CTL-mediated adaptive response only partly contributed to local tumor inhibition, and that tumor-resident innate effectors such as macrophages were also stimulated by anti-CD40/CpG therapy and subsequently involved in the anti-tumor response. While

macrophages, neutrophils, and other innate effectors may be capable of potent local anti-tumor effects, it is generally believed that these populations lack the persistence lifetime, antigen-specificity, and migratory capacity to exert inhibitory effects at distal tumor sites; conversely, tumor-specific CTL-mediated responses have been shown in a variety of pre-clinical and clinical settings to satisfy these criteria. Therefore, we sought to direct the subsequent work in this thesis towards the delivery of T cell-stimulatory agents, in an effort to concomitantly induce local, systemic, and memory anti-tumor immune responses against an established solid tumor.

CHAPTER 5

Potent stimulation of local, systemic, and memory anti-tumor immune responses via local liposome-anchored anti-CD137 + IL-2 therapy

5.1. Abstract

Earlier work conducted in this study had developed and validated our strategy of local liposome-anchored delivery, for the combinatorial anti-CD40 + CpG therapy of established solid tumors. Although the growth of primary treated B16 tumors was significantly inhibited, only a small fraction of mice developed fully curative responses or resistance against a secondary tumor challenge. Therefore, we sought to apply our liposome-coupled delivery strategy to the intra-tumoral administration of two highly potent, T cell-targeted immunomodulatory agents: anti-CD137 (anti-4-1BB) antibody and IL-2 cytokine. We hypothesized that the direct stimulation of cytotoxic T cells (which express both CD137 and IL-2R) would improve the efficacy of local, systemic, and memory anti-tumor immune responses in comparison to anti-CD40/CpG therapy, by priming a stronger tumor-specific adaptive response. As expected, intra-tumoral liposome-anchored anti-CD137 + IL-2 successfully inhibited the growth of primary treated tumors and induced complete cures in >50% of mice. Importantly, measurements of systemic exposure and toxicity following anti-CD137 + IL-2 therapy confirmed that our strategy of liposome-coupled delivery had restricted their bio-distribution and eliminated the inflammatory side effects associated with soluble delivery. In addition, 100% of mice that received primary anti-CD137 + IL-2 liposome therapy were able to reject a secondary tumor challenge on the opposite flank, inoculated ~1.5 weeks after the cessation of therapy, confirming the development of an anti-tumor memory response. Most strikingly, when mice bearing subcutaneous tumors

simultaneously on both flanks were treated in a single flank only, a significant delay in the progression of the distal untreated tumor was observed in all mice, as well as distal tumor rejection in a small fraction of animals, indicating the presence of disseminated, systemic tumor-specific immunity. By each of these measures, anti-CD137 + IL-2 liposome therapy provided a substantial improvement over the efficacy of the previously described anti-CD40/CpG liposome therapy

Analysis of tumor-infiltrating leukocyte (TIL) populations was performed in both the treated and distal untreated tumors to elucidate mechanisms by which these potent anti-tumor responses had been achieved. The successful inhibition of tumor growth was correlated with elevated levels of tumor-infiltrating $CD8^+$ CTLs, and decreased levels of regulatory T cells (Tregs). Furthermore, anti-CD137 and IL-2-conjugated liposomes were found to bind specifically to $CD8^+$ CTLs in the treated tumor, suggesting the stimulation of a potent CTL-mediated immune response. The depletion of $CD8^+$ cells prior to therapy confirmed that $CD8^+$ CTLs were essential in priming an effective anti-tumor response, while the depletion of NK cells (which can also express both IL-2R and CD137) had no distinguishable impact on therapeutic efficacy. Future studies will be aimed at achieving a 100% rejection rate of the treated and/or the distal untreated tumor, potentially by the combination with additional immunostimulatory agents. Nevertheless, the highly effective anti-tumor responses generated by locally administered, liposome-coupled anti-CD137 + IL-2 provided a potent illustration of the versatility and clinical relevance of the liposome delivery strategy developed over the course of this thesis.

5.2. Introduction

5.2.1. Motivation for the delivery of T cell-targeted immunomodulatory agents

We previously developed a strategy for the liposome-conjugated delivery of combinatorial anti-CD40/CpG therapy via intra-tumoral administration. The liposome-coupled anti-CD40/CpG therapy of subcutaneously established B16 tumors demonstrated the induction of potent local anti-tumor immune responses concurrent with the elimination of systemic inflammatory toxicity, but was unable to reproducibly elicit an effective systemic or memory anti-tumor response, as measured by the progression of distal secondary tumor challenges (refer to Chapter 4.4). Preliminary mechanistic experiments suggested only a weakly adaptive T cell-mediated response following anti-CD40/CpG therapy, consistent with the direct stimulation of local (tumor-resident) innate effectors such as macrophages by these two immuno-agonists, leading to an innate immune-dominated anti-tumor response (Chapter 4.4). Therefore, in order to develop a more potent and long-lasting adaptive immune response, we hypothesized that immunomodulatory agents that directly bind and activate tumor-specific cytotoxic T cells (CTLs) might prove more efficacious than anti-CD40 and CpG therapy.

T-cell immunomodulatory therapy has received particular focus for the treatment of advanced metastatic melanoma. In the clinical setting, the frequently disseminated nature of melanoma lesions (rendering surgery unfeasible), the documented presence of antigen-specific tumor-infiltrating lymphocytes in melanomas, and the isolation of clearly defined tumor-expressed antigens have combined to make melanoma an attractive candidate historically for both adoptive T cell therapies (ACT) and the use of immunotherapeutic agents aimed at stimulating endogenous T cells.[142-147] Indeed, the clinical approvals of ipilimumab (anit-CTLA-4) and Proleukin (IL-2) for the treatment of metastatic melanoma represent the most successful

examples of T cell-targeted immunotherapies to date, and ongoing studies combining anti-CTLA-4 therapy with melanoma antigen vaccination strategies have already yielded promising results in preliminary clinical evaluations.[18,148]

Similarly, in the pre-clinical B16 murine melanoma model, a number of recent studies have implicated the requirement for CTL-mediated responses, following a wide variety of anti-tumor immunotherapy strategies. Despite the weak immunogenicity of parental B16 tumors, tumor-infiltrating $CD8^+$ T cells that are reactive against self-antigens expressed in B16 melanoma have previously been reported, and are capable of mounting an effective anti-tumor response once the tolerance to self-antigens has been broken via immunostimulatory therapy.[138,149] For example, anti-CTLA-4 blockade in combination with GM-CSF therapy or with tumor antigen vaccination;[4,137,141] regulatory T cell depletion;[136,138,139] and other regimens of immunomodulatory antibody therapies[150-152] have all provoked increased infiltration and enhanced effector function of cytotoxic T cells in the B16 melanoma model. Therefore, we sought to achieve similarly efficacious priming of a B16-specific, CTL-mediated response, by choosing the appropriate immunostimulatory agents for liposome-coupled intra-tumoral delivery.

5.2.2. The use of anti-CD137 in cancer immunotherapy

Antibodies against the surface receptor CD137 (also known as 4-1BB) have demonstrated potent induction of anti-tumor immune responses in a variety of pre-clinical and early clinical studies.[26,153,154] Although initially discovered as a co-stimulatory receptor that is upregulated upon TCR activation in T cells, recent reports have indicated that CD137 is actually broadly expressed on a variety of immune cell populations, including activated and memory T cells (both $CD4^+$ and $CD8^+$), natural killer (NK) cells, natural killer T (NKT) cells, DCs, and regulatory T

cells, although its cognate ligand, CD137L, is restricted to expression on activated antigen-presenting cells such as macrophages, B cells, and DCs.[153,154] Triggering of CD137 by agonistic antibodies can thus compensate for the loss of CD137L signaling in the immunosuppressed tumor environment, directly providing a co-stimulatory signal to tumor antigen-specific CTLs or to the other aforementioned immune subsets and thereby inducing increases in activation, proliferation, resistance to apoptosis, and effector cytokine production.[153-157] Clinical trials of anti-CD137 therapy against melanoma, renal cancer, and ovarian cancer have reached Phase II in the US (Bristol Meyers Squibb),[26,158] while pre-clinical studies have demonstrated the efficacy of anti-CD137 immunotherapy against numerous murine models, including breast carcinoma, melanoma, lymphoma, renal carcinoma, thymoma, and colon cancer, whether alone or in combination with additional immunotherapeutics such as CpG, anti-CTLA-4, and others.[137,150,159-165] Furthermore, systemic or memory anti-tumor immunity has been demonstrated in a number of the aforementioned studies, including the ability to resist secondary tumor challenges,[161,162,164,165] or the measurement of tumor antigen-specific T cell responses following *in vitro* re-stimulation.[137,159] Therefore, anti-CD137 appears to be an attractive candidate for our strategy of using local liposome-coupled delivery to prime a systemically disseminated, tumor-specific immune response.

In the reports discussed above, the therapeutic activity of anti-CD137 has been primarily attributed to the direct stimulation of tumor-infiltrating $CD8^+$ or $CD4^+$ T cells, in keeping with the known expression profile of CD137 among leukocyte subsets. However, recent studies have also described two novel mechanisms of anti-CD137 activity: Kohrt et al observed that anti-CD137 significantly enhanced the ADCC functionality of CD137-expressing NK cells previously primed by encounter with rituximab-bound lymphoma cells or trastuzumab-bound

breast cancer cells, while Palazon et al discovered that anti-CD137 therapy stimulated tumor endothelium to induce the recruitment of activated T cells in a subcutaneously implanted colon carcinoma model.[166-168] Ongoing pre-clinical and clinical research studies have continued to investigate these potentially pleiotropic anti-tumor effects of anti-CD137.[26,167]

5.2.3. Systemic toxicity associated with anti-CD137 therapy

Agonists against the CD137 receptor have been shown to cause systemic inflammatory effects, consistent with its broadly immunostimulatory activity and similar to those previously described for anti-CD40 (refer to Chapter 3.2.1). For example, liver inflammatory damage, splenomegaly and lymphadenopathy, hematologic abnormalities such as lymphopenia and anemia, and diverse disruptions in lymphocyte trafficking have been observed in mice following systemic anti-CD137 injection.[169-171] Dose-dependent symptoms of liver toxicity, ranging from moderate to severe, have also been detected in human clinical trials with anti-CD137 therapy, accompanied by elevations in serum cytokines and other adverse events associated with systemic inflammation, such as fatigue.[26,158,172] Due to the broad expression profile of the CD137 receptor, studied have not yet determined conclusively whether these inflammatory toxicities are induced by the stimulation of particular leukocyte subsets, either systemically or differentially in particular organs, and/or by the binding to endothelial cells throughout the vasculature. Nevertheless, these findings present a clear motivation for liposome-anchored local delivery of this potent immuno-agonist.

5.2.4. IL-2 in cancer immunotherapy: established clinical efficacy and severe toxicity

Interleukin-2 (IL-2) is an immunostimulatory cytokine that binds to the IL-2 receptor (IL-2R) primarily expressed by T cells and NK cells. The binding of IL-2 stimulates the growth, proliferation, resistance to apoptosis, and differentiation of both $CD4^+$ and $CD8^+$ T cells. As a result of its potent immunostimulatory properties, the efficacy of IL-2 cytokine therapy has been well-established in a wide variety of pre-clinical murine tumor models.[173] After promising results were achieved in early clinical studies for the treatment of advanced cancers, IL-2 (Proleukin/Aldesleukin) was approved for the clinical immunotherapy of advanced metastatic melanoma and metastatic renal carcinoma.[174-180]

Surprisingly, despite its extensive record of pre-clinical success, recombinant IL-2 therapy has only achieved clinical responses, partial or complete, in approximately 15% of treated patients.[146,181] This can be attributed in part to the severity of the systemic side effects experienced by patients during intravenous IL-2 therapy, which limits the dosage and/or duration of therapy that can be administered.[180,182,183] The most common and significant toxicity caused by IL-2 therapy is known as capillary leak syndrome (CLS): the leakage and extravasation of plasma proteins and fluid into the extravascular space.[184] CLS can lead directly to hypotension, reduced organ perfusion, and pulmonary edema, and can result in fatality. To date, no alleviating treatments for CLS have yet been developed, and these symptoms of toxicity can only be reversed by the cessation of IL-2 therapy. Moreover, due to the potential lethality of these side effects, in-patient supervision and administration of IL-2 therapy is required, which substantially raises the overall expense of therapy for cancer patients.

More recently, various studies have examined alternative dosing regimens or administration routes for IL-2 therapy,[6,46,180,182,185,186] as well as combination therapies with additional immuno-

agonists such as anti-CD40 and other immunostimulatory antibodies.[30,79,105,161,187,188] A common objective of these efforts has been to improve on the narrow therapeutic window afforded by the anti-tumor efficacy and severe concurrent toxicity elicited by IL-2 administration. Although these various studies have all demonstrated significant increases in therapeutic potency relative to systemically infused IL-2 alone, none have clearly identified a strategy capable of completely abrogating the toxicity of systemic IL-2. Furthermore, previous biomaterial-based delivery strategies for IL-2 have all attempted to use the controlled release of vehicle-encapsulated IL-2 as a means to reduce systemic exposure and toxicity.[64,66,93,189] As illustrated by the biodistribution analyses described earlier in this thesis, the local release or delivery of protein therapeutics still results in systemic draining, exposure, and toxicity, so any pre-clinical safety profile based on therapeutic dosing in mice may not be translatable upon scale-up to human patients. Most recently, Levin et al have reported the development of a novel engineered IL-2 "superkine", capable of inducing potent anti-tumor responses in mice while significantly reducing pulmonary edema (a common symptom associated with IL-2-mediated inflammatory toxicity).[190] Again, whether these promising results can be directly translated into human patients remains to be determined. Taken together, these considerations clearly established that IL-2 would be a suitable candidate immunotherapy to be tested using our proposed strategy of locally-injected liposome-anchored delivery.

5.2.5. Bivalent IL-2 / Fc fusion protein for antibody-like conjugation to liposomes

In order to facilitate the conjugation of IL-2 cytokine to liposomes, we received a bivalent IL-2/Fc fusion protein from the laboratory of Dane Wittrup at MIT. The complete structure and sequence of the fusion protein is noted in Appendix 1. Briefly, a fusion protein was constructed

by Annie Gai et al (unpublished), in which wild-type murine IL-2 is expressed C-terminally of a murine IgG2a Fc sequence. The fusion protein was originally designed for the purpose of prolonging the circulation time of IL-2 following intravenous injection, and thus included a mutation (D265A) in the Fc portion to minimize binding interactions with low affinity IgG Fc receptors (FcγRIIB and FcγRIII), while binding to neonatal Fc receptor (FcRn) was not disrupted. The presence of disulfide bonds that link two IL-2/Fc chains at the hinge region into a bivalent structure (as in a native antibody) suggested that we should be able to couple the protein to liposome surfaces using a similar technique as our previously described conjugation protocol for anti-CD40 (Chapter 4.3.1). We also hypothesized that conjugating the IL-2/Fc fusion protein in this manner would ensure that the bioactive IL-2 portion would not be blocked or denatured, either during or after the liposome coupling process. Finally, we expected that the larger size of the bivalent IL-2/Fc (~90kDa) relative to free IL-2 cytokine (17.2kDa) could facilitate any purification and preparation required for the liposome coupling reaction.

5.3. Methods

5.3.1. Production of IL-2/Fc fusion protein using HEK293 Freestyle mammalian cells

HEK293 Freestyle ("293F") mammalian cells, generously donated by the Wittrup Lab, were used for the expression and production of the murine wild-type IL-2/Fc fusion protein. First, the IL-2/Fc DNA expression plasmid was transfected into DH5-alpha *E. coli* cells. After the growth of bacterial colonies on agar, plasmids were purified from bacterial lysates by Qiagen Mega-Prep plasmid purification kit, complexed with polyethyleneimine (PEI), and transfected into 293F mammalian cells for transient expression and secretion. Following 7 days of culture, supernatants were collected and the IL-2/Fc protein was isolated by gravity flow/elution through

protein A-linked agarose resin columns. Total protein was quantified by colorimetric BCA assay, while the quantification of IL-2 equivalence was performed by ELISA. In some experiments, a mutant IL-2/Fc fusion protein containing an E76G affinity mutation (for abrogated IL-2Rα binding) was prepared and used for liposome-coupled delivery. An identical protocol was used for the 293F production of mutant IL-2/Fc as for the wild-type IL-2/Fc described above.

5.3.2. Preparation and quantification of anti-CD137-liposomes and IL-2/Fc-liposomes

Liposomes were synthesized as described in Chapter 3.1, with a composition of cholesterol / DOPC / maleimide-PEG(2000)-DSPE / methoxy-PEG(2000)-DSPE. For anti-CD137 or rat IgG2a isotype antibody coupling, liposomes with a composition of 35/60/2.5/2.5 (by mol %) were used; for IL-2/Fc coupling, liposomes with a composition of 35/62.5/2.5/0 were prepared (methoxy-PEG-DSPE omitted). Prior to coupling, anti-CD137 (clone LOB12.3, Bio X Cell) or rat IgG2a isotype antibodies were concentrated to approximately 25-30mg/ml, while IL-2/Fc was concentrated to 12-18mg/ml (by total protein), equivalent to approximately 4-6mg/ml effective IL-2. Each agent was mixed with 1.8mM of dithiothreitol for 20min at room temperature, causing the reduction of hinge-region disulfide bonds and exposing of free reactive thiols. Following passage through desalting columns for the removal of DTT, antibodies or IL-2/Fc were immediately mixed with previously prepared, maleimide-functionalized liposomes in the presence of 10mM EDTA, at a conjugation ratio of 1mg Ab : 1.4μmol liposomes, or 1mg (effective) IL-2 : 5μmol liposomes. (Using the lipid compositions noted above, 1μmol of liposomes is roughly equivalent to 0.7mg of total lipid.) The maleimide-thiol coupling reaction was allowed to proceed overnight at room temperature; liposomes were then pelleted and washed

of unbound antibody or IL-2 by table-top or high-speed airfuge centrifugation. Finally, liposomes were syringe-extruded through 200nm polycarbonate membranes prior to use, resulting in a mean diameter of 150-190nm as measured by dynamic light scattering, which is comparable to the size of the anti-CD40/CpG liposomes developed in Chapter 4. The conjugation of mutant (E76G) IL-2/Fc to liposomes was performed exactly as for wild-type IL-2/Fc.

Quantification of liposome-coupled anti-CD137 or IL-2 for dose equilibration was performed by first dissolving liposomes in a 0.5% solution of the surfactant Tween 20. Solubilized antibody was then measured by a sandwich ELISA similar to that used in the previous quantification of anti-CD40: plates were coated with anti-human IgG, followed by the use of a recombinant CD137/human Fc fusion protein as the capture agent, HRP-conjugated anti-rat IgG as the detection agent, and an HRP-sensitive substrate for colorimetric reading. Solubilized IL-2 was detected using routine sandwich ELISA (R&D Systems).

Liposome-coupled IL-15 super-agonist (IL-15 cytokine + IL-15Rα) was also prepared for an early experiment. A commercially bought IL-15Rα/Fc fusion (R&D Systems) was treated with DTT reduction and coupled to maleimide-functionalized liposomes, according to the protocol described above. After washing to remove unbound IL-15Rα, soluble IL-15 cytokine was added, and captured onto liposome-coupled IL-15Rα. Quantification of conjugated IL-15 super-agonist was measured by dissolving liposomes and performing a sandwich ELISA against IL-15.

5.3.3. Assessing *in vitro* bioactivity of anti-CD137-liposomes and IL-2/Fc-liposomes

To confirm that the bioactivity of anti-CD137 and IL-2/Fc was not lost following liposomal coupling, liposomes were incubated with primary murine splenocyte cultures and assayed for T

cell binding and stimulation. For the testing of anti-CD137-liposomes, splenocytes were obtained from naïve mice and stimulated with concavalin A and IL-7 for two days for non-specific T cell blasting, followed by 10ng/ml of IL-2 for an additional two days. After the combined four days of culture, cultures consisted of over 85% T cells (combined $CD4^+$ and $CD8^+$). Anti-CD137-liposomes or soluble anti-CD137 were then added to a final effective concentration of 5 μg/ml for the indicated times, either as a pulse/wash or in continuous incubation for up to 24 hours. The binding of fluorescently labeled anti-CD137-liposomes was imaged by confocal microscopy (after washing and re-plating cells in fresh medium), while the T cell-stimulatory capacity of anti-CD137-liposomes versus soluble anti-CD137 was assayed by the measurement of IFNγ secretion into culture supernatants. The internalization of liposomes was probed using a trypan blue fluorescence quenching assay, in which cells were incubated with anti-CD137-liposomes for 4hr or 24hr (as above), then analyzed by flow cytometry before or after a 2min pulse of 0.2% Trypan Blue used to quench any extracellular fluorescence (from non-internalized membrane-bound liposomes).

For the testing of IL-2/Fc liposomes, splenocytes were again obtained from naïve mice and stimulated with concavalin A and IL-7 for two days. Soluble IL-2 or IL-2/Fc liposomes were then added to the splenocytes cultures for an additional two days, at a final effective concentration of 20ng/ml. Binding of fluorescently labeled IL-2/Fc liposomes to T cells was detected by confocal microscopy and by flow cytometry, while IL-2 stimulatory activity was confirmed by measuring the proliferation of $CD4^+$ and $CD8^+$ T cells in response to the indicated dosages.

5.3.4. Intra-tumoral therapy of primary subcutaneous B16 tumors using anti-CD137-liposomes and IL-2/Fc-liposomes

Female C57BL/6 mice (6 or 7 weeks) were implanted subcutaneously with 50,000 B16F10 cells on either hind flank. Tumors were allowed to establish for 9 or 10 days prior to the start of therapy, at which point the average tumor area was ~15mm^2. Mice then received intra-tumoral or intra-peritoneal injections of anti-CD137 and IL-2/Fc therapy (or other agents as indicated), either in combination or as monotherapies, in soluble or liposome-coupled form. Three doses were administered in total over the course of one week (3 or 4 days between injections), at equivalent dosages of 100μg of anti-CD137 ± 20μg of IL-2 (effective) per injection, unless otherwise noted. Tumor growths were monitored for up to 60 days post-tumor inoculation, and mice were euthanized if tumors exceeded 100 mm^2, per institutional guidelines. In some mice, serum was collected at various timepoints by retro-orbital bleeding.

Weight changes, normalized to the first therapeutic dosage, were tracked daily as a measurement of overall body condition and systemic toxicity. In addition, the collected serum samples were analyzed by sandwich ELISA for circulating levels of anti-CD137 or IL-2 (refer to Chapter 5.3.2), as well as markers of inflammatory toxicity such as systemically released TNFα, IL-6, or the hepatic enzyme alanine transaminase.

Where noted, an antibody against the TRP-1 protein (clone TA99, Bio X Cell) expressed on the surface of B16 melanoma cells was added to the regimen of intra-tumoral liposome-coupled anti-CD137 + IL-2/Fc therapy. TA99 was administered via intra-peritoneal injection in doses of 50μg or 250μg per injection, either alone or in combination with intra-tumoral liposome therapy, according to the same treatment schedule of 3 doses over the course of one week.

5.3.5. Secondary and distal tumor challenges to assess systemic and memory anti-tumor immune responses

To test the persistence and memory of anti-tumor responses primed by anti-CD137 + IL-2/Fc therapy, surviving mice received a secondary tumor challenge of 50,000 B16F10 cells on the opposite flank, on day 27 post-primary tumor inoculation. This corresponds to at least 10 days following the cessation of primary tumor therapy, ensuring the complete clearance of any residual, systemically circulating levels of either therapeutic agent. Secondary tumor inoculations were left untreated, and subsequently monitored along with the primary tumors. In mice where the day 27 secondary challenge failed to grow into a visible or palpable tumor, an additional secondary challenge of 50,000 B16F10 cells was administered 4 weeks later, on day 55. Mice were euthanized if either primary or secondary tumor growths exceeded $100mm^2$ in area.

To test for the systemic dissemination of anti-tumor immunity primed by local anti-CD137 + IL-2/Fc therapy at the primary tumor, mice were initially inoculated with 50,000 B16F10 cells simultaneously on each hind flank. Tumors were allowed to grow for 9-10 days on both flanks, and mice were removed from therapeutic analysis if tumors failed to establish visible masses on both flanks. Tumors on one flank received intra-tumoral, liposome-coupled anti-CD137 + IL-2/Fc therapy according to the dosage regimen described above in Chapter 5.3.4, while the opposite tumor was left untreated. Mice were euthanized if tumor growths on either flank exceeded $100mm^2$ in area.

Where indicated, the intra-tumoral liposome-coupled therapy of 2 tumor-bearing mice was combined with various doses of soluble anti-CD137 + IL-2/Fc, which were administered systemically via intra-peritoneal injection. Systemic soluble injections were performed

simultaneous with intra-tumoral liposome therapy (one flank only) according to the same treatment schedule. Control mice received systemic soluble therapy in the absence of intra-tumoral liposome therapy.

5.3.6. Depletion studies to determine contributions of CD8+ T cells and NK cells

We had previously validated the use of depletion antibodies to eliminate over 98% of $CD8^+$ and $CD4^+$ expressing cells in tumors, lymphoid organs, and circulation (Chapter 4.3.3). A similar antibody regimen was used to deplete $CD8^+$ cells and $NK1.1^+$ cells (including NK cells and NKT cells). 400μg per dose of anti-CD8a (clone 2.43, Bio X Cell) or anti-NK1.1 (clone PK136, Bio X Cell) was injected intra-peritoneally on days 7, 12, and 16 post-tumor inoculation, in mice bearing 2 simultaneously implanted subcutaneous B16 tumors. Intra-tumoral liposome-coupled anti-CD137 + IL-2/Fc therapy was then carried out on one flank on days 9, 12, and 16, according to the treatment regimen described above (Chapter 5.3.4). Control mice received depletion antibodies without any intra-tumoral immunotherapy.

5.3.7. Analysis of tumor-infiltrating leukocyte (TIL) populations following liposome-coupled anti-CD137 + IL-2/Fc therapy

For the analysis of tumor-infiltrating leukocyte (TIL) populations and their changes in response to anti-CD137 + IL-2/Fc liposome therapy, mice were inoculated with either one or two simultaneous tumors and treated according to the dosing regimen described above for therapy experiments (Chapter 5.3.4). The fluorescent dye DiD was incorporated (at 0.1%) into liposomes to track the binding and distribution of anti-CD137-liposomes and IL-2/Fc liposomes or control IgG-liposomes *in vivo*. At various timepoints before, during, or after the course of

treatment, mice were euthanized and the tumors, spleens, and draining (inguinal) lymph nodes were harvested. Tissues were mechanically dissociated and filtered to obtain single-cell suspensions, and then stained with antibodies against CD45 (common leukocyte antigen), CD3, CD8, NK1.1, CD11c, or F4/80 for analysis by flow cytometry, to compare the levels of tumor-infiltrating $CD3^+CD8^+$ T cells, NK cells, dendritic cells, and macrophages following injections of therapeutic or control IgG liposomes. CD45 expression was used to separate leukocyte subsets from tumor cells and any other non-leukocyte populations such as stromal or endothelial cells. In some samples, staining antibodies against CD25 (IL-2Rα) and CD137 were included in the flow cytometry analysis to compare the changing expression levels of these receptors over the course of therapy. Co-localization of the fluorescent liposome label with these various immune subsets was also examined, in both treated and distal tumors, the spleen, and the draining and distal lymph nodes, to determine the specificity of anti-CD137 and IL-2/Fc liposome binding compared to control IgG liposomes.

Tumor-infiltrating levels of regulatory T cells ($CD4^+Foxp3^+$) were also examined, either before, during, or after the course of treatment. Tissues were harvested as above, processed into cell suspensions, and surface stained with anti-CD4 antibody. Cells were then fixed and permeabilized prior to intracellular staining using an anti-Foxp3 antibody, and analyzed by flow cytometry. Defined volumes of cell suspensions were used to enable the calculation of total cell counts within an entire tumor mass, according to the gated populations measured by flow cytometry.

5.3.8. Histological analysis of anti-CD137-liposome and IL-2/Fc-liposome biodistributions *in vivo*

For the histological analysis of liposome biodistribution, B16 tumors were implanted on both flanks and treated intra-tumorally (one flank only) with a single dose of DiD-labeled anti-CD137-liposomes and IL-2/Fc-liposomes. 24 hours post-injection, the treated and distal tumors, as well as the draining and distal lymph nodes, were harvested and snap-frozen in liquid nitrogen for cryosectioning. Tissue slices were obtained and imaged directly by confocal microscopy to investigate the distribution of injected liposomes.

5.4. Results and Discussion

5.4.1. Screening candidate immunotherapies for the priming of potent adaptive anti-tumor immunity

In the preceding chapters of this thesis, we developed a strategy for the local liposome-anchored delivery of anti-CD40 + CpG therapy for the treatment of established B16 tumors. Although this combination therapy induced the potent inhibition of primary tumor growth (Figure 4.4), the majority of mice were unable to reject a secondary tumor challenge, indicating the insufficient priming of an adaptive anti-tumor immune response (Figure 4.11). Therefore, we performed a pilot screen of additional candidate immunotherapies, to test their ability to stimulate protective immunity against a secondary tumor challenge as well as their suitability for liposome-coupled delivery.

Since anti-CD137 has previously been reported to mediate highly potent anti-tumor responses, via direct stimulation of tumor-specific $CD8^+$ T cells,[153] we decided to test the liposome-conjugated delivery of this antibody for B16 tumor therapy. As shown in Figure 5.1a,

a short regimen of intra-tumoral therapy with anti-CD137-coupled liposomes (2 doses only, at ~70μg per dose) provided only a modest inhibition of primary B16 tumor growth, with the majority of tumors progressing rapidly by about three weeks post-inoculation. Surprisingly, the addition of anti-CD40-coupled liposomes, prepared as described previously in Chapter 4, did not yield any significant therapeutic benefit above anti-CD137-liposomes alone (Figure 5.1a).

Liposomes bearing surface-coupled IL-15 superagonist (IL-15Rα pre-complexed with IL-15 cytokine) were also prepared as described in Chapter 5.3.2., and combined with anti-CD137-liposomes for a pilot regimen of intra-tumoral therapy. IL-15 superagonist has been shown in a variety of pre-clinical tumor models to potently stimulate the proliferation and effector functions of CTLs and NK cells.[191,192] However, due to the low efficiency of coupling (<5%), only a total of ~10μg/dose of IL-15 superagonist could be administered following liposome conjugation, representing a substantially lower dose than has previously been used for local therapies against B16 tumors.[51] As a result, the combination of liposome-coupled IL-15 superagonist with anti-CD137 was also unable to consistently induce a potent anti-tumor immune response, even at the primary treated tumor (Figure 5.1a). Given the small fraction of effective responses observed, and the low number of overall long-term surviving mice, secondary challenge studies were not carried out subsequent to the primary liposome-coupled therapies described above.

We next investigated the use of IL-2 cytokine in the intra-tumoral treatment of subcutaneous B16 tumors. Similar to IL-15 superagonist, IL-2 has previously been well-established as a potent stimulant for CTL and NK cell activity and proliferation (as introduced in Chapter 5.2.4). Furthermore, the donation of the IL-2/Fc fusion protein from the Wittrup Lab (refer to Chapter 5.2.5 or Appendices) provided a convenient means by which the cytokine could theoretically be conjugated to the surface of liposomes at a high efficiency. Therefore, we tested the use of the

IL-2/Fc fusion, either alone or in combination with anti-CD137, for the primary inhibition of B16 tumors and the subsequent induction of secondary tumor rejection. For this experiment, a 2-dose regimen of therapy was administered intra-tumorally in soluble form, for the purpose of expediting the screening process.

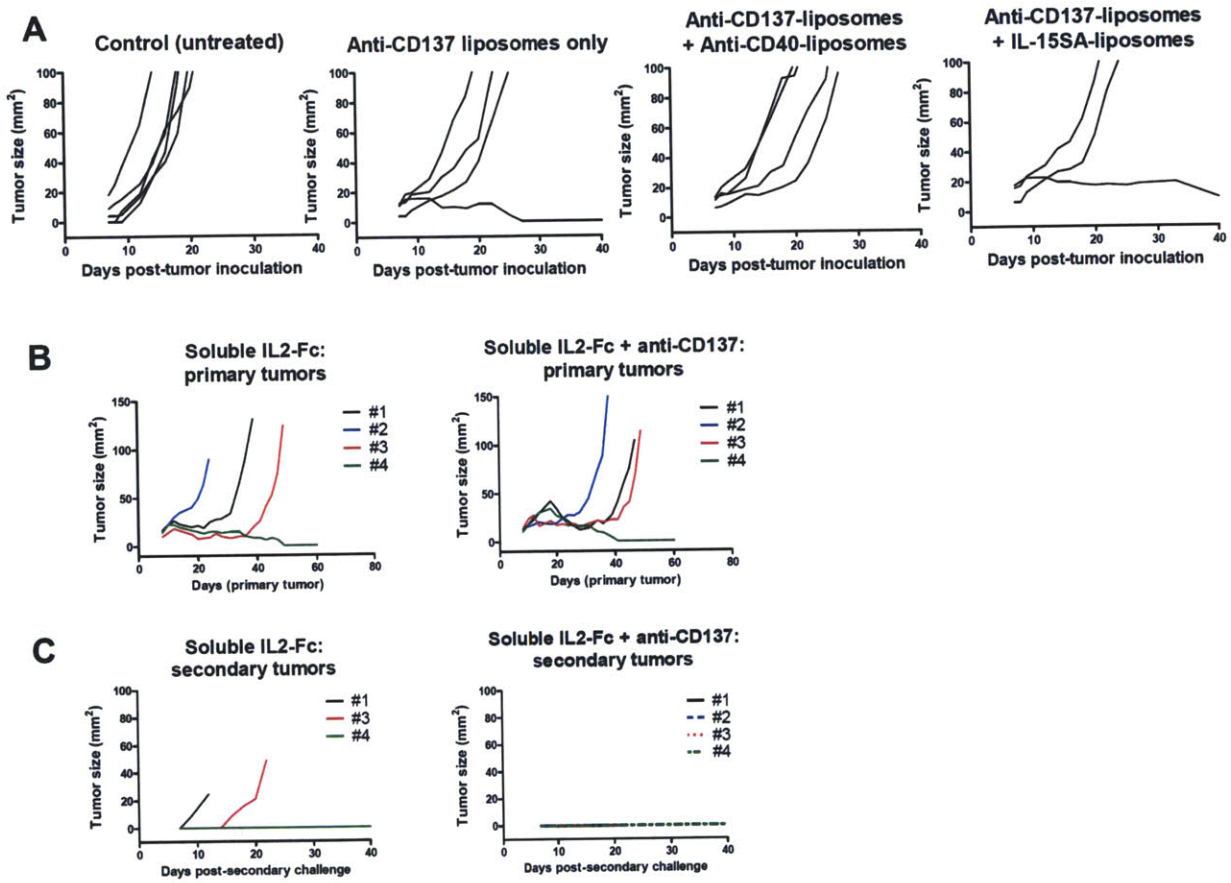

Figure 5.1. Pilot screens of candidate immunotherapies for improved priming of adaptive anti-tumor immune responses. A) Individual tumor growths (n=3 or 4) of mice treated with 2 intra-tumoral injections of liposome-coupled anti-CD137 only, liposomal anti-CD137 + anti-CD40, or liposomal anti-CD137 + IL-15-superagonist (SA), on days 8 and 14. B) Individual growths (n=4) of the primary treated tumors in mice receiving 2 intra-tumoral injections of soluble IL-2/Fc or soluble IL-2/Fc + anti-CD137, on days 8 and 12. C) Corresponding growths of secondary tumors inoculated in mice following primary intra-tumoral therapy with soluble IL-2/Fc or IL-2/Fc + anti-CD137. Secondary challenges were inoculated into all surviving mice at day 27 of primary tumor growth.

As shown in Figure 5.1b, soluble IL-2/Fc alone provided a significant, but inconsistent, inhibition of the primary treated tumor growth, while the combination of soluble IL-2/Fc + anti-CD137 further enhanced the delay in tumor progression, in the majority of treated tumors. Strikingly, when the surviving mice were re-challenged with a secondary inoculation (50,000 B16F10 cells) on day 27 post-primary inoculation, all mice (4 of 4) that had received the combination of soluble IL-2/Fc + anti-CD137 therapy were able to reject the secondary tumor (Figure 5.1c). Conversely, of the mice that had received soluble IL-2/Fc therapy alone, only 1 out of 3 initial primary survivors demonstrated protective immunity against the secondary challenge. Based on these preliminary results, we decided to focus subsequent experiments on developing and optimizing the liposome-coupled delivery of anti-CD137 + IL-2/Fc combination therapy. Our principal objective, as previously stated, continued to be the use of liposome-anchored delivery to achieve similarly efficacious anti-tumor responses, while eliminating any inflammatory toxicities induced by this potent combination of immunostimulatory agonists.

5.4.2. Synthesis and *in vitro* bioactivity of anti-CD137-liposomes and IL-2/Fc liposomes

Having previously developed and validated a strategy for the maleimide-thiol coupling of anti-CD40 to the surface of liposomes (Chapters 3-4), we adapted this technique for the conjugation of both anti-CD137 and the IL-2/Fc fusion protein. Briefly, anti-CD137 and IL-2/Fc were separately treated with 1.8mM DTT to reduce disulfide bonds in the Fc chain hinge region, exposing free thiols for reaction with maleimide-functionalized liposomes. The reaction of each therapeutic agent with previously prepared liposomes was also performed separately. Coupling efficiencies of approximately 10-15% for anti-CD137 and 20-25% for IL-2/Fc were achieved, corresponding to a final conjugation of 100-150μg anti-CD137 per mg of total lipid, and 57-71μg

IL-2 (effective) per mg of lipid. Following syringe extrusion through a 200nm membrane, anti-CD137-liposomes and IL-2/Fc-liposomes were recovered with mean diameters of 150-190nm by dynamic laser scattering measurement. Prior to *in vivo* injection for anti-tumor therapy, the two species of liposomes were simply mixed together, for a final effective dose of 100μg anti-CD137 + 20μg IL-2 per injection.

Mixed primary splenocyte cultures from naïve C57BL6 mice (untreated and tumor-free) were used to first confirm the bioactivity of either liposome-coupled anti-CD137 or IL-2/Fc *in vitro*. For anti-CD137-liposomes, naïve splenocytes were activated in culture for 2d using concavalin A and IL-7, followed by incubation with soluble recombinant IL-2 cytokine for 2d, to stimulate T cell proliferation, resulting in cultures that consisted of over ~85% T cells (including $CD4^+$ and $CD8^+$ cells) by day 4. Anti-CD137-liposomes or soluble anti-CD137 were then added at an effective final concentration of 5μg/ml, in a pulse of 2hr or 6hr, or continuous incubation over 24hr. After a total of 24hr, the culture supernatants were collected and analyzed by ELISA for IFNγ levels, as a measure of T cell stimulation. Figure 5.2a shows that the addition of anti-CD137-liposomes at this dose induced a significant increase in IFNγ secretion compared to untreated or control IgG-liposome treated cultures, and that the level of IFNγ production increased in correlation with a greater incubation time of anti-CD137-liposomes. Interestingly, anti-CD137-liposomes in this *in vitro* assay induced an even more potent IFNγ response than an equivalent dose of soluble anti-CD137 (Figure 5.2a), in either the pulsed or continuously stimulated cultures. This clearly confirmed that the coupling of anti-CD137 to liposome surfaces via maleimide-thiol conjugation had not caused any detectable loss in the stimulatory activity of the agonistic antibody.

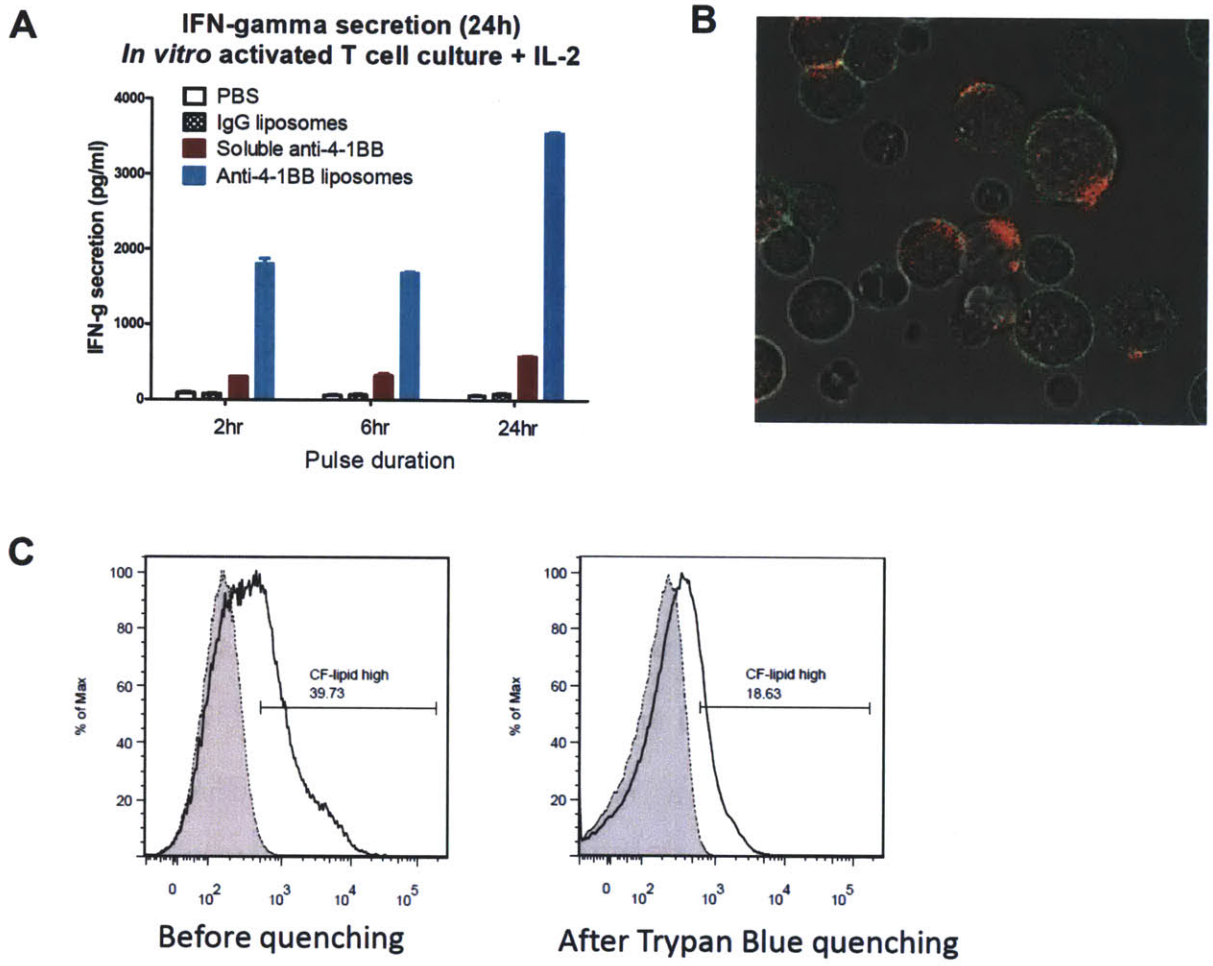

Figure 5.2. *In vitro* binding and bioactivity of anti-CD137-coupled liposomes on primary stimulated splenocyte cultures. A) Secretion of IFNγ by *in vitro* activated splenocyte cultures following the addition of soluble or liposome-coupled anti-CD137 (anti-4-1BB). Naïve splenocytes were activated for 2d with concavalin A + IL-7, then additionally stimulated for 2d with IL-2, resulting in cultures consisting of >85% T cells. On day 4, anti-CD137 was added for the indicated pulses, and supernatants were collected after 24hr for the measurement of IFNγ by ELISA. B) Confocal imaging of T cells incubated for 24hr with anti-CD137-liposomes, showing specific binding and aggregation of fluorescently labeled liposomes (red) on T cells (green). C) Flow cytometry analysis showing the quenching of extracellular fluorescence from cell surface-bound liposomes by addition of Trypan Blue. Activated T cells were incubated with labeled anti-CD137-liposomes for 24hr as in parts a-b, then measured by flow cytometry (open histograms), before (left) or after (right) the addition of the quenching agent. Filled histograms represent background fluorescence of cells in the absence of liposome incubation.

Confocal imaging of splenocytes after 5hr (not shown) or 24hr (Figure 5.2b) of continuous incubation with anti-CD137-liposomes indicated that both $CD4^+$ and $CD8^+$ T cells were able to

bind anti-CD137-coupled liposomes. Importantly, liposomes were capable of efficient binding in the presence of complete serum-containing medium, which includes proteases and lipases that could hypothetically degrade or hamper the specificity of antibody-coupled liposomes. Furthermore, a large proportion of fluorescently labeled liposomes appeared to remain attached to the surface of T cells in membrane-localized, aggregated "patches" of fluorescence, even after a full 24hr of culture. We speculated that this occurred via the antibody/liposome-mediated crosslinking of CD137 receptors on the cell surface, due to the multivalent nature of anti-CD137 conjugated on the surfaces of liposomes. In turn, this might have restricted the ability of T cells to internalize either the CD137 receptor itself or the agonistic antibody when presented on liposomes, thereby resulting in continual stimulation and the induction of unexpectedly potent levels of IFNγ production that surpassed the response to soluble anti-CD137 (Figure 5.2a).We validated this hypothesis by performing a Trypan Blue fluorescence quenching assay, in which cells were incubated with labeled anti-CD137-liposomes for 4hr or 24hr, then analyzed by flow cytometry with or without the addition of a pulse of Trypan Blue to quench any extracellular fluorescence. The addition of Trypan Blue serves to quench any fluorescence from non-internalized, membrane-bound liposomes; therefore, any remaining fluorescent signal following Trypan Blue quenching represents the level of previously internalized liposomes. As shown in Figure 5.2c, there was a substantial loss of detectable fluorescence following quenching, indicating that a large of fraction of anti-CD137-liposomes had indeed remained membrane-bound on the surface of T cells, and thus had avoided internalization and subsequent degradation.

Similarly, for the *in vitro* confirmation of liposome-coupled IL-2/Fc bioactivity, we again used primary mixed splenocyte cultures, activated for 2d by concavalin A + IL-7. On day 2, either soluble free IL-2 or IL-2/Fc-liposomes were added to the cultures at a final effective

concentration of 20ng/ml, and the proliferation of $CD4^+$ and $CD8^+$ T cells was quantified by flow cytometry two days later. Figure 5.3a illustrates that IL-2/Fc-liposomes were able to induce a comparable amount of T cell proliferation as soluble IL-2 (baseline normalized to live cell counts in the absence of IL-2 stimulation), confirming that the bioactivity of IL-2 was not abrogated by the presence of the Fc fusion chains nor by the conjugation to liposomes. The slightly lower level of liposome-induced $CD4^+$ and $CD8^+$ T cell proliferation relative to soluble IL-2 treated cultures might reflect imprecise quantification of the amount of IL-2 coupled to liposomes, since increasing the amount of IL-2/Fc-liposomes added to the cultures resulted in a dose-dependent increase in proliferation for both T-cell compartments (not shown).

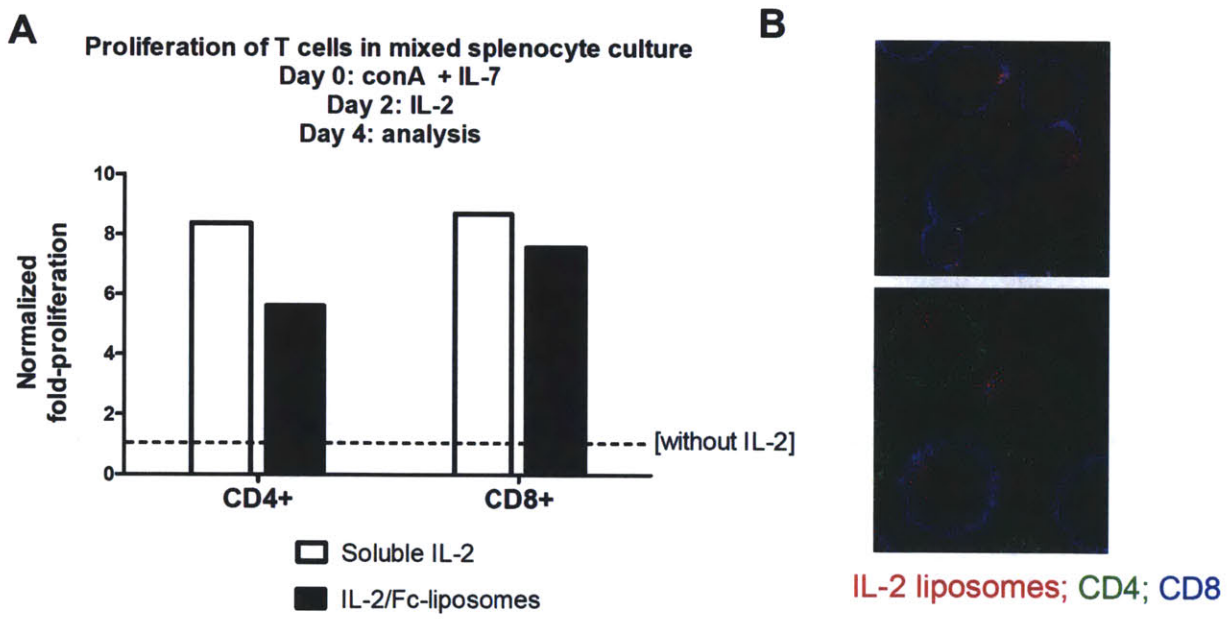

Figure 5.3. *In vitro* binding and bioactivity of IL-2/Fc-coupled liposomes on primary stimulated splenocyte cultures. A) Proliferation of $CD4^+$ and $CD8^+$ T cells from primary splenocyte cultures, activated with concavalin A + IL-7 on d0 and stimulated with soluble (open bars) or liposome-coupled (solid bars) IL-2/Fc from d2 to d4. Cell counts were obtained by flow cytometry and normalized to the level of viable T cells in the absence of IL-2 (dotted line). B) Confocal imaging demonstrating specific binding of IL-2/Fc liposomes to $CD4^+$ (green) or $CD8^+$ (blue) T cells, following 5hr of incubation on d2 of *in vitro* splenocyte culture, as described for part (a).

In addition, confocal microscopy was performed to directly image the binding of IL-2/Fc-liposomes to both CD4+ and CD8+ cells, as shown in Figure 5.3b. T-cell specific binding could be observed after less than 2 hours of incubation in the presence of serum-containing medium, followed by the washing and re-plating of cells in fresh medium. Contrary to the imaging of anti-CD137-liposomes in splenocyte cultures (Figure 5.2b), only a limited amount of fluorescently labeled liposomes could be detected on the surface of any given T cell, and considerable internalization of IL-2/Fc liposomes was observed. Differences between the T cell-binding capacities of the two liposome-coupled agents may simply reflect differences in the surface expression levels of CD137 and IL-2Rα. Nevertheless, taken together, these *in vitro* splenocyte culture assays convincingly demonstrated that the bioactivity of both immunostimulatory agonists was maintained following their conjugations onto liposomes for delivery.

5.4.3. Potent inhibition and cure of primary tumors with minimal systemic toxicity via intra-tumoral liposome-coupled anti-CD137 + IL-2/Fc therapy

We then proceeded to test the anti-tumor efficacy of anti-CD137-liposomes and IL-2/Fc-liposomes *in vivo*. C57BL/6 mice (6-8 weeks old, female) were inoculated on one flank with 50,000 B16F10 tumor cells, and tumors were allowed to establish for 9-10 days, reaching an average size of ~15mm^2 prior to the start of therapy. Mice were treated with 3 injections of intra-tumoral therapy over the course of one week (days 9/12/16 or 10/13/17), using saline control (PBS), rat isotype IgG-liposomes, anti-CD137-liposomes only, IL-2/Fc-liposomes only, combined liposomes, or combined soluble anti-CD137 + IL-2/Fc, at a dosage of 100μg anti-CD137 and 20μg effective IL-2 per injection. Figure 5.4a illustrates the individual tumor

growths in response to the various liposome-delivered therapies. As expected, liposome-coupled monotherapies (anti-CD137 or IL-2/Fc alone) induced only a modest delay in tumor progression compared to PBS-treated controls, although 1 of 4 mice treated with IL-2/Fc-liposomes alone was able to achieve a completely curative response. These results were comparable to the anti-tumor responses described earlier following soluble IL-2 or anti-CD137 monotherapies (Figure 5.1b). On the other hand, the combination of anti-CD137-liposomes + IL-2/Fc-liposomes successfully stimulated highly potent anti-tumor immune responses at the primary treated tumor (Figure 5.4a): 9 out of 14 mice achieved durable tumor regression and cures, where tumors remained undetectable for over 50 days or until the cessation of monitoring. Furthermore, the remaining 5/14 mice treated with liposome combination therapy all showed significant delays in tumor progression, indicating the priming of at least a transiently effective anti-tumor immune response. Anti-tumor responses to combined anti-CD137 and IL-2/Fc liposome therapy were compiled from multiple independent experiments, confirming the robustness of the current delivery strategy. Overall, the efficacy of liposome-coupled anti-CD137 + IL-2/Fc therapy constituted a substantial improvement over the primary responses achieved by intra-tumoral anti-CD40/CpG liposome therapy (Figure 4.4, Chapter 4.4.2).

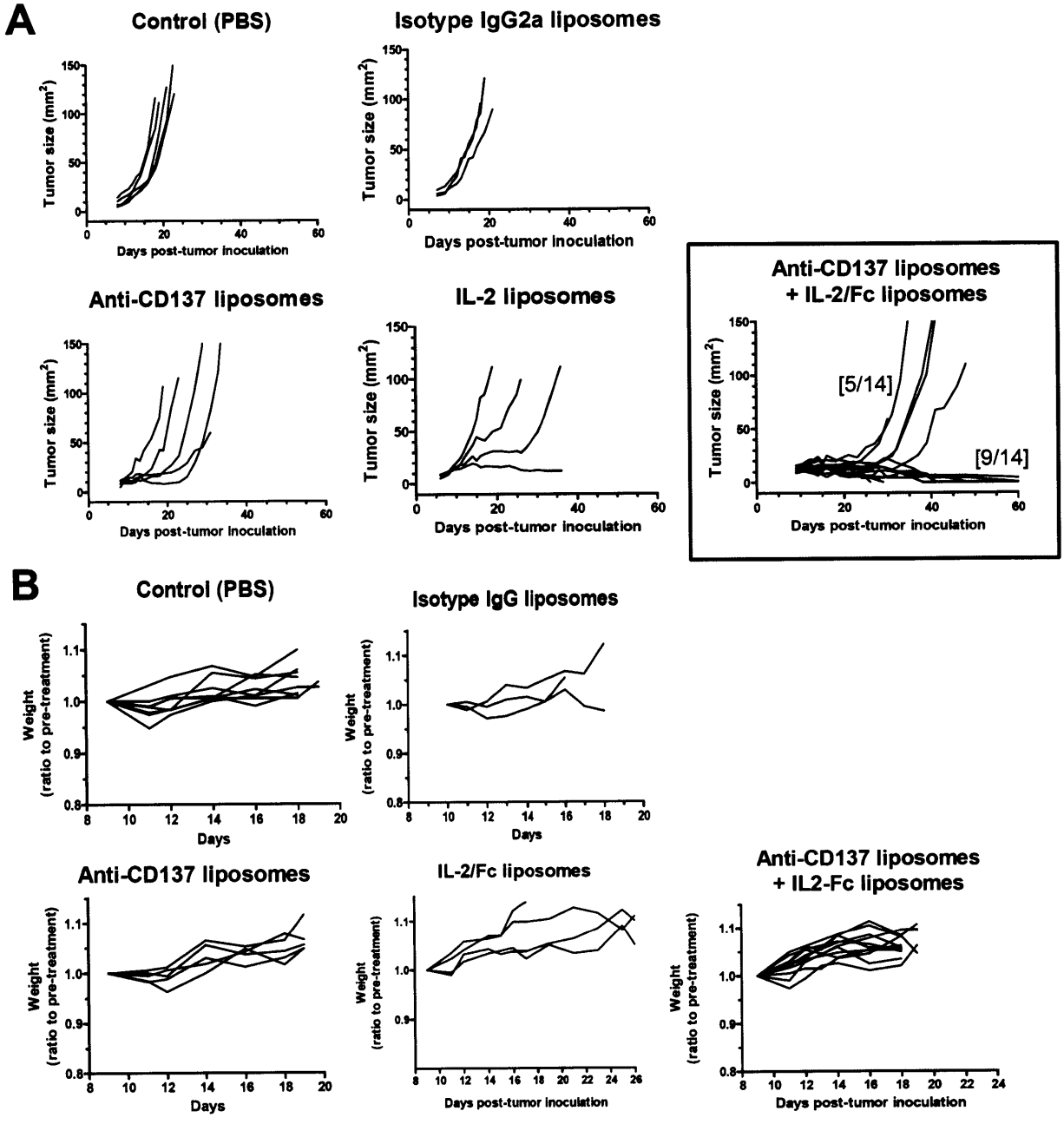

Figure 5.4. Highly potent inhibition of primary treated B16 tumors in the absence of systemic toxicity, via intra-tumoral liposome-coupled anti-CD137 + IL-2/Fc therapy. A) Individual growths of primary tumors treated with PBS, isotype-coupled liposomes, anti-CD137-liposomes only (n=5), IL-2/Fc-liposomes only (n=4), or combined anti-CD137-liposomes + IL-2/Fc liposomes (n=14). Mice received intra-tumoral treatments on days 9/12/16 or 10/13/17, at equivalent doses of 100μg anti-CD137 and/or 20μg IL-2 per injection. Bracketed numbers indicate fractions of delayed progressing tumors versus complete cures. B) Individual weight changes, represented as a ratio to the pre-treatment weight, in mice treated with intra-tumoral therapy as described for part (a).

Weight changes of mice treated with liposome-coupled anti-CD137 + IL-2/Fc were also tracked over the course of therapy, as an overall measure of body condition and systemic inflammatory toxicity. As shown in Figure 5.4b, no detectable symptoms of systemic toxicity were observed in liposome-treated mice compared to saline control mice, whether in response to combination anti-CD137 + IL-2/Fc therapy or to either agent alone. This suggested that liposome-coupled delivery had again successfully eliminated systemic inflammatory side effects, as expected based on the previous results obtained using anti-CD40/CpG liposome therapy (Figure 4.5, Chapter 4.4.2).

For comparison, B16 tumor-bearing mice were also treated with soluble anti-CD137 + IL-2/Fc combination therapy, according to the same dosing schedule of three injections within one week. In separate experiments, intra-tumoral or systemic (intra-peritoneal) injections were administered at an equivalent full dose of 100μg soluble anti-CD137 + 20μg (effective) soluble IL-2/Fc per injection. The individual tumor growths and weight changes in response to soluble intra-tumoral therapy are shown below in Figure 5.5. Although equivalent full doses of soluble intra-tumoral therapy proved to be highly efficacious at inducing primary tumor regression, resulting in complete cures in 100% of treated mice (Figure 5.5a), extremely severe or lethal inflammatory toxicities were observed in all mice (Figure 5.5b). Significant weight losses were measured in the majority of mice (>10% of initial weight in some mice), beginning one or two days after the first injection and continuing throughout the treatment regimen, along with a variety of side effects including fatigue, sluggishness, shivering, severe local tissue ulceration/necrosis, and local limb paralysis. In all, 2 out of 8 mice that received full doses of soluble intra-tumoral therapy perished during or after the treatment course, despite having completely eliminated any visible tumor burden at the injected site (Figure 5.5b). Not

surprisingly, systemic (intra-peritoneal) injections of soluble therapy at the full dose of 100μg anti-CD137 + 20μg effective IL-2 proved to be even more lethal, with 3 out of 5 treated mice perishing from inflammatory toxic effects even before the completion of the three-dose regimen (data not shown).

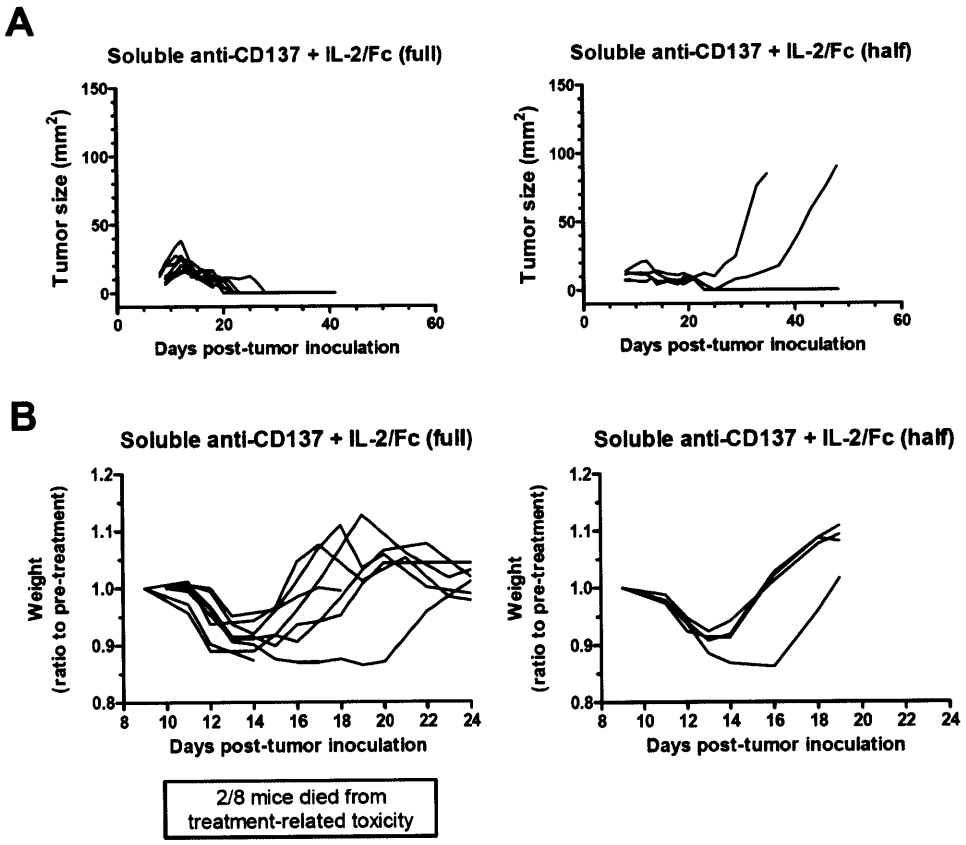

Figure 5.5. Potent therapeutic efficacy concurrent with severe or lethal systemic toxicity induced by intra-tumorally injected, soluble anti-CD137 + IL-2/Fc combination therapy. A) Individual tumor growths in mice receiving soluble intra-tumoral therapy on days 9/12/16 or 10/13/17, at a full dose of 100μg anti-CD137 + 20μg IL-2/Fc per injection (left panels, n=8) or at half of that dose per injection (right panels, n=4). B) Weight changes in mice treated with soluble intra-tumoral therapy as described for part (a), demonstrating severe inflammatory toxicities, including lethality.

To determine whether locally injected soluble anti-CD137 + IL-2/Fc therapy could be titrated to achieve an appropriate therapeutic window of efficacy and reduced toxicity, a group of mice was treated with half-doses of combination therapy (50μg anti-CD137 + 10μg IL-2/Fc per

injection), according to the same treatment schedule. Although no toxicity-induced fatalities occurred, significant weight losses up to ~10% of the initial weight could still be detected, for several days through the course of therapy (Figure 5.5b). However, at this reduced dose of soluble therapy, only 2 of 4 mice achieved completely curative responses, while the other 2 mice eventually succumbed to tumor progression, albeit with a substantial delay compared to untreated controls (Figure 5.5a compared to Figure 5.4a). Taken together, these results clearly illuminate the advantage of controlling the bio-distribution of such potent immunostimulatory agents, thereby providing a therapeutic window by which effective anti-tumor immune responses can be induced without causing highly toxic systemic inflammatory effects.

To confirm that liposome-coupled delivery had indeed minimized the leakage and systemic exposure of anti-CD137 and IL-2 following intra-tumoral injection, blood samples were collected at 18hr post-injection (single dose). Acellular plasma fractions were then analyzed by ELISA for the circulating levels of each immunotherapeutic agent. Figure 5.6 shows that liposome-anchored delivery almost completely eliminated the drainage of both anti-CD137 (5.6a) and IL-2/Fc (5.6b) into systemic circulation, consistent with the aforementioned absence of observable systemic toxicity as measured by overall weight loss (Figure 5.4b). In contrast, intra-tumoral injections of soluble combined anti-CD137 + IL-2/Fc resulted in a high level of systemic exposure to both agonists, which was correlated with the severe and sometimes fatal symptoms of toxicity described above (Figure 5.5b). The respective systemic levels attained with soluble or liposome-coupled anti-CD137 + IL-2/Fc therapy matched our expectation that liposome-mediated delivery would be able to locally sequester these agonists, based on our previous experience using anti-CD40 + CpG combination therapy in soluble or liposome-coupled form (Chapter 4.4).

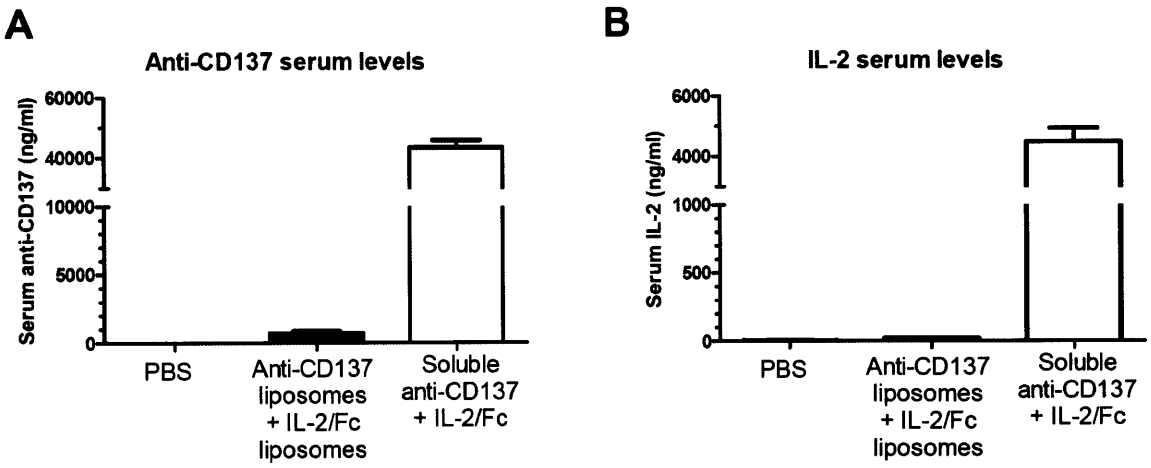

Figure 5.6. Systemic circulating levels of anti-CD137 and IL-2/Fc following the soluble or liposome-anchored intra-tumoral injection of combination therapy. A,B) Serum measurements of anti-CD137 or IL-2 by ELISA at 18hr post-injection ($n \geq 4$ per group), illustrating the ability of liposome-coupled delivery to locally restrict the *in vivo* bio-distribution of these potent agonists and minimize systemic exposure.

5.4.4. Rejection of secondary tumor challenge and inhibition of simultaneous distal tumors following primary anti-CD137 + IL-2/Fc liposome therapy

Having established the potency of local liposome-coupled anti-CD137 + IL-2/Fc therapy at the primary treated tumor, we next examined whether an adaptive anti-tumor immune response had been effectively primed. Since anti-CD137 and IL-2/Fc have been shown in previous studies to induce the activation of tumor-specific cytotoxic T cells (refer to Chapter 5.2), we hypothesized that a CTL-mediated response would be able to disseminate systemically and inhibit the growth of distal identical tumors. Therefore, we tested the potency of the systemically disseminated immune response in two contexts: 1) the secondary inoculation of a distal tumor post-primary tumor therapy, as a measure of memory anti-tumor immunity and as a model of tumor recurrence or metastatic outgrowth; and 2) the simultaneous inoculation of a distal tumor that remains untreated while the primary tumor receives anti-CD137 + IL-2/Fc

therapy, to mimic the clinical setting of multiple disseminated tumor lesions (as frequently found in melanoma patients).

To assess the ability of local anti-CD137 + IL-2/Fc therapy to inhibit a secondary distal tumor challenge, mice were inoculated with a primary tumor and treated intra-tumorally according to the same dosages and schedule (days 9/12/16) as described earlier. On day 27 post-primary inoculation, all surviving mice that had received anti-CD137 + IL-2/Fc therapy, either in soluble or liposome-conjugated form, were inoculated on the distal flank with 50,000 B16F10 tumor cells. Strikingly, in two independent experiments, 100% of primary treated mice completely rejected the secondary tumor challenge, regardless of whether anti-CD137 and IL-2/Fc had been administered as soluble (4 out of 4 mice) or liposome-coupled (7 out of 7 mice) therapy. Mice were monitored until at least 28 days post-secondary inoculation, and in all mice, the secondary challenge was completely unable to establish and grow into any detectable tumor mass (Figure 5.7). Importantly, inoculations performed in naïve mice (no primary tumor or immunotherapy), using the same batch of tumor cells, established progressing tumors in 100% of mice, confirming the viability of these tumor cells at the time of inoculation (Figure 5.7). Similarly, previous experiments had also shown that secondary tumor challenges in untreated primary tumor-bearing mice result in 100% secondary progression as well (Figure 4.11a). An additional distal tumor challenge was then performed on day 55, on mice that had rejected the day 27 secondary challenge and had not yet succumbed to primary tumor progression. The day 55 re-challenge was again completely rejected in 100% of inoculated mice, including 3 out of 3 animals that had initially received liposome-coupled primary therapy. Taken together, these results demonstrated that local liposome-coupled anti-CD137 + IL-2/Fc therapy had successfully primed an adaptive immune response capable of targeting distal tumor cells.

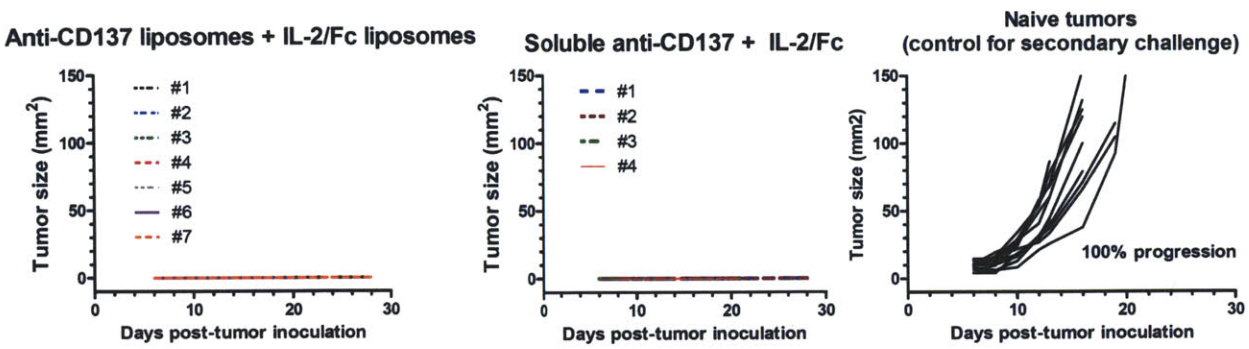

Figure 5.7. Rejection of distal secondary tumor challenge in mice, following local anti-CD137 + IL-2/Fc primary therapy in soluble or liposome-coupled form. Mice received primary intra-tumoral injections of combination therapy on days 9/12/16, as previously described. Secondary tumor challenges in the distal flank were inoculated on all surviving mice at day 27 of primary tumor growth (n=7 for liposome-treated, n=4 soluble-treated). Simultaneous primary inoculations into naïve mice yielded 100% tumor progression (right panel).

Somewhat surprisingly, symptoms of melanin-associated autoimmunity such as vitiligo were not consistently observed in mice that had been treated with either soluble or liposome-coupled anti-CD137 + IL-2/Fc therapy, despite the clear indications of a systemically disseminated immune response against B16 tumors. While previous reports have described a correlation between autoimmune vitiligo and effective anti-tumor immunity in the B16 tumor model,[138,149] unpublished observations in our work and in the Wittrup Lab have suggested that the presence or absence of vitiligo is not a reliable indication of the efficacy of therapy. These conflicting conclusions may simply reflect slight differences in the tumor model setting used in the various studies.

We speculated that the secondary tumor rejection described above was most likely mediated by the systemic dissemination of tumor-specific CTL effectors, capable of recognizing and directly killing tumor cells at the site of secondary inoculation before a solid tumor mass can be established, with its plethora of immuno-suppressive mechanisms. With this in mind, a model of 2 simultaneous tumor inoculations (in which only one tumor site is treated) presents the most

difficult challenge for local therapy, as it requires a locally primed immune response to not only target and infiltrate the distal tumor, but to also overcome the established immuno-suppressive microenvironment at the distal tumor.

To test the proximal and distal efficacy of liposome-coupled anti-CD137 + IL-2/Fc therapy in this highly challenging setting, 50,000 B16F10 cells were simultaneously inoculated on both hind flanks and first allowed to establish for 9-10 days. Mice then received intra-tumoral anti-CD137 + IL-2/Fc liposome therapy on one flank only, on days 9/12/16 or 10/13/16, at 100μg antibody + 20μg IL-2 per dose. Figure 5.8a shows the average growths of treated and distal tumors following liposome-coupled therapy, compiled from three independent experiments, while Figure 5.8b illustrates the individual growth kinetics of distal untreated tumors. Consistent with previous experiments (Figure 5.4a), progression of the treated tumor was either significantly delayed or completely cured. Notably, distal tumor growths were also consistently inhibited following local liposome-coupled therapy, achieving a significant delay in progression compared to control mice (Figure 5.8a,b). Although the majority of treated mice did eventually succumb to progression of the distal tumor, a small fraction (2 out of 9) appeared to successfully reject the distal tumor, with no observable tumor growth for over 50 days post-inoculation (Figure 5.8b). Furthermore, Figure 5.8c shows that intra-tumoral liposome therapy provided a significant improvement in overall survival compared to control mice, in this 2-tumor setting. Thus we have clearly demonstrated that liposome-delivered anti-CD137 + IL-2/Fc is capable of eliciting highly potent local as well as systemic anti-tumor immune responses, despite the weakly immunogenic and aggressive nature of the B16 melanoma model.

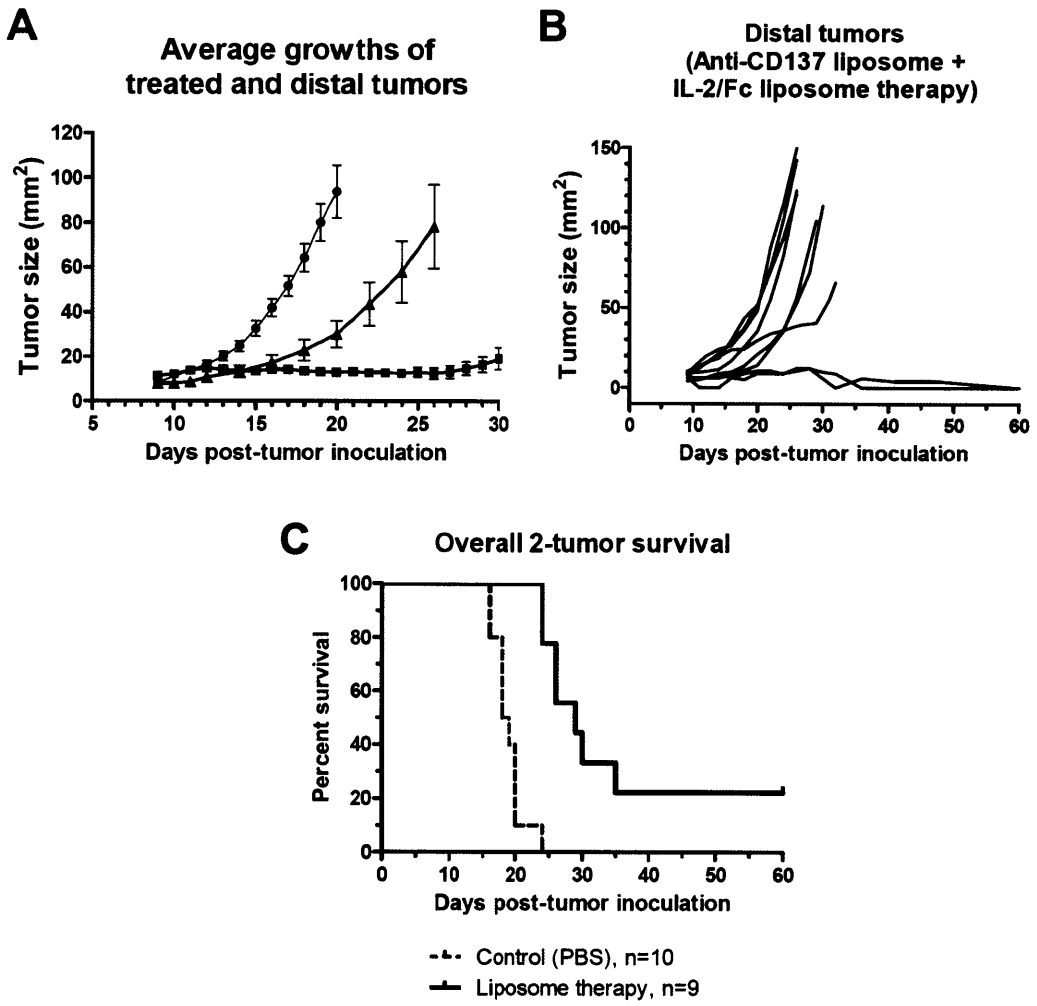

Figure 5.8. Inhibition of simultaneous distal tumors following liposome-coupled anti-CD137 + IL-2/Fc therapy at a primary tumor site. A) Average growths of the primary treated tumor (squares) or the distal untreated tumor (triangles) in mice receiving intra-tumoral liposome-coupled combination therapy, on one flank only. Mice were inoculated with simultaneous tumors on both flanks, and treated on one side on days 9/12/16 or 10/13/16 as previously described. Distal tumors were significantly inhibited compared to PBS-treated controls (circles). B) Individual growth curves (n=9 in total) of simultaneous distal (untreated) tumors in mice that received intra-tumoral therapy at the primary tumor. C) Overall survival of mice bearing 2 simultaneous tumors, following anti-CD137 + IL-2/Fc liposome therapy (solid line) or PBS control treatment (dashed line) on one flank only, as for parts a-b. Mice were euthanized if any individual tumor on either flank exceeded 100mm^2.

It should be noted that by using intra-tumoral liposome-coupled delivery, we have ensured that any tumor-inhibitory effects at the distal site have occurred via the dissemination of the immune response from the local priming site, as opposed to the systemic leakage of soluble

therapeutic agents reaching the distal tumor. The ability to reject a simultaneously growing distal tumor without requiring a systemically administered therapy, even if only in a small fraction of mice, represents an extremely promising development for potential translation into the clinical treatment of patients bearing multiple disseminated lesions. By maintaining the local sequestration of therapy, via our strategy of liposomal coupling or a comparable delivery vehicle, highly potent immunotherapeutic agents (such as the anti-CD137 and IL-2 used in this study) could potentially be administered to a single lesion for the induction of anti-tumor responses throughout multiple malignant sites.

5.4.5. Modified therapies and combination treatments for the potential enhancement of anti-tumor efficacy

The previous experiments using liposome-coupled anti-CD137 + IL-2/Fc therapy had demonstrated the induction of potent local and systemic anti-tumor immunity, as indicated by the large proportion of complete cures attained at primary treated tumors and the inhibition of simultaneous distal untreated tumors. We sought to further enhance the efficacy of liposome-coupled therapy with the dual goals of consistently obtaining 100% rejection of primary tumors, and improving the anti-tumor responses at the distal tumor so as to achieve a greater delay in tumor progression or a greater percentage of complete cures.

We first investigated the use of a mutated IL-2/Fc fusion protein, developed by Gai et al (Wittrup Lab), in place of the wild-type IL-2/Fc fusion administered previously. The mutant IL-2/Fc, containing an E76G point mutation, had been shown to induce greater levels of T and NK cell proliferation *in vivo* relative to the wild-type IL-2/Fc fusion, despite having an extremely weak (or near-zero) binding affinity for the IL-2Rα chain (CD25) (data not shown). We

hypothesized that the increased stimulation of CTL and NK cell proliferation via mutant IL-2/Fc might enhance the overall efficacy of our liposome-coupled therapy, relative to wild-type IL-2/Fc. Therefore, we tested the use of mutant IL-2/Fc-liposomes, in combination with anti-CD137-liposomes as described earlier, for the local treatment of B16 tumors. Mice received 3 doses of intra-tumoral liposome-coupled therapy, consisting of 100μg anti-CD137 (as before) + approximately 8-10μg mutant IL-2/Fc per dose, on days 10/13/17. A substantially lower dose of mutant IL-2/Fc was injected compared to previous experiments with wild-type IL-2/Fc, due to the relatively poor conjugation efficiency of the mutant to liposomes. Disappointingly, the use of mutant IL-2/Fc-liposomes did not provide any additional therapeutic benefit compared to wild-type IL-2/Fc (Figure 5.9a), with only 2 of 4 treated mice showing completely curative responses. Moreover, when challenged with a secondary tumor on the distal flank (day 27), 1 of 3 surviving mice showed visible progression of the secondary inoculation into a palpable tumor mass, indicating the insufficient priming of a memory anti-tumor immune response. The lack of improvement in therapeutic efficacy, when substituting the E76G mutant for wild-type IL-2, was consistent with other results obtained in parallel by Gai et al (Wittrup Lab). Consequently, the use of the mutant IL-2/Fc was not further pursued in this thesis.

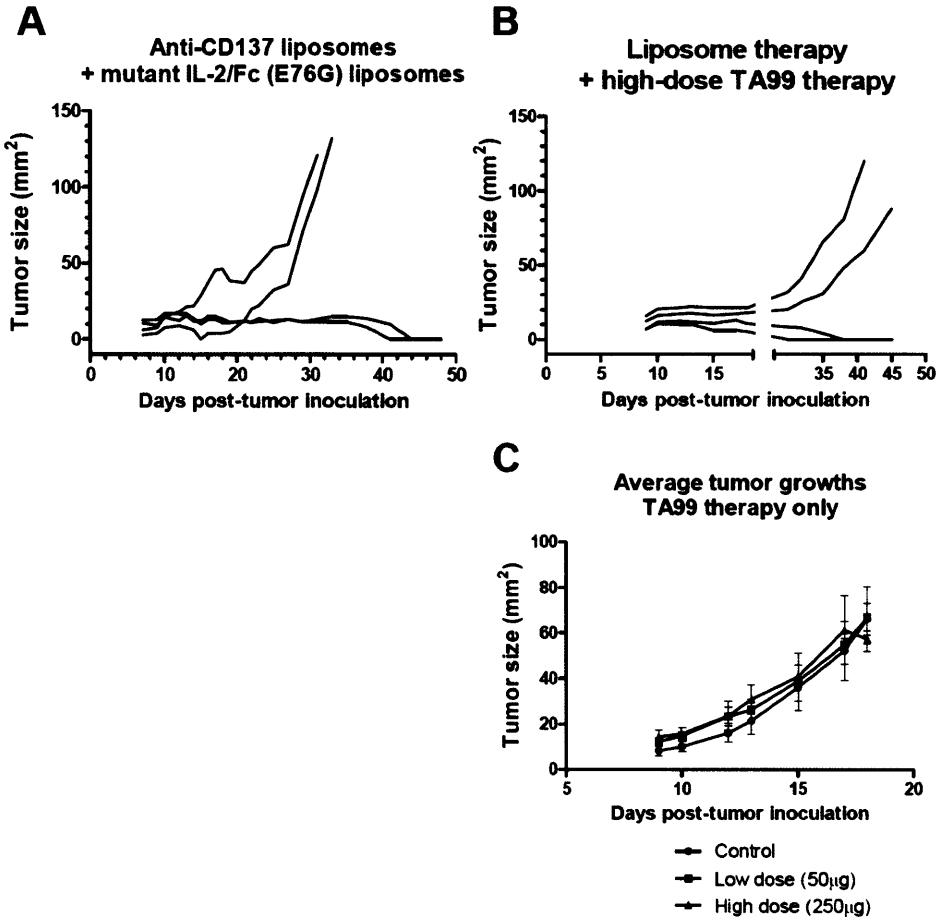

Figure 5.9. Modified therapeutic regimens fail to significantly improve on the efficacy of liposome-coupled anti-CD137 + IL-2/Fc treatment. A) Individual tumor growths (n=4) in mice treated intra-tumorally with liposome-coupled anti-CD137 + mutant IL-2/Fc (E76G). Mice received intra-tumoral injections on days 10/13/17, at 100μg anti-CD137 + 8-10μg mutant IL-2/Fc per dose. B) Individual tumor growths (n=4) in mice receiving intra-peritoneal TA99 antibody therapy, in addition to intra-tumoral liposome-coupled anti-CD137 + IL-2/Fc (wild-type) combination therapy. Mice were treated on days 10/13/17 with 250μg TA99 per intra-peritoneal dose, and local liposome therapy as previously described. C) Average tumor growths (n=4 per group) of mice receiving intra-peritoneal TA99 antibody therapy alone on days 10/13/17, illustrating lack of efficacy at 50μg (squares) or 250μg (triangles) per dose. Average tumor growth in PBS-treated mice is overlaid (circles).

Another potential strategy for enhancing the response to immunomodulatory tumor therapies is to combine the use of a tumor cell-binding antibody, capable of directly eliciting antibody-dependent cellular cytotoxicity (ADCC) or complement-dependent cytotoxicity (CDC) against the targeted tumor cells. Antibodies that target tumor-expressed antigens for the induction of

ADCC and CDC have been developed and used in a wide variety of pre-clinical and clinical settings, including the targeting of EGFR, ERBB2, EpCAM, CD20, CD30, and many others.[14,172,193] In the case of the murine B16 melanoma model, the anti-TRP-1 antibody TA99 has previously demonstrated the ability to induce tumor cell apoptosis *in vivo*.[194-196] Therefore, we investigated whether the addition of TA99 therapy to our established regimen of anti-CD137 + IL-2/Fc therapy could result in an improved, or potentially synergistic, anti-tumor response at the primary treated site.

B16 tumors were allowed to establish on one flank for 10 days prior to the start of therapy. On days 10/13/17, mice received intra-peritoneal injections of soluble TA99 antibody, at 50μg (low-dose) or 250μg (high-dose) per injection. Systemic delivery of the soluble TA99 was used to more closely mimic the clinical administration of tumor-targeting antibodies; since TA99 does not exhibit immunomodulatory effects, the resulting systemic exposure to the antibody did not induce any detectable inflammatory toxicities. In addition, some mice received intra-tumoral injections of liposome-coupled anti-CD137 + (wild-type) IL-2/Fc therapy, also on days 10/13/17, a similar regimen as had previously been used in our immunotherapy experiments (Chapter 5.4.3). As shown in Figure 5.9b, the combination of high-dose TA99 with liposome-coupled immunotherapy did not induce any significant delays in primary tumor progression compared to immunotherapy alone (Figure 5.4, Chapter 5.4.3), nor did it increase the percentage of complete cures achieved. In fact, the systemic administration of TA99 antibody had a negligible effect on directly inhibiting the rate of B16 tumor growth, as illustrated by comparing the average tumor sizes in untreated mice to mice that received TA99 alone, without immunotherapy (Figure 5.9c). It is likely that the dosages and timepoints of TA99 therapy administered in this study were simply unable to achieve sufficient levels of infiltration in the established B16 solid tumors, and

thus could not reach the critical local antibody concentration necessary for any detectable therapeutic activity.

Finally, we investigated the possibility of incorporating a low dose of systemic soluble immunotherapy (anti-CD137 + IL-2/Fc) in combination with our strategy of locally injected liposome-coupled immunotherapy. Since the principal concern with soluble immuno-agonist therapy is the extent to which it can cause systemic inflammatory toxicities, we attempted to determine a therapeutic window in which a sufficiently low dose of systemic soluble therapy could induce a slight delay in tumor progression without eliciting any toxic side effects. Given that local liposome-coupled therapy had not been able to consistently cure distal tumors, in the setting of the simultaneous 2-tumor model (Chapter 5.4.4), we further hypothesized that a low dose of systemic soluble immunotherapy might transiently inhibit the progression of multiple tumors on both flanks, and that the adaptive immune response primed by a full regimen of local liposome-coupled therapy might subsequently succeed at completely rejecting the distal tumor.

To assess this hypothesis, mice were inoculated with B16 tumors on both flanks, and therapy was administered on days 9/12/16. Intra-tumoral liposome-delivered therapy consisted of 100μg anti-CD137 + 20μg IL-2/Fc per injection as before, while the low-dose systemic soluble therapy was injected intra-peritoneally on the same days at doses of 10μg anti-CD137 + 2μg IL-2/Fc per injection. At this dose of soluble therapy, with or without local liposome therapy, no observable symptoms of inflammatory toxicity were elicited, as indicated by the weight changes in treated mice (Figure 5.10a). However, the administration of low-dose systemic soluble therapy also provided no detectable improvement in anti-tumor efficacy over local liposome-coupled therapy alone. As shown in Figure 5.10b, neither the average kinetics of tumor progression nor the percentage of complete cures achieved was enhanced by the addition of systemic soluble therapy

at this dose, whether at the primary tumor (i.e. the site of liposome-coupled treatment) or at the distal tumor (refer to Figures 5.4a and 5.8b for comparison). When the systemic soluble dose was increased to 20μg anti-CD137 + 4μg IL-2/Fc, symptoms of inflammatory toxicity began to be observed regardless of the inclusion of local liposome therapy (Figure 5.10c). Overall, we concluded from these results that the addition of systemically delivered soluble therapy did not provide any practical therapeutic advantage over the use of intra-tumoral liposome-anchored therapy alone.

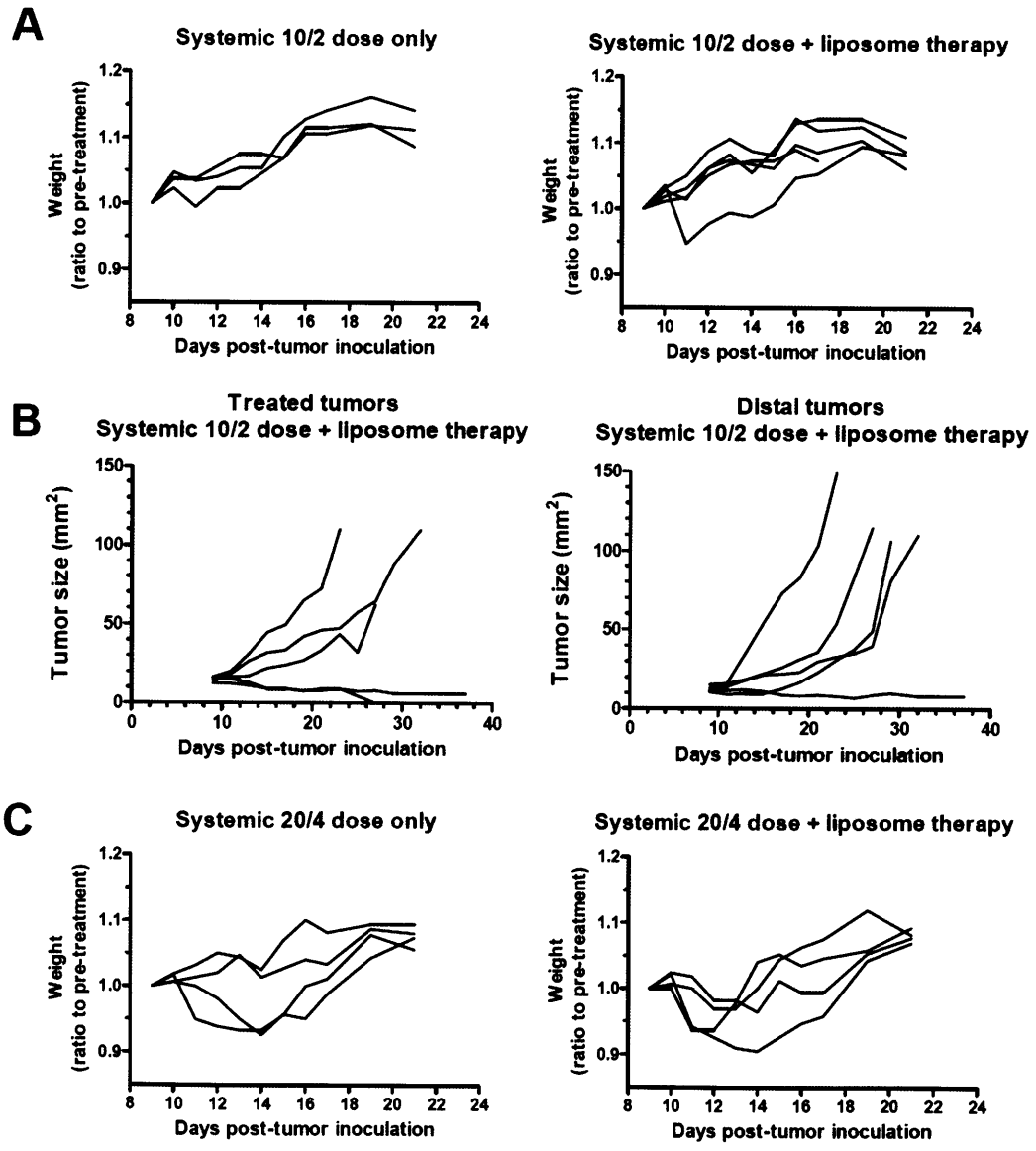

Figure 5.10. Lack of an effective therapeutic window for the addition of systemic soluble anti-CD137 + IL-2/Fc therapy to the established regimen of local liposome-coupled therapy. A) Weight changes in mice receiving a low non-toxic dose of systemic soluble anti-CD137 + IL-2/Fc therapy. Mice were treated with soluble intra-peritoneal doses of combination therapy (10μg anti-CD137 + 2μg IL-2/Fc per dose) on days 9/12/16, with or without full doses of local liposome-coupled combination therapy as previously described. B) Individual growth curves of mice that received a non-toxic dose of systemic soluble anti-CD137 + IL-2/Fc therapy (respectively 10μg + 2μg per dose) in addition to intra-tumoral liposome-coupled therapy (full doses as previously described) on days 9/12/16. Mice were simultaneously inoculated with tumors on both flanks; intra-tumorally injected tumors are shown in the left panel, and distal tumors shown in the right panel. C) Weight changes in mice receiving moderately toxic doses of systemic soluble anti-CD137 + IL-2/Fc therapy (20μg anti-CD137 + 4μg IL-2/Fc per injection) on days 9/12/16, with or without a full regimen of intra-tumoral liposome-coupled combination therapy.

5.4.6. *In vivo* distribution of anti-CD137-liposomes and IL-2/Fc-liposomes and specificity of binding following intra-tumoral therapy

The preceding series of experiments confirmed that locally injected anti-CD137-liposome + IL-2/Fc-liposome therapy, without any further addition, remained the most effective strategy for eliciting local and systemic anti-tumor immunity in the complete absence of systemic toxicity. Therefore, for the remainder of this thesis, we focused on gaining a fuller understanding of the immunological mechanisms by which these potent anti-tumor responses had been induced by this liposome-delivered therapy.

As reviewed in Chapters 5.2.2 and 5.2.4, anti-CD137 and IL-2 have been shown to stimulate effective anti-tumor responses primarily via the activation of cytotoxic $CD8^+$ T cells, in a variety of pre-clinical models and clinical settings.[146,153,154,180,182] Given the potent level of local, systemic and memory immune responses attained in the current thesis, we speculated that CTLs were the principal effectors being primed by liposome-coupled anti-CD137 and IL-2/Fc therapy. In order to test this hypothesis, the *in vivo* bio-distribution of fluorescent DiD-labeled liposomes bearing anti-CD137 and IL-2/Fc was examined in detail, following intra-tumoral administration.

Mice were inoculated with subcutaneous B16 tumors on both flanks, then treated with 2 doses of local liposome-coupled therapy (100μg Ab + 20μg IL-2 as before) on days 10 and 13 post-inoculation. On days 15 or 16, the treated and distal tumors, the proximal and distal lymph nodes, and the spleen were harvested from mice; processed into single-cell suspensions; stained for a variety of immunological cell populations; and finally analyzed by flow cytometry, for the co-localization of liposomes with various immune cell subsets. Isotype rat IgG2a-conjugated liposomes were compared to anti-CD137 or IL-2/Fc liposomes, to determine the binding specificity of the therapeutic liposomes via their intended receptors, relative to levels of non-specific Fc-mediated binding or uptake by phagocytic antigen-presenting cells (APCs).

Figures 5.11a and 5.11b illustrate the binding specificity of DiD-labeled anti-CD137 and IL-2/Fc liposomes for $CD8^+$ T cells in locally treated tumors. The majority of CTLs in the injected tumor were positive for DiD in therapeutic liposome-treated mice (mean 67±6%), while a significantly lower percentage of CTLs were DiD^+ in mice receiving IgG liposomes (mean 21±3%). Similarly, the overall geometric mean fluorescent intensity (geo-MFI) of DiD on the CTLs recovered from treated tumors was substantially higher following therapeutic liposome treatment (mean 3100±1400 RFU), compared to IgG liposome treatment (mean 79±16 RFU). Thus, therapeutic liposomes had successfully bound to local (tumor-infiltrating) $CD8^+$ T cells at a much greater extent than IgG liposomes, as we had expected given the known expression levels of the receptors CD137 and IL-2Rα on these cells. Conversely, no detectable levels of DiD fluorescence were found on CTLs in the distal tumors, whether in therapeutic or IgG liposome-treated mice, confirming that locally injected liposomes were unable to drain into systemic circulation and directly access the distal tumor (Figure 5.11a).

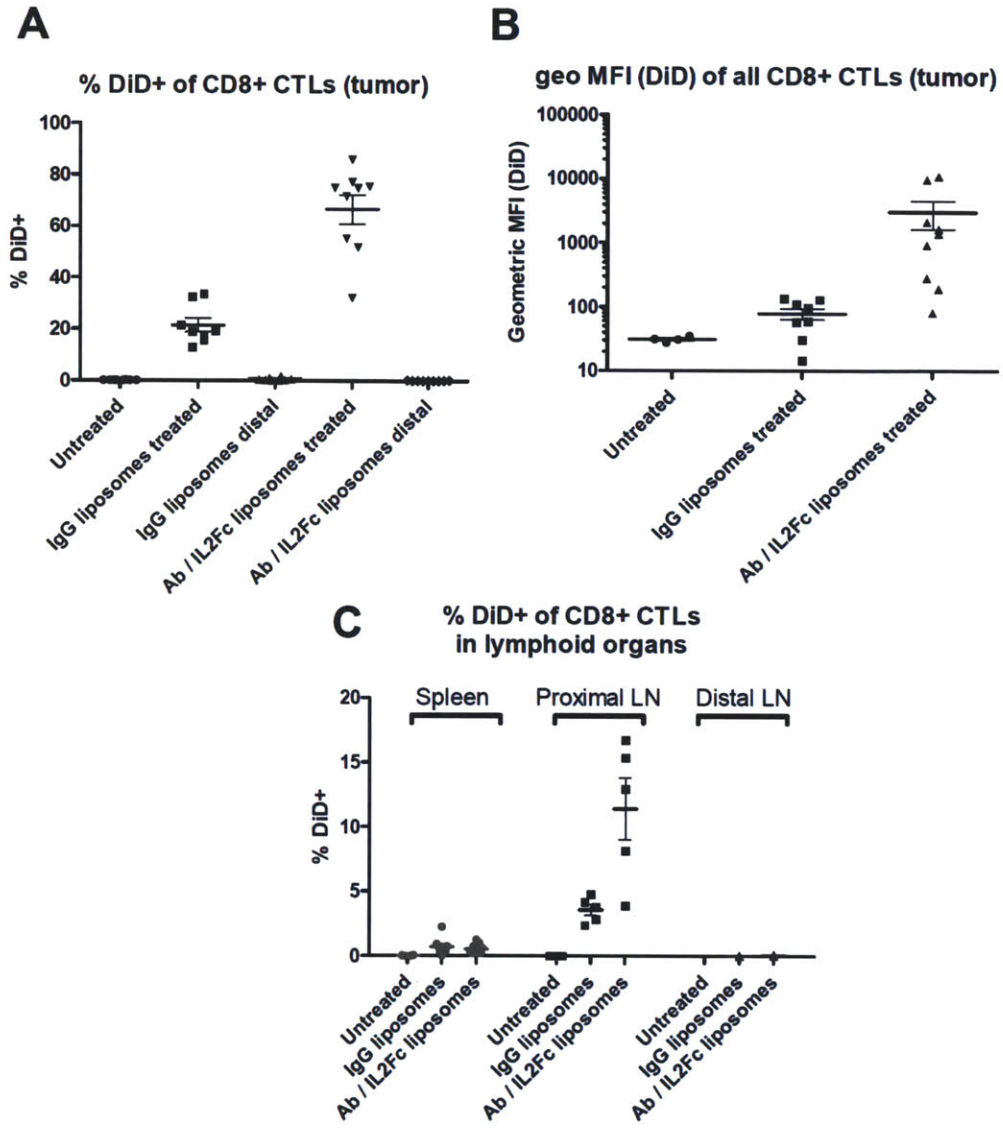

Figure 5.11. Binding specificity of anti-CD137-liposomes and IL-2/Fc liposomes to $CD8^+$ CTLs at the treated tumor and proximal LN. A) Percentage of tumor-resident $CD8^+$ CTLs positive for the fluorescent DiD label incorporated into IgG control or anti-CD137 and IL-2/Fc-coupled liposomes. Mice bearing 2 simultaneous tumors received intra-tumoral injections of labeled IgG-liposomes or combination therapeutic liposomes into one tumor, on days 10 and 13 (n=8 per group); the treated and distal tumors were recovered on days 15 or 16 and analyzed by flow cytometry. B) Geometric mean fluorescent intensity (MFI) of DiD signal on all $CD8^+$ CTLs recovered from primary treated tumors. Mice received intra-tumoral injections of labeled IgG-liposomes or combination therapeutic liposomes as described for part (a). C) Percentage of $CD8^+$ CTLs positive for DiD fluorescence in various lymphoid organs. Mice received intra-tumoral injections of DiD-labeled IgG-liposomes or combination therapeutic liposomes as described for part (a) (n=5 per group); spleens and tumor-draining inguinal lymph nodes (proximal to the treated tumor, or on the distal flank) were excised on days 15 or 16 and analyzed by flow cytometry.

Measurements of DiD co-localization with CTLs in proximal and distal lymphoid organs demonstrated a similar pattern of binding specificity, with significantly higher levels of CTL binding in the proximal lymph node by therapeutic anti-CD137 and IL-2/Fc liposomes than by IgG isotype liposomes (mean 11±2% vs. 3.6±0.4%, Figure 5.11c). Whether DiD-labeled liposomes had accessed the proximal lymph node via direct lymphatic draining, or via cell-mediated trafficking, was not explicitly determined in this experiment. Analysis of the distal lymph node and the spleen again confirmed the minimal systemic exposure to locally injected liposomes, as negligible levels of DiD fluorescence could be detected in these distal tissues (Figure 5.11c). Overall, these results clearly established the ability of therapeutic anti-CD137 and IL-2/Fc liposomes to directly target and bind to CTLs for the local stimulation of potent, tumor-specific immune responses.

In addition to the analysis of CTLs at tumors and lymphoid organs, we decided to investigate other immune subsets that might also be capable of binding or taking up therapeutic liposomes, both specifically (via the intended receptors) or non-specifically (via Fc-mediated interactions or phagocytosis). NK cells were analyzed because of their reported ability to respond to both anti-CD137 and IL-2 stimulation,[154,166,197] while dendritic cells (DCs) and macrophages (MPs) were analyzed because of their phagocytic capabilities, Fc receptor expression, and known infiltration into solid tumor masses.[2,198] Figures 5.12a and 5.12b illustrate respectively the percentages of DiD fluorescent co-localization with each of these immune subsets at the local injected tumor, and the overall geometric MFI of DiD in each of these subsets. Only the analysis from the treated tumor is shown, as no observable DiD fluorescence was detected at the distal tumor.

As expected, local tumor-infiltrating NK cells bound a significantly greater level of therapeutic liposomes than IgG liposomes (Figure 5.12a, mean 60±6% vs. 22±2%), suggesting

that liposome-coupled anti-CD137 and IL-2/Fc therapy may have been able to target NK cells and induce NK cell-mediated effects in addition to a CTL-mediated response. A similar increase in specific binding was measured by quantifying the geometric MFI of DiD fluorescence in NK cells at the treated tumor (Figure 5.12b). Somewhat surprisingly, the DiD fluorescence from therapeutic liposomes also co-localized with DCs and macrophages at the treated tumor at a higher percentage than IgG liposomes (Figure 5.12a, mean 48±6% vs. 28±2% for DCs and mean 64±7% vs. 35±3% for macrophages). Although we had expected that therapeutic and IgG liposomes would co-localize equally with these subsets of APCs, due to non-specific and possibly Fc-mediated interactions, the expression of CD137 has in fact been reported on activated DCs and macrophages.[153] Therefore, it is possible that anti-CD137-liposomes may have exhibited preferential targeting for DCs and macrophages as well. However, differences between therapeutic and IgG treatments in the overall geometric DiD MFI of these two cell populations remained either modest or statistically insignificant (Figure 5.12b). Finally, the percentage of DiD^+ co-localization with NK cells, DCs, or macrophages in the proximal lymph node was statistically indistinguishable between therapeutic and IgG treatments (Figure 5.12c). Taken together, these results suggested that while anti-CD137-liposomes and IL-2/Fc liposomes may have exhibited some degree of specific binding to each of these immune populations, it is likely that in addition to CTLs, only NK cells were directly stimulated by therapeutic liposomes to contribute significantly to the locally primed anti-tumor immune response.

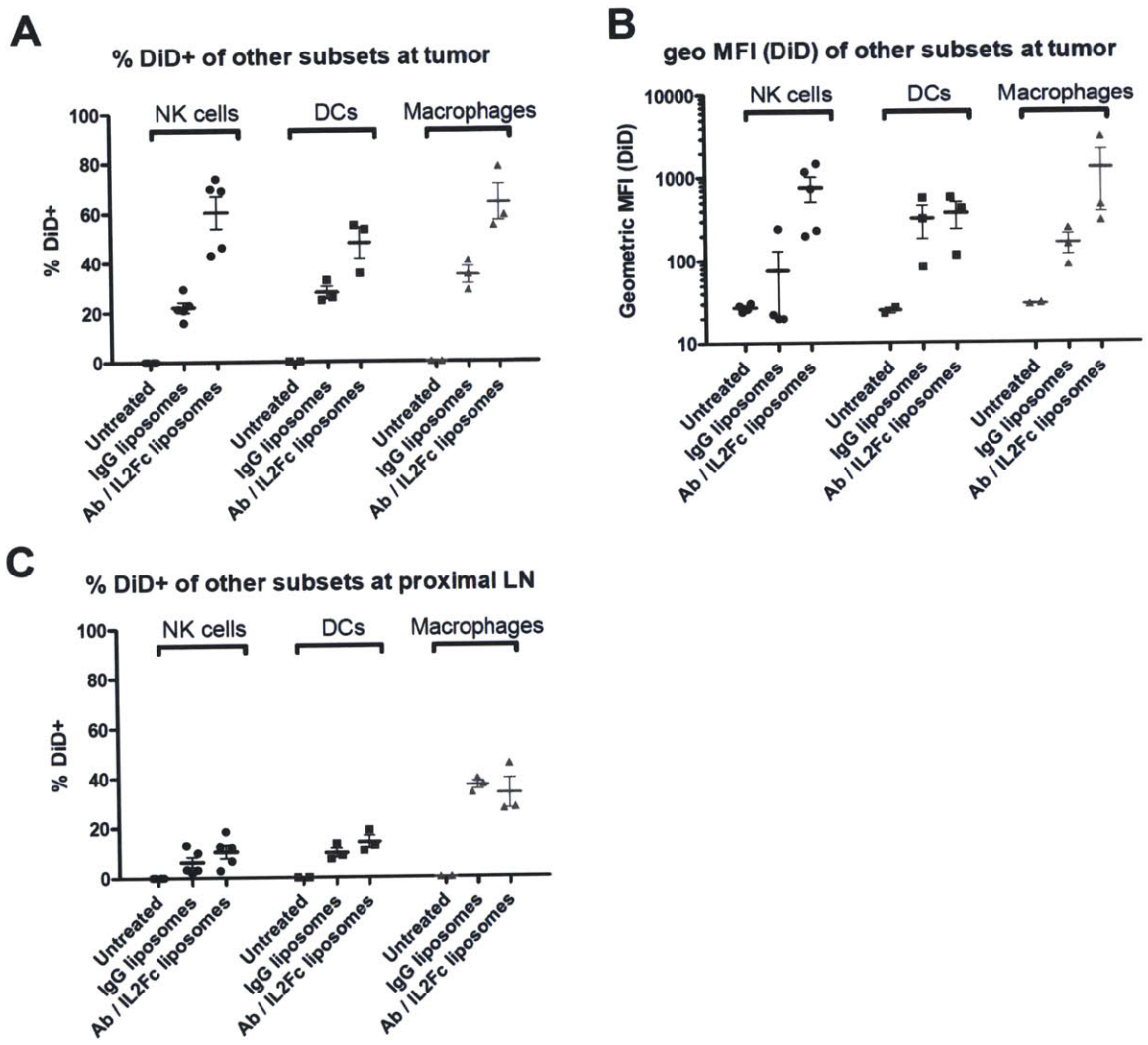

Figure 5.12. Specific binding or non-specific uptake of therapeutic vs. IgG liposomes by NK cells, DCs, and macrophages, at the treated tumor and proximal LN. A) Percentages of tumor-resident NK cells, DCs, and macrophages positive for the fluorescent DiD label incorporated into IgG control or anti-CD137 and IL-2/Fc-coupled liposomes. Mice received intra-tumoral injections of labeled IgG-liposomes or combination therapeutic liposomes on days 10 and 13 (n=3 or 5 per group), and the treated tumors were recovered on days 15 or 16 and analyzed by flow cytometry. B) Geometric mean fluorescent intensity (MFI) of DiD signal on immune subsets recovered from primary treated tumors. Mice received intra-tumoral injections of labeled IgG-liposomes or combination therapeutic liposomes as described for part (a). C) Percentage of NK cells, DCs, and macrophages positive for DiD fluorescence in the tumor-proximal lymph node. Mice received intra-tumoral injections of DiD-labeled IgG-liposomes or combination therapeutic liposomes as described for part (a), and the tumor-draining inguinal lymph node proximal to the treated tumor was excised on days 15 or 16 and analyzed by flow cytometry.

5.4.7. Changing the balance of tumor-infiltrating leukocyte populations via intra-tumoral liposome-coupled anti-CD137 + IL-2/Fc therapy

While the flow cytometry analysis described above had shown the specificity of liposome targeting, it did not distinguish the exact mechanisms by which tumor progression was either completely halted or transiently inhibited, in the injected or distal tumors respectively. Therefore we analyzed the population levels of various tumor-infiltrating leukocytes in either the treated or distal tumors, to elucidate whether anti-CD137 + IL-2/Fc liposome therapy had successfully skewed the tumor environment from a tumor-induced immuno-suppressive phenotype towards an immune-activated, tumor-inhibitory balance.

Since anti-CD137 and IL-2 are known to stimulate the activation and proliferation of $CD8^+$ CTLs, we first investigated whether the level of CTL infiltration was enhanced following liposome-coupled therapy. The infiltration of CTLs into solid tumors has been shown to correlate with improved overall prognosis, in both pre-clinical tumor models and human patients. Tumors were inoculated on both flanks of mice, and therapeutic or IgG-coupled liposomes were injected intra-tumorally on days 10 and 13, followed by the analysis of excised tumor tissues by flow cytometry on days 15 or 16. As shown in Figure 5.13a, the intra-tumoral administration of anti-CD137 + IL-2/Fc liposomes induced a dramatic increase in the concentration of $CD8^+$ T cells (normalized to the total tumor volume) within the treated tumor by day 15 or 16, reaching a mean level of 1100±260 CTLs per mm^3 of tumor. This increase in CTL density within the therapeutically treated tumors correlated with the strong inhibition of tumor growth, as we had previously shown in Figure 5.4 (Chapter 5.4.3). In contrast, the injection of control IgG-coupled liposomes had no observable effect on $CD8^+$ CTL infiltration, yielding a mean level of only 90±55 CTLs/mm^3 tumor, which was not a statistically significant increase above the mean level

of CTLs (74±27 cells/mm^3 tumor) in non-injected mice (Figure 5.13a). Correspondingly, IgG-treated tumors progressed at a rapid rate similar to untreated mice. Clearly, this illustrated that the liposome-coupled anti-CD137 + IL-2/Fc therapy had primed a potent tumor-specific CTL response, at least at the locally injected tumor. Whether the increased concentration of CTLs in treated tumors was a result of enhanced tumor infiltration by CTLs, increased proliferation of CTLs already present within the tumor (which might previously have been impaired or tolerized), or a combination of both mechanisms, was not explicitly determined.

A slight increase in CTL levels was also observed in the distal tumors of therapeutic liposome-treated mice (Figure 5.13a), up to a mean of 640±300 CTLs/mm^3 tumor. Although this did not represent a statistically significant increase above the CTL levels measured in non-injected or IgG-treated mice ($p=0.089$ by unpaired t-test, Figure 5.13a), it appeared to correlate with a modest inhibition of tumor progression, consistent with the results obtained previously in our simultaneous 2-tumor therapy experiments (Figure 5.8, Chapter 5.4.4). The high degree of variability in CTL levels at the distal tumors of individual mice might account for the similar amount of variability observed in the therapeutic inhibition of distal tumor growths (Figure 5.8b). Since no amount of fluorescent labeled liposomes was observed attached to these CTLs at the distal tumor (Figure 5.11a), and we had previously established that liposome-delivered intra-tumoral therapies could not directly access the distal tumor, it is unlikely that increases in CTL levels at the distal tumor of therapeutically treated mice was the direct result of proliferation by CTLs already resident in that tumor. Instead, these results suggested that a tumor-specific adaptive immune response had in fact been successfully primed at the primary treated tumor and/or its tumor-proximal lymph node, and had subsequently disseminated systemically in order to target and attack distal tumor growths, as per our initial hypothesis (Chapter 5.4.4).

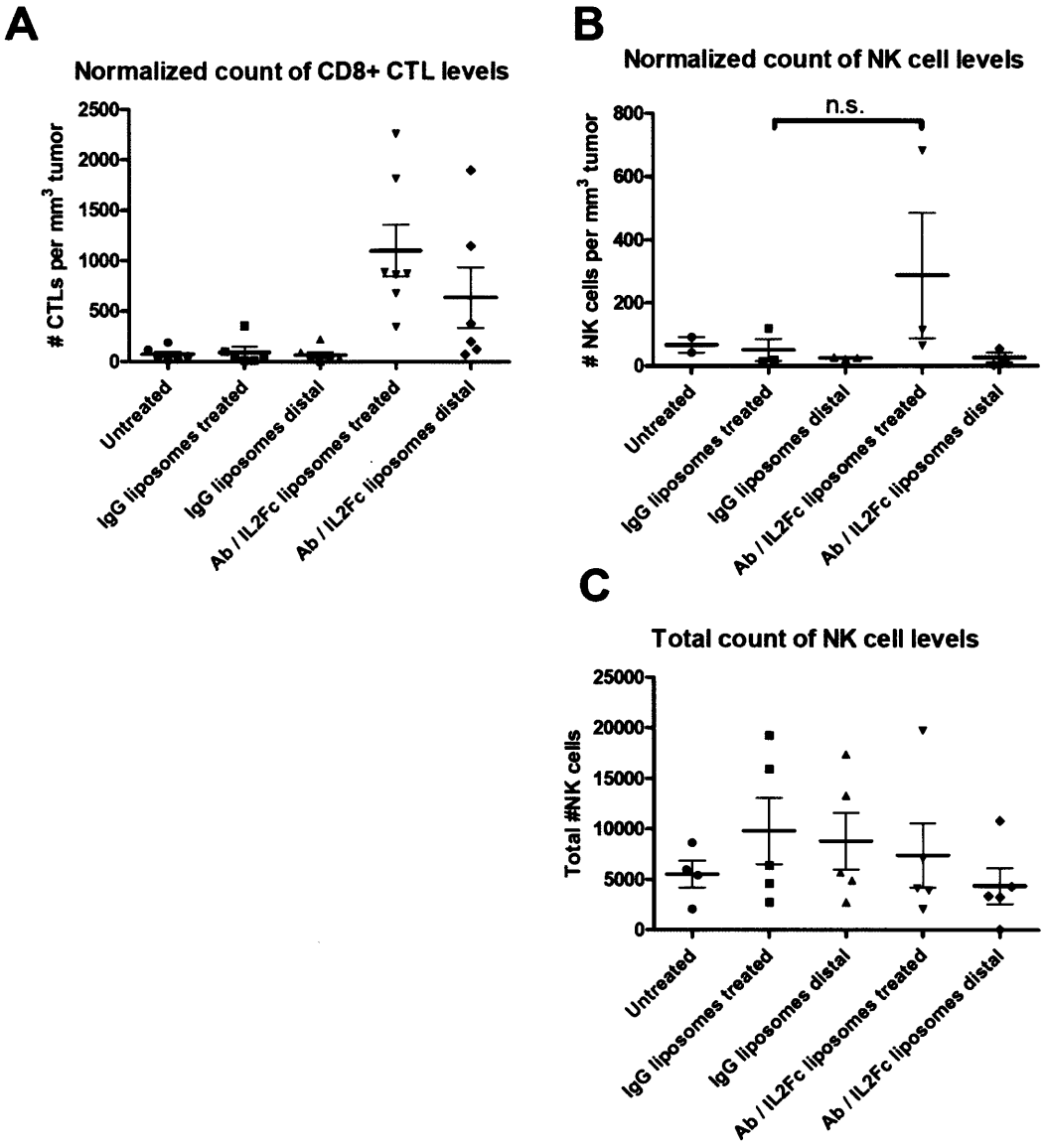

Figure 5.13. Liposome-coupled anti-CD137 + IL-2/Fc therapy induced an increase in tumor-infiltrating CTLs, but not NK cells, at the treated and distal tumors. A) Tumor-infiltrating levels of CD8+ CTLs in response to liposome-coupled anti-CD137 + IL-2/Fc therapy. Mice bearing 2 simultaneous tumors received intra-tumoral injections of IgG-coupled liposomes or combination of anti-CD137 + IL-2/Fc-coupled liposomes in one tumor only, on days 10 and 13 (n=5 to 7 per group); treated and distal tumors were then harvested on day 15 or 16 for flow cytometry analysis. CD8+ CTL counts were normalized to the tumor volume measured at the time of excision. B,C) Tumor-infiltrating levels of NK cells in response to liposome-coupled anti-CD137 + IL-2/Fc therapy. Mice bearing 2 simultaneous tumors were treated intra-tumorally in one tumor on days 10 and 13 as described for part (a) (n=3 or 5 per group), then analyzed on day 15 or 16. NK cell counts are plotted as the total number recovered in excised tumors (B), or normalized to the tumor volume at excision (C).

As previously discussed in Chapters 5.2.2 and 5.2.4, anti-CD137 and IL-2 therapies have also been shown to target NK cells, resulting in increased proliferation and anti-tumor effector functions. Therefore, we performed a similar analysis on the infiltrating levels of NK cells at day 15, following 2 doses of liposome-delivered therapy on days 10 and 13. As shown in Figures 5.13b-c, anti-CD137 + IL-2/Fc liposome therapy did not significantly enhance the infiltrating levels of NK cells in either the treated or distal tumors (with the exception of a single outlier), compared to non-injected or IgG-liposome treated mice ($p=0.3$ by unpaired t-test). Even though the bio-distribution analysis of fluorescently labeled liposomes had shown that anti-CD137 and IL-2/Fc-coupled liposomes could bind to NK cells already present at the treated tumor (Figure 5.12a), there was no apparent stimulation of NK cell proliferation or increased recruitment into the tumor tissue. Nevertheless, these results do not rule out the possibility that anti-CD137 and IL-2/Fc liposome therapy had affected the functional phenotype of tumor-resident NK cells, thereby inducing a more potent level of anti-tumor activity.

A common characteristic of tumor-induced immunosuppression is the substantial recruitment and infiltration of regulatory T cells (Tregs), which can hamper or induce the tolerization of a variety of different immune effector cells.[2,146,198] Moreover, the depletion of Tregs has been shown to induce potent tumor inhibition or regression, specifically in the B16 tumor model as well as in other murine tumors.[136,138,139,159] To investigate whether our strategy of liposome-coupled anti-CD137 + IL-2/Fc therapy had succeeded in counteracting tumor-induced immunosuppressive mechanisms, we quantified the tumor-infiltrating levels of Tregs by flow cytometry on day 16 post-inoculation, following intra-tumoral therapeutic-liposome or IgG-liposome treatments on days 10 and 13 as before. Figure 5.14a shows the absolute counts of Tregs ($CD4^+Foxp3^+$ cells) isolated from the treated or distal tumors. Anti-CD137 + IL-2/Fc

liposome therapy caused an enormous reduction in total Treg levels within the treated tumor, with a mean level of 720 ± 130 Tregs per tumor, compared to 24,000 ± 7000 Tregs in IgG-treated tumors and 25,000 ± 7000 Tregs in non-injected mice. As expected, this dramatic decrease in Treg levels correlated with the potent inhibition of primary tumor progression in therapeutically treated mice, while the elevated levels of Tregs in IgG-treated or non-injected mice correlated with continual tumor progression. Interestingly, no significant reductions in Treg levels were observed in the distal tumors of therapeutically treated mice (Figure 5.14a, mean count 23,000 ± 7000 Tregs). This finding is consistent with our previous analyses indicating that locally injected liposome therapies were restricted from systemic draining and thus could not directly access the distal tumor. As a result, this suggested that liposome-coupled therapies administered intra-tumorally at the primary tumor were unable to impact the immuno-suppressive environment already established at the distal tumor.

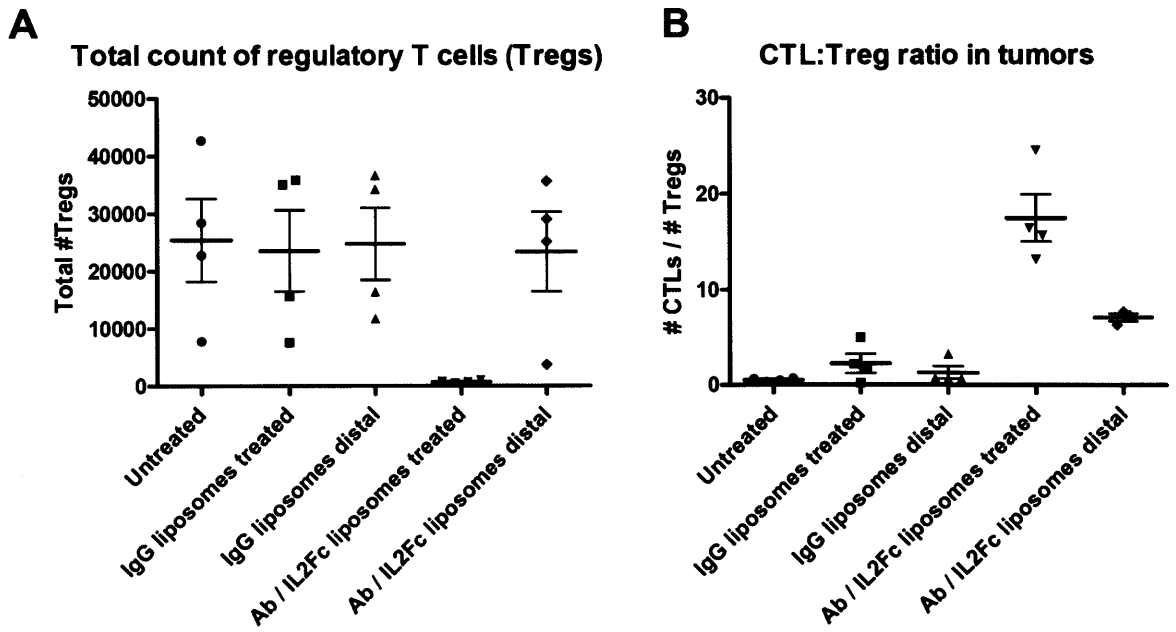

Figure 5.14. Reduced infiltration of regulatory T cells and the overall priming of increased CTL:Treg ratios in therapeutic liposome-treated tumors. A) Tumor-infiltrating levels of regulatory T cells (Tregs) following intra-tumoral therapy with control IgG-liposomes or

combination anti-CD137 + IL-2/Fc liposomes (n=4 per group). Mice bearing 2 simultaneous tumors were injected at one tumor only on days 10 and 13, and the treated and distal tumors were excised for flow cytometry analysis on day 16. Tregs were defined by CD4+Foxp3+ expression, via intracellular staining. Total Treg counts recovered from the excised tumors are plotted. B) Ratio of tumor-infiltrating counts of CTLs to Treg cells following liposome-coupled anti-CD137 + IL-2/Fc therapy, as a measure of the immuno-activatory versus immuno-suppressive balance in the tumor environment. Mice were treated intra-tumorally as described in part (a), and the treated and distal tumors were excised on day 16 for flow cytometry measurement of Treg and CTL counts.

By combining our analyses of the tumor-infiltrating levels of CTLs (Figure 5.13a) and regulatory T cells, a plot of CTL:Treg ratios (by total cell count) was then constructed to provide an overall measure of the balance of immune-activating versus immunosuppressive mechanisms in the tumor environment. As shown in Figure 5.14b, intra-tumoral therapy using liposome-coupled anti-CD137 + IL-2/Fc primed a substantial increase of the CTL:Treg ratio (mean of 17.4±2.5) at the treated tumor, indicating a dramatic shift in the balance of tumor-infiltrating lymphocytes towards an activated immune response. This represented a statistically significant increase compared to the CTL:Treg ratios measured in either IgG-treated tumors or non-injected mice (Figure 5.14b). In the distal tumors of therapeutically treated mice, the CTL:Treg ratio was also significantly enhanced (mean ratio of 7.1±0.4) compared to IgG-treated tumors or untreated mice. This immune priming effect, however, was not as potent as in primary therapeutically-treated tumors, since only an increase in CTLs was observed in the distal tumors without a concurrent decrease in Tregs. Overall, these trends matched the therapeutic results previously observed in the local liposome-coupled treatment of mice bearing 2 simultaneous tumors (Figure 5.8): the highly potent skewing of TIL phenotypes towards immune activation in primary treated tumors correlated with significant tumor inhibition and completely curative responses, while the comparatively modest shift of TIL phenotypes in distal tumors led to more moderate and inconsistent levels of tumor growth inhibition.

5.4.8. CD8 and NK cell depletion studies to elucidate mechanisms of effective anti-CD137 + IL-2/Fc liposome therapy

The analyses of liposome bio-distribution *in vivo* (Chapter 5.4.6) and the changes in tumor-infiltrating leukocyte (TIL) populations (Chapter 5.4.7) had implicated $CD8^+$ CTLs as the principal immune effectors involved in the anti-tumor response following anti-CD137 + IL-2/Fc liposome therapy. In order to conclusively demonstrate the priming of a CTL-mediated response, depletion studies were performed to test the therapeutic efficacy of liposome-delivered anti-CD137 and IL-2/Fc on both treated and distal tumors, in the absence of $CD8^+$ T cells. Additionally, since previous reports have described the stimulation of NK cells via anti-CD137 and IL-2 therapy,[167,197,199] and our distribution analysis had shown the binding of therapeutic liposomes to tumor-resident NK cells, the efficacy of liposome-delivered therapy was also examined in mice depleted of NK cells. The depletions of these two respective subsets was carried out by the systemic (intraperitoneal) administration of anti-CD8a or anti-NK1.1 antibodies on days 7/12/16, thus encompassing the start of anti-tumor liposome-coupled therapy and continuing throughout the course of the therapeutic regimen (intra-tumoral liposomes on days 9/12/16, as described in Chapter 5.3.4). Validation of the depletion schedule had previously been performed (refer to Chapter 4.4.4), ensuring >98% depletion of the targeted population in lymphoid organs, systemic circulation, as well as peripheral tissues such as subcutaneous tumors.

Figure 5.15a shows the individual tumor growths in mice depleted of CD8-expressing cells, while Figures 5.15c and 5.15d contain the average growth rates of treated and distal tumors respectively, with or without subset depletion. In the absence of any intra-tumoral liposome therapy, tumor growths in CD8-depleted mice progressed as rapidly as in non-depleted mice, indicating that the depletion regimen did not have any intrinsic effects on the growth of B16

tumors (refer to Figure 5.4a for comparison). Notably, when CD8-depleted mice were treated with liposome-coupled anti-CD137 + IL-2/Fc, both the treated tumors and distal tumors continued to rapidly progress, at nearly the same rate as in control, non-treated mice (Figures 5.15a,c,d). Only a slight delay in tumor progression was observed at the treated tumor in CD8-depleted mice, without any long-term curative responses. This dramatic loss in therapeutic efficacy convincingly demonstrated the absolute requirement for $CD8^+$ T cells, in mediating the anti-tumor immune response primed by local anti-CD137 + IL-2/Fc liposome-coupled therapy.

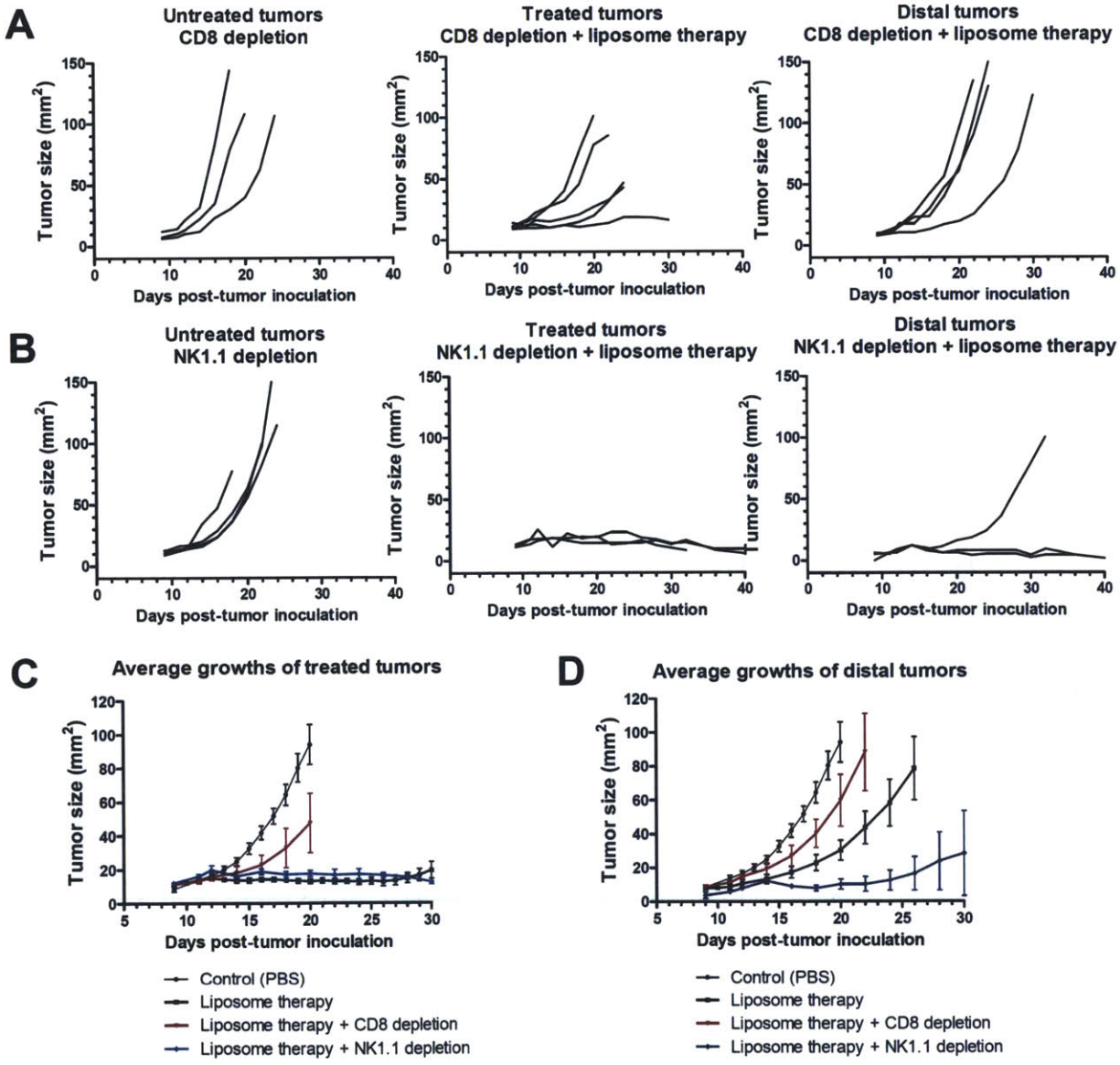

Figure 5.15. Requirement for $CD8^+$ CTLs, but not NK cells, in the priming of an effective anti-tumor immune response via liposome-coupled anti-CD137 + IL-2/Fc therapy. A,B) Individual tumor growths (n=3 to 5 per group) in CD8-depleted mice (A) or NK1.1-depleted mice (B), bearing 2 simultaneous tumors. Mice received depleting antibodies prior to the start of therapy, and continuing through the treatment regimen. Intra-tumoral injections were administered on days 9/12/16 in one tumor only, consisting of PBS control (left panels) or anti-CD137 + IL-2/Fc-coupled liposomes (middle and right panels, showing the primary treated tumor and distal tumor respectively). C) Average tumor growths on the primary liposome-treated flank of non-depleted mice (thick black line), CD8-depleted mice (red line), or NK1.1-depleted mice (blue line) (n=3 to 5 per group). Mice bearing 2 tumors were intra-tumorally treated on one flank as described for parts a-b. Control mice (thin black line) received neither immunotherapy nor any depletion regimen. D) Average tumor growths on the distal untreated flank of non-depleted mice (thick black line), CD8-depleted mice (red), or NK1.1-depleted mice (blue), corresponding to the liposome-treated mice shown in part (c).

In complete contrast to the lack of therapeutic responses observed in CD8-depleted mice, no loss of efficacy was detected in NK-depleted mice compared to non-depleted mice following liposome-anchored anti-CD137 + IL-2/Fc therapy, as shown in Figures 5.15b-d. In this particular experiment, all 3 of the treated tumors in NK-depleted mice exhibited durable complete cures, while distal tumors were also either significantly inhibited or completely rejected (Figure 5.15b). Control NK-depleted mice that did not receive any liposome therapy showed rapid tumor progression as expected. Therefore, the therapeutic response following liposome-coupled immunotherapy in NK-depleted mice was at least as potent as the anti-tumor responses primed by the treatment of non-depleted mice (Figure 5.15c,d), demonstrating that NK cells were not an essential component in the priming of anti-tumor immunity by anti-CD137 + IL-2/Fc liposomes. In fact, there even appeared to be a slight enhancement in the inhibition of the distal tumor in NK-depleted mice (n=3) compared to non-depleted mice (averages shown in Figure 5.15d), although conclusively determining whether or not this was a real phenomenon will require this experiment to be repeated using larger groups of mice. We speculated that even though therapeutic liposomes had bound to tumor-resident NK cells at a high level following

intra-tumoral delivery (Figure 5.12), the relatively low number of NK cells compared to tumor-infiltrating CTLs might explain the insignificance of NK-mediated effects in the overall anti-tumor response. Taken together, the results of lipsosome-coupled anti-CD137 + IL-2/Fc therapy in either CD8-depleted or NK-depleted mice clearly illustrated that a CTL-mediated response was required for effective local and distal tumor inhibition, consistent with our hypothesis of a locally primed adaptive immune response leading to the systemic dissemination of potent anti-tumor immunity.

5.5. Summary and Conclusions

The third aim of this thesis focused on the optimization and characterization of a highly potent combination of liposome-delivered therapy, for the local treatment of established B16 tumors in mice. By adapting the liposome-coupled delivery strategy previously developed in the first two sections of this study (Chapters 3-4), a combination of anti-CD137-liposomes and IL-2/Fc-liposomes was administered via intra-tumoral injection to induce the priming of local, systemic, and memory anti-tumor immunity. Anti-CD137 + IL-2/Fc liposome therapy stimulated the potent inhibition of primary treated tumors, including durable complete cures in the majority of mice, while significantly delaying the progression of simultaneous distal tumors as well. Secondary tumor re-challenges were also rejected in 100% of liposome-treated mice, confirming the priming of protective anti-tumor immunity that persisted for at least 8 weeks. Importantly, systemic exposure to these potent immuno-agonists and the associated inflammatory toxicities were minimized by the use of liposome-coupled delivery, enabling the spatially restricted administration of therapeutic dosages that proved to be severely toxic and even lethal when injected in freely soluble form, despite being administered intra-tumorally.

A series of mechanistic experiments was conducted to elucidate the primary effectors of the activated anti-tumor immune response. Given the apparent ability of the locally primed anti-tumor response to target either simultaneous or secondary distal tumors, we speculated that anti-CD137 + IL-2/Fc therapy had primarily activated a CTL-mediated adaptive immune response. Although anti-CD137-liposomes and IL-2/Fc-liposomes were observed to bind to both $CD8^+$ CTLs and NK cells within the primary treated tumor, subsequent depletion studies confirmed that only CTLs were essential for the efficacy of this therapy, at both the treated and distal tumors. Furthermore, analysis of tumor-infiltrating immunological populations showed that the local liposome delivery of anti-CD137 and IL-2/Fc resulted in significantly elevated levels of CTLs while reducing levels of Tregs in primary treated tumors, consistent with the highly potent inhibition of tumor growth. On the other hand, distal tumors exhibited more modest and variable increases in CTL levels and no detectable decrease in Treg levels, and therefore achieved only moderate delays in tumor progression. Nevertheless, these combined results successfully proved our hypothesis that the use of liposome-anchored anti-CD137 and IL-2, two immunomodulatory agents that directly target and stimulate CTLs, would be capable of generating a stronger adaptive immune response against B16 tumors than the previous regimen of anti-CD40/CpG liposome therapy.

In the greater context of translating liposome-delivered immunotherapies into a clinical setting, the anti-tumor responses and minimal toxicity achieved here via the combination of anti-CD137 + IL-2/Fc liposomes illustrated that local liposome-coupled delivery can actually provide a significantly broader therapeutic window than the direct injection of soluble agents. By simply applying the previously established strategy of liposome surface coupling to these two highly potent immunotherapeutics, we also demonstrated the versatility of such a strategy in general, for

the delivery of any antibody or protein therapeutic against cancer. Given the wide range of immunostimulatory agonists currently being tested in pre-clinical and clinical phase trials, the therapeutic liposome conjugation strategy described in this chapter represents a promising tool that could be used to substantially improve the clinical prospects and applicability of many such compounds.

CHAPTER 6: Overall Conclusions and Future Outlook

6.1. Ongoing and future studies

Certain analyses of the immunological mechanisms of the anti-tumor response remain ongoing. For example, a complete understanding of the mechanism by which distal tumor growth is inhibited by local liposome-coupled anti-CD137 + IL-2/Fc therapy has not yet been attained. It is possible that tumor antigen-specific CTLs that have been activated by local therapy are able to migrate from the primary treated tumor and home to the distal tumor site to enact a cytotoxic response. Alternatively, *de novo* tumor-specific CTL effectors capable of accessing the distal tumor may have been primed at the tumor-draining lymph node on the treated flank, due to an increase in tumor antigen release from the treated tumor and/or the enhanced activation of tumor antigen-bearing APCs, following liposome-delivered immunotherapy. In addition, the ability of primary treated mice to completely reject a distal secondary tumor challenge at both 11 and 39 days post-therapy (days 27 and 55 in total) implies the long-lived persistence of tumor-specific CTLs that are capable of targeting and destroying a new tumor inoculation in peripheral tissues. Whether these CTLs are of a central memory or effector memory phenotype (i.e. whether they remain circulating, peripherally located, or lymphoid-resident) has not yet been determined. Obtaining a fuller understanding of the mechanisms for distal or secondary tumor inhibition might enable further improvements or optimization of the therapeutic regimen, in order to achieve a consistent rejection of multiple disseminated tumors.

The tumor antigen specificity of the CTL-mediated response following anti-CD137 + IL-2/Fc therapy has also not been examined. For instance, peptide-specific tetramer staining of CTLs

following liposome-coupled immunotherapy could be used to determine the breadth of the anti-tumor immune response. An analysis of the CTL responses in individual treated mice might illustrate differences between mice that successfully attained complete cures of the primary tumor (representing the majority of anti-CD137 + IL-2/Fc treated mice) or even complete cures of the simultaneous distal tumor, compared to mice that eventually succumbed to primary tumor progression in a delayed fashion. In turn, this could illuminate whether antigenic variation in the primary tumor might be responsible for the long-term immune evasion observed in this minority of liposome-treated mice that displayed sub-optimal therapeutic efficacy.

Finally, the liposome-coupled delivery strategy described in this thesis has only been tested in subcutaneously implanted B16 tumors to date. If the local and systemic therapeutic potency of this strategy could be shown in additional murine tumor models, it would convincingly demonstrate the broad applicability of this delivery for clinical translation. While the use of anti-CD137 and IL-2 may not necessarily provide the maximal level of efficacy in other pre-clinical tumor models or in clinical human patients, additional immunotherapeutic agents (such as anti-CTLA-4, anti-PD-1, IL-12, IL-15, and many others) could be tested either in addition to, or in place of these agonists, given the versatility of the reaction scheme and the liposome carrier described here. Conventional cancer treatment modalities such as chemotherapy, local radiation, and surgical intervention could also be investigated in combination with the liposome-coupled delivery of potent immunotherapy, as a potential strategy to treat well-established, large bulky tumor lesions in either ectopic or orthotopic models of cancer.

6.2. General conclusions and scope of thesis

The overall objective of this study was to develop and characterize a nanoparticle-based delivery strategy, as a conceptual framework for the local administration of immunostimulatory agents in the treatment of established solid tumors. Over the course of this thesis, we have demonstrated the use of a versatile and reproducible conjugation technique for the stable coupling of multiple immuno-agonists to polymeric and liposomal nanoparticles; we have validated the local sequestration of nanoparticle-delivered therapeutic agents following intra-tumoral administration *in vivo*, enabling the minimization of systemic exposure and elimination of inflammatory toxicities; and we have achieved the successful priming of highly potent local and systemic anti-tumor immune responses via this nanoparticle-mediated therapeutic strategy. Although there are already a wide variety of immunomodulatory antibodies and cytokine therapies being investigated in pre-clinical and clinical studies, a common obstacle to their clinical translation remains the frequent induction of significant dose-limiting toxicities, resulting in a narrow or completely ineffective therapeutic window for treatment. Thus, the liposome-coupled delivery method that was developed and optimized in this thesis represents a generalizable strategy that could potentially improve the clinical applicability of many such therapies for cancer treatment.

In the clinical patient setting, accessible solid tumors are most likely to be resected or treated with local radiation, while the use of immunomodulatory agents usually represents either a neo-adjuvant therapy or post-surgical treatment to combat minimal residual disease. However, a major unmet need in many types of human cancers is the capability to diagnose, treat, and/or prevent tumor recurrences and metastatic outgrowths. Therefore, an essential consideration for the clinical translation of any cancer immunotherapy is the ability to target secondary or distal

sites of tumor growth, via the systemic dissemination and durable persistence of an adaptive, tumor-specific immune response. In this current study, our initial formulation of liposome-coupled, combinatorial anti-CD40+CpG therapy did not consistently induce an effective level of systemic anti-tumor immunity, despite having achieved the potent local inhibition of primary treated tumors. This motivated the switch to the delivery of anti-CD137 and IL-2 combination therapy, which was subsequently found to be highly successful in controlling or rejecting the growths of primary tumors, secondary tumor challenges, and simultaneous distal untreated tumors. Notably, these therapeutic results were attained using the highly aggressive, poorly immunogenic B16F10 melanoma model, which does not express any foreign (non-murine) or transduced antigens that could be targeted more easily by an endogenous immune response in these mice. As such, the use of the B16F10 tumor model mimics the clinical setting of many types of human cancers that similarly lack the expression of non-self-antigens, and are thus extremely challenging to target via tumor-specific immune responses. Nevertheless, the ability of liposome-coupled anti-CD137 + IL-2 combination therapy to induce such effective anti-tumor responses in the current study illustrates that the administration of potent immunostimulatory agents remains a highly promising strategy for cancer therapy, if accompanied by an appropriate delivery method for the reduction of associated toxicities.

In a broader sense, the developments and results described in this thesis represent an amalgamation of engineering principles with a highly relevant, clinically-targeted biological outcome. The design, *in vitro* and *in vivo* characterizations, and optimization of the liposome-mediated delivery strategy were carried out systematically in order to attain the desired therapeutic results, followed by detailed mechanistic analyses of the observed biological responses. Taken together, a strong understanding of both the immunological and biomaterial-

associated aspects of this project was developed, laying the foundation for further improvements to the clinical applicability of this work.

APPENDICES

Appendix 1: Structure and sequence of IL-2/Fc fusion protein (DNA plasmid donated by Annie Gai, laboratory of Dane Wittrup, MIT)

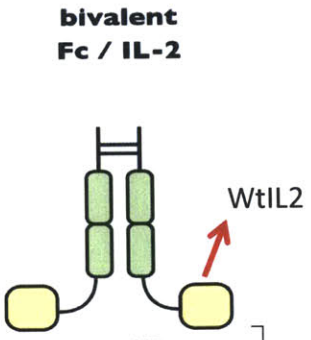

Total Number of Residues: 397
M.W.:44783 g/mol (one strand; bivalent around 90 kDa)
Extinction Coefficient (Secreted Protein): 38555 cm^{-1} M^{-1}
Extinction Coefficient (Cytosolic Protein): 37930 cm^{-1} M^{-1}

Fc D265A mutation:
No interaction with low affinity IgG Fc receptor (FcγRIIB, FcγRIII)

Ala	19	Asx	0	Cys	10	Asp	19
Glu	25	Phe	16	Gly	15	His	14
Ile	16	Lys	22	Leu	37	Met	9
Asn	15	Pro	28	Gln	30	Arg	17
Ser	36	The	28	Val	29	Trp	5
Tyr	7	Glx	0				

Peptide Sequence:

EPRVPITQNPCPPLKECPPCAAPDLLGGPSVFIFPPKIKDVLMISLSPMVTCVVVAVSEDDPDVQISWFVNNVEVHT
AQTQTHREDYNSTLRVVSALPIQHQDWMSGKEFKCKVNNRALPSPIEKTISKPRGPVRAPQVYVLPPPAEEMTKKEF
SLTCMITGFLPAEIAVDWTSNGRTEQNYKNTATVLDSDGSYFMYSKLRVQKSTWERGSLFACSVVHEGLHNHLTTKT
ISRSLGKGGGSAPTSSSTSSSTAEAQQQQQQQQQQQQHLEQLLMDLQELLSRMENYRNLKLPRMLTFKFYLPKQATE
LKDLQCLEDELGPLRHVLDLTQSKSFQLEDAENFISNIRVTVVKLKGSDNTFECQFDDESATVVDFLRRWIAFCQSI
ISTSPQHHHHHH

DNA sequence:

gWIZ - D265A Fc - wt IL2
.....CTGCAG - human LC leader - D265A mIgG2a Fc - GGGS linker - wt mIL2 - HHHHHH tag - STOP - CAGCTG.....

ATGAGGGTCCCCGCTCAGCTCCTGGGGCTCCTGCTGCTCTGGCTCCCAGGTGCACGATGTGAGCCCAGAGTGCCCATAACACAGAA
CCCCTGTCCTCCACTCAAAGAGTGTCCCCCATGCGCAGCTCCAGACCTCTTGGGTGGACCATCCGTCTTCATCTTCCCTCCAAAGA
TCAAGGATGTACTCATGATCTCCCTGAGCCCCATGGTCACATGTGTGGTGGTGGCCGTGAGCGAGGATGACCCAGACGTCCAGATC
AGCTGGTTTGTGAACAACGTGGAAGTACACACAGCTCAGACACAAACCCATAGAGAGGATTACAACAGTACTCTCCGGGTGGTCAG
TGCCCTCCCCATCCAGCACCAGGACTGGATGAGTGGCAAGGAGTTCAAATGCAAGGTCAACAACAGAGCCCTCCCATCCCCCATCG
AGAAAACCATCTCAAAACCCAGAGGGCCAGTAAGAGCTCCACAGGTATATGTCTTGCCTCCACCAGCAGAAGAGATGACTAAGAAA
GAGTTCAGTCTGACCTGCATGATCACAGGCTTCTTACCTGCCGAAATTGCTGTGGACTGGACCAGCAATGGGCGTACAGAGCAAAA
CTACAAGAACACCGCAACAGTCCTGGACTCTGATGGTTCTTACTTCATGTACAGCAAGCTCAGAGTACAAAAGAGCACTTGGGAAA
GAGGAAGTCTTTTCGCCTGCTCAGTGGTCCACGAGGGTCTGCACAATCACCTTACGACTAAGACCATCTCCCGGTCTCTGGGTAAA
GGAGGGGGCTCCGCACCCACTTCAAGCTCCACTTCAAGCTCTACAGCGGAAGCACAGCAGCAGCAGCAGCAGCAGCAGCAGCA
GCAGCACCTGGAGCAGCTGTTGATGGACCTACAGGAGCTCCTGAGCAGGATGGAGAATTACAGGAACCTGAAACTCCCCAGGATGC
TCACCTTCAAATTTTACTTGCCCAAGCAGGCCACAGAATTGAAAGATCTTCAGTGCCTAGAAGATGAACTTGGACCTCTGCGGCAT
GTTCTGGATTTGACTCAAAGCAAAAGCTTTCAATTGGAAGATGCTGAGAATTTCATCAGCAATATCAGAGTAACTGTTGTAAAACT
AAAGGGCTCTGACAACACATTTGAGTGCCAATTCGATGATGAGTCAGCAACTGTGGTGGACTTTCTGAGGAGATGGATAGCCTTCT
GTCAAAGCATCATCTCAACAAGCCCTCAACACCATCACCACCATCACTGATAA

Appendix 2: Selected experimental protocols

A2-1. Cell culture protocols

a) B16F10 cell culture and tumor inoculation:

Source: ATCC
Culture media: High-glucose DMEM, supplemented with 10% FCS and Pen/Strep.

Cell culture:
Cells were cultured in $25cm^2$ or $75cm^2$ tissue culture flasks, and split every 2-3 days. To passage cultures, cells were rinsed with serum-free medium, then incubated with Trypsin/EDTA until all adherent cells had detached. Cells were washed once in complete DMEM, then re-plated at a dilution of approximately 1:10 to 1:15.

Tumor inoculation:
Cells were detached from culture flasks, and washed once in complete DMEM. Cells were then washed 3x in serum-free HBSS, prior to counting and final re-suspension in HBSS at ~$0.5x10^6$ cells/ml. For each tumor inoculum, 50000 cells were used, or ~100µl of cell suspension.
Mice were shaved prior to the preparation of tumor cells, to minimize the time of cells being kept on ice before injection. Subcutaneous injections were performed in the lower back/hind flank region, on either side or on both sides, as indicated for various experiments.

b) HEK293-Freestyle cell transfection for IL-2/Fc production:

Source: Invitrogen, via Wittrup Laboratory
Culture media: 293 Freestyle medium (Invitrogen), no supplement required.

Cell culture:
Cells were cultured in round-bottom TC flasks, on shaker in incubator, and split every 2-3 days, when cell density reached ~1-$2x10^6$ cells/ml. Media was pre-warmed, then cells were diluted into fresh media to ~$0.4x10^6$ cells/ml.

IL-2/Fc plasmid transfection into 293F cells:

1. Count and dilute 500 million cells, to concentration of 1 million cells/ml. Transfer to large 2L roller bottle (pink cap), max 500ml per bottle. Make sure if you lay the bottle on its side, the media inside isn't enough to reach the filter on the cap.
2. Warm up 20ml of Opti-Pro serum-free transfection medium to room temp. Thaw out PEI
3. Add 1ml of PEI to 9ml of Opti-Pro media. Mix gently, sit at room temp for 10min.
4. Meanwhile, add 0.5mg of IL-2 DNA plasmid to 10ml of Opti-Pro media. Mix gently. Sterile-filter using syringe filter, but don't use needle.
5. Add DNA to PEI, mix gently, sit at room temp another 10min.
6. Add DNA/PEI mixture dropwise (20ml total volume) to the batch of 500 million cells. Swirl bottle around while adding, for immediate mixing.
7. Incubate in incubator, flat on a roller, for 7 days, for IL-2 production.

IL-2/Fc recovery and purification:

1. After 7 days of roller culture, centrifuge entire volume 15min at 1600rpm, 4degC, to pellet out the cells.
2. Sterile-filter the supernatant by pouring through bottle-top vacuum filter, in TC hood.
3. Add 1/10th volume of sterile 10x PBS, to the recovered SN (e.g. 50ml of 10x PBS to one batch of 500ml culture supernatant). This is to equilibrate pH and osmolarity with the purification resin/columns, which are going to be rinsed with 1x PBS. Supernatant can be stored at 4C, up to a couple of weeks, if not doing column purification immediately.
4. Prepare columns with 3-4ml of protein A-linked agarose bead resin (Millipore).
5. Rinse columns 3-4x with 25-30ml of 1x PBS.
6. Gently add the culture supernatant, and try to minimize disturbing the beads at the bottom of the column. After filling column, let sit 5-10 min to let beads settle a bit, before opening valve to start flowthrough.
7. Open valve very slightly to allow liquid to drip through slowly.
8. Take flow-through and repeat passage through column one more time.
9. Rinse columns with 25-30ml of 1x PBS. (pre-elution rinse)
10. Add 30ml of IgG elution buffer (Pierce) to each column. Let beads settle 5-10min, then allow flow-through. This elution should contain the purified IL-2/Fc.
11. Rinse columns again with 25-30ml of 1x PBS. (post-elution rinse)
12. Meanwhile, add 3-4ml of 1M Tris buffer (approx. pH 8), per 30ml of recovered elution volume, to bring pH of the recovered IL-2 back to neutral, then store recovered IL-2 in fridge.
13. After final rinse of columns, add 4ml of PBS + 0.05% NaN3 for storage, then store columns at 4degC.
14. Concentration of IL-2/Fc post-recovery: Rinse 3 or 4 centrifuge spin filter tubes (Amicon, 30kDa MWCO) with 10-12ml PBS, by spinning down 5min at 6000rpm. Remove any PBS that didn't spin through. Add 15ml of recovered IL-2/Fc solution per tube. Spin 20min at 5000rpm, 15degC. Recover concentrated IL-2 solution, which shouldn't spin through (IL-2/Fc construct is above the 30kDa MWCO). Protein tends to stick a bit to the membrane filter, so make sure to pipet up/down a few times against the membrane when recovering the concentrated solution. Repeat until all recovered IL-2/Fc solution has been concentrated.
15. Should be able to concentrate one batch of supernatant (initial 500ml in culture) to about 2.5-4ml final volume, with a final yield of about 6-8mg of total protein (by BCA assay).
16. Once concentration is finished, sterile-filter IL-2/Fc solution using Costar 0.22um membrane filter tubes. Spin 1min at 12000g. Store IL-2/Fc at 4degC, or -80degC for long-term.

c) DH5-alpha bacterial cell transformation for production of IL-2/Fc plasmid:

1. Thaw transformation-competent DH5α cells on ice.
2. Mix ~3ug IL-2/Fc plasmid with 30ul TE buffer.
3. Add 7ul of DNA to 50ul of DH5α cells. Leave on ice for 30min. Heat-shock in 40degC water bath for 42 seconds, then return to ice for 2min.
4. Add 500ul SOC medium and shake at 220pm in 37degC, for 1hr.
5. Plate and streak 10-20ul cells onto 1.5% agar LB with kanamycin (50ug/ml final antibiotic concentration). Incubate plates at 37degC.

6. 18hr post-plating, pick colony and inoculate starter culture in 5ml of LB-kanamycin. After 6-8hr culture (220rpm at 37degC), inoculate batch cultures.
7. After 24hr culture, pellet cells at 7500g for 15min, then discard supernatant.
8. Proceed to DNA plasmid purification from bacterial cell pellets, according to Qiagen Maxi-Prep (Mega/Giga) instructions.

A2-2. Preparation of anti-CD40/CpG liposomes

Anti-CD40: clone FGK4.5 from Bio-X-Cell

1) Liposome preparation:
composition (mol%) = 55/35/5/5
= DOPC/cholesterol/maleimide-PEG2000-DSPE/methoxy-PEG2000-DSPE (Avanti Lipids)

per 5 umol batch of liposomes:
202ul DOPC (10.68mg/ml stock)
680ul cholesterol (1mg/ml stock)
134ul maleimide-PEG2k (5.53mg/ml stock)
280ul empty PEG2k (2.5mg/ml stock)

- Vacuum-dry lipids
- Re-suspend by vortexing in sterile PBS at 15umol/ml. Sonicate with ice bath for ~4-5min at alternating 6-8 Watts.
- Centrifuge at 16000g for 1-2min, to pellet any debris from sonicator tip. Keep supernatant containing liposomes.
- Extrude liposomes (optional). Without extrusion, the sonicated liposomes should already be down to <200nm.
- Use ~2.5umol liposomes per starting mg of antibody to be conjugated.

2) Antibody preparation (recommended for higher efficiency binding):
- Add 1ml PBS into Amicon 10k or 30k MWCO centrifugal filter column, spin through at 5000rpm for 7min to rinse membrane. Use centrifuge at 15-25 degC. Remove any PBS that didn't spin through.
- Add anti-CD40 into column, spin at 5000rpm for 10-12min, collect concentrated Ab solution. Repeat if necessary, until reaching an antibody concentration of 15-20mg/ml.

3) Antibody reduction for free thiols:
- Add EDTA (final concentration of 10mM) to concentrated antibody solution
- Add 10x molar excess of DTT (relative to antibody), or a maximum of 1.8mM DTT (final concentration), and mix by pipetting to minimize air bubbles. Let sit 20-25min at room temp.

4) Mixing reactive antibody with liposomes:
- Simultaneously prepare Zeba desalt columns (7k MWCO, Pierce) by rinsing/spinning 3-4x with 10mM EDTA in PBS (spin 1min at 1000g), and prepare the previously synthesized maleimide-functionalized liposomes by adding EDTA to a final concentration of 10mM.

- When antibody reduction is finished, pass through Zeba column to remove DTT (spin 2min at 1000g).
- Mix reduced Ab immediately with liposomes, allow conjugation to proceed overnight or a minimum of 8 hours.
- Liposome + Ab mixture may turn cloudy (aggregation), if conjugation is happening at high efficiency, but not necessarily. May depend on the antibody/protein being conjugated.

5) Washing and purification:
- After conjugation, wash liposomes 3x with PBS. If liposomes have aggregated visibly, use tabletop centrifuge: spin at 18000g at 4 degC for 5min. Otherwise, if liposomes have not visibly aggregated/precipitated, use the airfuge to pellet liposomes: spin at max speed for 20-30min.
- After washing, re-suspend conjugated liposomes in PBS at about 10umol/ml.

6) Add CpG-lipid conjugate to washed anti-CD40-coupled liposomes:
- Mix approximately 3nmol CpG-lipid (FAM-labeled) per 1umol starting liposome amount. Let sit at room temp for at least 1-2hr.
- Insertion efficiency should be ~80-90%. To wash, pellet liposomes again by tabletop centrifuge (max speed, 5min), and rinse 3x with PBS.
- Re-suspend in PBS in desired volume for injection, ~150ul per ~1umol liposome dose (per mouse).

7) Size re-extrusion of aCD40/CpG liposome aggregates:
- Use 200nm filter membranes to extrude (syringe extrusion, equipment from Avanti Lipids), which results in liposomes that are ~150nm in diameter by DLS.
- If the liposome suspension is concentrated, the liposomes can re-aggregate again after the size extrusion, especially if stored at 4degC.
- If liposomes need to be stored at 4C for a while before injection, recommend doing the size re-extrusion just prior to injection, and then do not put them back in 4degC or into ice, to avoid re-aggregation.
- Alternatively, re-wash the liposomes after storage, before re-extruding, to remove any additional CpG that has leaked off the liposomes (since the CpG is just inserted and not actually conjugated like the antibody). Generally, if stored at 4C in PBS, there should be minimal loss of either the Ab or CpG.

8) Quantification:
- Perform size re-extrusion of anti-CD40/CpG liposomes prior to quantification
- Remove a sample of re-extruded liposomes and dilute 1:10 into PBS + 1% BSA, followed by additional dilution 1:100 into PBS + 0.5% Tween 20, for liposome disruption.
- Measure the solubilized anti-CD40 by sandwich ELISA, as described in Chapter 3.3.

A2-3. Preparation of anti-CD137-liposomes and IL-2/Fc-liposomes

Anti-CD137: clone LOB12.3 from Bio-X-Cell
IL-2/Fc: produced in-lab as described in Appendices 1 and A2-1b

1) Liposome preparation as described in Appendix A2-2 for anti-CD40 conjugation
For anti-CD137-liposomes: use composition (mol%) = 60/35/2.5/2.5
= DOPC/cholesterol/maleimide-PEG2000-DSPE/methoxy-PEG2000-DSPE (Avanti Lipids)
For IL-2/Fc-liposomes: use composition (mol%) = 62.5/35/2.5
= DOPC/cholesterol/maleimide-PEG2000-DSPE (Avanti Lipids)

2) Prepare anti-CD137 or IL-2/Fc by DTT reduction, similar to anti-CD40 preparation:
- Concentrate antibody to ~25-30mg/ml and IL-2/Fc to ~13-18mg/ml (total protein) by centrifugation in Amicon filter columns (30kDa MWCO), as described in Appendix A2-2.
- Add EDTA (final concentration of 10mM) to concentrated protein solutions
- Add DTT to a final concentration of 1.8mM DTT, and mix by pipetting to minimize air bubbles. Let sit 20-25min at room temp.
- After DTT reduction, desalt using Zeba columns (7kDa MWCO, Pierce)
- Mix with prepared maleimide-functionalized liposomes in presence of 10mM EDTA, and allow reactions to proceed overnight or at least 8 hours, at room temperature.

Conjugation ratios:
1.4umol liposomes per starting mg of anti-CD137
5umol liposomes per starting mg of IL-2 (effective), equivalent to ~3mg of total IL-2/Fc protein

3) Washing and purification / membrane re-extrusion / quantification:
- All can be performed identically as with anti-CD40-coupled liposomes (described in Appendix A2-2)

A2-4. Harvesting and processing of tissues for flow cytometry analysis and histology

Extract spleen and lymph nodes as usual, and store in RPMI medium with 10% FCS, on ice. Extract tumors from subcutaneous space by cutting back surrounding skin, then using razor blade to slice or scrape away the tumor mass. Avoid including the outer layer of skin, as this will produce a lot of non-cellular debris in later processing and analysis. Store tumor tissues in RPMI medium with 10% FCS as well, on ice.

For histology (cryosectioning):
Fill plastic moulds with appropriate volume of OCT embedding compound. Place and orient the desired tissue into the OCT, and snap-freeze using liquid nitrogen. Store intact samples at -80 degC until cryosectioning, and store cryosectioned slices at -20degC or colder. Antibody staining of cryosections was performed using the same dilutions as listed below (for flow).

For flow cytometry analysis:
1. Optionally, add collagenase to intact tissue samples, to facilitate subsequent processing of tissues and cell recovery. Digest for a maximum of 15-20min at 37degC, to avoid inducing cell death.

2. Mechanically dissociate all tissues into single-cell suspensions by grinding with syringe plungers through 40um or 70um nylon cell strainers, and rinsing through with complete RPMI

medium. Use of complete medium enhances cell viability after dissociation and re-suspension. Keep tissues and cell suspensions on ice as much as possible.

3. For spleens, pellet cells and then re-suspend in ACK Lysis Buffer (4ml per spleen), for 3-4min, at room temperature, in order to remove red blood cells. When finished, add an equal volume of complete medium to wash cells; pellet, re-suspend, and pass through nylon cell strainers again to ensure removal of aggregates and cell debris.

4. Wash all samples 2x with flow cytometry staining buffer (PBS + 1% BSA), then proceed to staining.

5. Cell staining for FACS analysis
Cells were stained with the following antibodies at the indicated dilutions, for 30-60min at 4degC or on ice.
- purified anti-CD16/32 (Fc block), 1:100
- CD45 (common leukocyte marker), 1:50
- CD11c, 1:50 - F4/80, 1:50
- CD3, 1:100 - CD8, 1:100
- CD4, 1:100 - NK1.1, 1:50

6. For intracellular staining of Foxp3, the kit from eBioscience was used, containing anti-Foxp3 antibody, and all fixation and permeabilization buffers. All procedures were carried out according to the manufacturer's instructions.

7. Gating of flow cytometry data: tumor-infiltrating leukocytes were first gated by forward and side scatter, and then by CD45+ expression, according to comparison with spleen and lymph node samples. Of the CD45+ cells, CD8+ CTLs were gated by CD3+CD8+ expression; macrophages were gated by F4/80+ expression; (conventional) dendritic cells were gated by CD11c+F4/80- expression; NK cells were gated by NK1.1+F4/80- expression; regulatory T cells were gated by CD4+Foxp3+ expression (including both CD25+ and CD25- cells).

A2-5. Sandwich ELISA for antibody quantification

1. Coat 96-well plates overnight using goat anti-human IgG (R&D Systems), at concentration of 2ug/ml in PBS.
2. Wash plate 3-4x using PBS + Tween20
3. Add 200ng/ml recombinant mouse CD40/human Fc fusion protein, or recombinant mouse CD137/human Fc fusion protein (both from R&D Systems), for 2hr. Wash as in step 2.
4. Add samples and 2-fold dilution standard curve, with maximum standard point of 10ng/ml anti-CD40 or anti-CD137. Incubate 2hr, then wash as in step 2.
5. Add 160ng/ml of HRP-conjugated goat anti-rat IgG (eBioscience), and incubate 2hr. Wash as in step 2.
6. Develop plate using HRP-sensitive colorimetric substrate.

Appendix 3: References

1. Swann JB, Smyth MJ. 2007. Immune Surveillance of Tumors. J Clin Invest 117(5):1137-1146.
2. Whiteside TL. 2008. The Tumor Microenvironment and Its Role in Promoting Tumor Growth. Oncogene 27(45):5904-5912.
3. Vicari AP, Chiodoni C, Vaure C, Ait-Yahia S, Dercamp C, Matsos F, Reynard O, Taverne C, Merle P, Colombo MP, O'Garra A, Trinchieri G, Caux C. 2002. Reversal of Tumor-Induced Dendritic Cell Paralysis by Cpg Immunostimulatory Oligonucleotide and Anti-Interleukin 10 Receptor Antibody. Journal of Experimental Medicine 196(4):541-549.
4. Curran MA, Montalvo W, Yagita H, Allison JP. 2010. Pd-1 and Ctla-4 Combination Blockade Expands Infiltrating T Cells and Reduces Regulatory T and Myeloid Cells within B16 Melanoma Tumors. Proc Natl Acad Sci U S A 107(9):4275-4280.
5. Kortylewski M, Swiderski P, Herrmann A, Wang L, Kowolik C, Kujawski M, Lee H, Scuto A, Liu Y, Yang C, Deng J, Soifer HS, Raubitschek A, Forman S, Rossi JJ, Pardoll DM, Jove R, Yu H. 2009. In Vivo Delivery of Sirna to Immune Cells by Conjugation to a Tlr9 Agonist Enhances Antitumor Immune Responses. Nat Biotechnol 27(10):925-932.
6. Radny P, Caroli UM, Bauer J, Paul T, Schlegel C, Eigentler TK, Weide B, Schwarz M, Garbe C. 2003. Phase Ii Trial of Intralesional Therapy with Interleukin-2 in Soft-Tissue Melanoma Metastases. Br J Cancer 89(9):1620-1626.
7. Yang Y, Huang CT, Huang X, Pardoll DM. 2004. Persistent Toll-Like Receptor Signals Are Required for Reversal of Regulatory T Cell-Mediated Cd8 Tolerance. Nat Immunol 5(5):508-515.
8. Houot R, Levy R. 2009. T-Cell Modulation Combined with Intratumoral Cpg Cures Lymphoma in a Mouse Model without the Need for Chemotherapy. Blood 113(15):3546-3552.
9. Jackaman C, Lew AM, Zhan Y, Allan JE, Koloska B, Graham PT, Robinson BW, Nelson DJ. 2008. Deliberately Provoking Local Inflammation Drives Tumors to Become Their Own Protective Vaccine Site. Int Immunol 20(11):1467-1479.
10. Gattinoni L, Powell DJ, Jr., Rosenberg SA, Restifo NP. 2006. Adoptive Immunotherapy for Cancer: Building on Success. Nat Rev Immunol 6(5):383-393.
11. Restifo NP, Dudley ME, Rosenberg SA. 2012. Adoptive Immunotherapy for Cancer: Harnessing the T Cell Response. Nat Rev Immunol 12(4):269-281.
12. Pardoll DM. 2012. The Blockade of Immune Checkpoints in Cancer Immunotherapy. Nat Rev Cancer 12(4):252-264.
13. Topalian SL, Weiner GJ, Pardoll DM. 2011. Cancer Immunotherapy Comes of Age. J Clin Oncol 29(36):4828-4836.
14. Vanneman M, Dranoff G. 2012. Combining Immunotherapy and Targeted Therapies in Cancer Treatment. Nat Rev Cancer 12(4):237-251.
15. FDA. 2012. Vaccines, Blood, and Biologics - Approved Products. http://www.fda.gov/BiologicsBloodVaccines/CellularGeneTherapyProducts/ApprovedProducts/default.htm. February 5, 2012
16. Pardoll DM. 1995. Paracrine Cytokine Adjuvants in Cancer Immunotherapy. Annu Rev Immunol 13(1):399-415.
17. Attia P, Phan GQ, Maker AV, Robinson MR, Quezado MM, Yang JC, Sherry RM, Topalian SL, Kammula US, Royal RE, Restifo NP, Haworth LR, Levy C, Mavroukakis SA, Nichol G, Yellin MJ, Rosenberg SA. 2005. Autoimmunity Correlates with Tumor Regression in

Patients with Metastatic Melanoma Treated with Anti-Cytotoxic T-Lymphocyte Antigen-4. J Clin Oncol 23(25):6043-6053.
18. Phan GQ, Yang JC, Sherry RM, Hwu P, Topalian SL, Schwartzentruber DJ, Restifo NP, Haworth LR, Seipp CA, Freezer LJ, Morton KE, Mavroukakis SA, Duray PH, Steinberg SM, Allison JP, Davis TA, Rosenberg SA. 2003. Cancer Regression and Autoimmunity Induced by Cytotoxic T Lymphocyte-Associated Antigen 4 Blockade in Patients with Metastatic Melanoma. Proc Natl Acad Sci U S A 100(14):8372-8377.
19. Elgueta R, Benson MJ, de Vries VC, Wasiuk A, Guo Y, Noelle RJ. 2009. Molecular Mechanism and Function of Cd40/Cd40l Engagement in the Immune System. Immunol Rev 229(1):152-172.
20. Biber JL, Jabbour S, Parihar R, Dierksheide J, Hu Y, Baumann H, Bouchard P, Caligiuri MA, Carson W. 2002. Administration of Two Macrophage-Derived Interferon-Γ-Inducing Factors (Il-12 and Il-15) Induces a Lethal Systemic Inflammatory Response in Mice That Is Dependent on Natural Killer Cells but Does Not Require Interferon-Γ. Cellular immunology 216(1):31-42.
21. Carson WE, Dierksheide JE, Jabbour S, Anghelina M, Bouchard P, Ku G, Yu H, Baumann H, Shah MH, Cooper MA, Durbin J, Caligiuri MA. 2000. Coadministration of Interleukin-18 and Interleukin-12 Induces a Fatal Inflammatory Response in Mice: Critical Role of Natural Killer Cell Interferon-Gamma Production and Stat-Mediated Signal Transduction. Blood 96(4):1465-1473.
22. Ruter J, Antonia SJ, Burris HA, Huhn RD, Vonderheide RH. 2010. Immune Modulation with Weekly Dosing of an Agonist Cd40 Antibody in a Phase I Study of Patients with Advanced Solid Tumors. Cancer Biol Ther 10(10):983-993.
23. Vonderheide RH, Flaherty KT, Khalil M, Stumacher MS, Bajor DL, Hutnick NA, Sullivan P, Mahany JJ, Gallagher M, Kramer A, Green SJ, O'Dwyer PJ, Running KL, Huhn RD, Antonia SJ. 2007. Clinical Activity and Immune Modulation in Cancer Patients Treated with Cp-870,893, a Novel Cd40 Agonist Monoclonal Antibody. J Clin Oncol 25(7):876-883.
24. Advani R, Forero-Torres A, Furman RR, Rosenblatt JD, Younes A, Ren H, Harrop K, Whiting N, Drachman JG. 2009. Phase I Study of the Humanized Anti-Cd40 Monoclonal Antibody Dacetuzumab in Refractory or Recurrent Non-Hodgkin's Lymphoma. J Clin Oncol 27(26):4371-4377.
25. Hussein M, Berenson JR, Niesvizky R, Munshi N, Matous J, Sobecks R, Harrop K, Drachman JG, Whiting N. 2010. A Phase I Multidose Study of Dacetuzumab (Sgn-40; Humanized Anti-Cd40 Monoclonal Antibody) in Patients with Multiple Myeloma. Haematologica 95(5):845-848.
26. Ascierto PA, Simeone E, Sznol M, Fu YX, Melero I. 2010. Clinical Experiences with Anti-Cd137 and Anti-Pd1 Therapeutic Antibodies. Semin Oncol 37(5):508-516.
27. Suntharalingam G, Perry MR, Ward S, Brett SJ, Castello-Cortes A, Brunner MD, Panoskaltsis N. 2006. Cytokine Storm in a Phase 1 Trial of the Anti-Cd28 Monoclonal Antibody Tgn1412. N Engl J Med 355(10):1018-1028.
28. Gardner K. 2006. Cytokine Storm and an Anti-Cd28 Monoclonal Antibody. N Engl J Med 355(24):2591-2592; author reply 2593-2594.
29. Ahonen CL, Wasiuk A, Fuse S, Turk MJ, Ernstoff MS, Suriawinata AA, Gorham JD, Kedl RM, Usherwood EJ, Noelle RJ. 2008. Enhanced Efficacy and Reduced Toxicity of Multifactorial Adjuvants Compared with Unitary Adjuvants as Cancer Vaccines. Blood 111(6):3116-3125.

30. Hamzah J, Nelson D, Moldenhauer G, Arnold B, Hammerling GJ, Ganss R. 2008. Vascular Targeting of Anti-Cd40 Antibodies and Il-2 into Autochthonous Tumors Enhances Immunotherapy in Mice. J Clin Invest 118(5):1691-1699.
31. Hamzah J, Altin JG, Herringson T, Parish CR, Hammerling GJ, O'Donoghue H, Ganss R. 2009. Targeted Liposomal Delivery of Tlr9 Ligands Activates Spontaneous Antitumor Immunity in an Autochthonous Cancer Model. J Immunol 183(2):1091-1098.
32. Johnson EE, Lum HD, Rakhmilevich AL, Schmidt BE, Furlong M, Buhtoiarov IN, Hank JA, Raubitschek A, Colcher D, Reisfeld RA, Gillies SD, Sondel PM. 2008. Intratumoral Immunocytokine Treatment Results in Enhanced Antitumor Effects. Cancer Immunol Immunother 57(12):1891-1902.
33. Gimbel MI, Delman KA, Zager JS. 2008. Therapy for Unresectable Recurrent and in-Transit Extremity Melanoma. Cancer Control 15(3):225-232.
34. Mundt AJ, Vijayakumar S, Nemunaitis J, Sandler A, Schwartz H, Hanna N, Peabody T, Senzer N, Chu K, Rasmussen CS, Kessler PD, Rasmussen HS, Warso M, Kufe DW, Gupta TD, Weichselbaum RR. 2004. A Phase I Trial of Tnferade Biologic in Patients with Soft Tissue Sarcoma in the Extremities. Clin Cancer Res 10(17):5747-5753.
35. Den Otter W, Jacobs JJ, Battermann JJ, Hordijk GJ, Krastev Z, Moiseeva EV, Stewart RJ, Ziekman PG, Koten JW. 2008. Local Therapy of Cancer with Free Il-2. Cancer Immunol Immunother 57(7):931-950.
36. Grasso M, Torelli F, Scannapieco G, Franzoso F, Lania C. 2001. Neoadiuvant Treatment with Intravesical Interleukin-2 for Recurrent Superficial Transitional Bladder Carcinoma Ta-T1/G1-2. Journal of Immunotherapy 24(2):184-187.
37. van Mierlo GJD, den Boer AT, Medema JP, van der Voort EIH, Fransen MF, Offringa R, Melief CJM, Toes REM. 2002. Cd40 Stimulation Leads to Effective Therapy of Cd40− Tumors through Induction of Strong Systemic Cytotoxic T Lymphocyte Immunity. Proceedings of the National Academy of Sciences 99(8):5561.
38. Heckelsmiller K, Rall K, Beck S, Schlamp A, Seiderer J, Jahrsdorfer B, Krug A, Rothenfusser S, Endres S, Hartmann G. 2002. Peritumoral Cpg DNA Elicits a Coordinated Response of Cd8 T Cells and Innate Effectors to Cure Established Tumors in a Murine Colon Carcinoma Model. J Immunol 169(7):3892-3899.
39. Simmons AD, Moskalenko M, Creson J, Fang J, Yi S, VanRoey MJ, Allison JP, Jooss K. 2008. Local Secretion of Anti-Ctla-4 Enhances the Therapeutic Efficacy of a Cancer Immunotherapy with Reduced Evidence of Systemic Autoimmunity. Cancer Immunol Immunother 57(8):1263-1270.
40. Galili U, Wigglesworth K, Abdel-Motal UM. 2007. Intratumoral Injection of A-Gal Glycolipids Induces Xenograft-Like Destruction and Conversion of Lesions into Endogenous Vaccines. The Journal of Immunology 178(7):4676.
41. Broomfield SA, van der Most RG, Prosser AC, Mahendran S, Tovey MG, Smyth MJ, Robinson BW, Currie AJ. 2009. Locally Administered Tlr7 Agonists Drive Systemic Antitumor Immune Responses That Are Enhanced by Anti-Cd40 Immunotherapy. J Immunol 182(9):5217-5224.
42. Broderick L, Yokota SJ, Reineke J, Mathiowitz E, Stewart CC, Barcos M, Kelleher RJ, Jr., Bankert RB. 2005. Human Cd4+ Effector Memory T Cells Persisting in the Microenvironment of Lung Cancer Xenografts Are Activated by Local Delivery of Il-12 to Proliferate, Produce Ifn-Gamma, and Eradicate Tumor Cells. J Immunol 174(2):898-906.

43. Brody JD, Ai WZ, Czerwinski DK, Torchia JA, Levy M, Advani RH, Kim YH, Hoppe RT, Knox SJ, Shin LK, Wapnir I, Tibshirani RJ, Levy R. 2010. In Situ Vaccination with a Tlr9 Agonist Induces Systemic Lymphoma Regression: A Phase I/Ii Study. J Clin Oncol 28(28):4324-4332.
44. French RR, Chan HTC, Tutt AL, Glennie MJ. 1999. Cd40 Antibody Evokes a Cytotoxic T-Cell Response That Eradicates Lymphoma and Bypasses T-Cell Help. Nature medicine 5(5):548-553.
45. Tutt AL, O'Brien L, Hussain A, Crowther GR, French RR, Glennie MJ. 2002. T Cell Immunity to Lymphoma Following Treatment with Anti-Cd40 Monoclonal Antibody. J Immunol 168(6):2720-2728.
46. Eton O, Rosenblum MG, Legha SS, Zhang W, Jo East M, Bedikian A, Papadopoulos N, Buzaid A, Benjamin RS. 2002. Phase I Trial of Subcutaneous Recombinant Human Interleukin-2 in Patients with Metastatic Melanoma. Cancer 95(1):127-134.
47. Portielje JE, Kruit WH, Eerenberg AJ, Schuler M, Sparreboom A, Lamers CH, Gratama JW, Stoter G, Huber C, Hack CE. 2005. Subcutaneous Injection of Interleukin 12 Induces Systemic Inflammatory Responses in Humans: Implications for the Use of Il-12 as Vaccine Adjuvant. Cancer Immunol Immunother 54(1):37-43.
48. Portielje JE, Kruit WH, Schuler M, Beck J, Lamers CH, Stoter G, Huber C, de Boer-Dennert M, Rakhit A, Bolhuis RL, Aulitzky WE. 1999. Phase I Study of Subcutaneously Administered Recombinant Human Interleukin 12 in Patients with Advanced Renal Cell Cancer. Clin Cancer Res 5(12):3983-3989.
49. Hanes J, Sills A, Zhao Z, Suh KW, Tyler B, DiMeco F, Brat DJ, Choti MA, Leong KW, Pardoll DM, Brem H. 2001. Controlled Local Delivery of Interleukin-2 by Biodegradable Polymers Protects Animals from Experimental Brain Tumors and Liver Tumors. Pharm Res 18(7):899-906.
50. Bourquin C, Anz D, Zwiorek K, Lanz AL, Fuchs S, Weigel S, Wurzenberger C, von der Borch P, Golic M, Moder S, Winter G, Coester C, Endres S. 2008. Targeting Cpg Oligonucleotides to the Lymph Node by Nanoparticles Elicits Efficient Antitumoral Immunity. J Immunol 181(5):2990-2998.
51. Hori Y, Stern PJ, Hynes RO, Irvine DJ. 2009. Engulfing Tumors with Synthetic Extracellular Matrices for Cancer Immunotherapy. Biomaterials 30(35):6757-6767.
52. Hill HC, Conway TF, Jr., Sabel MS, Jong YS, Mathiowitz E, Bankert RB, Egilmez NK. 2002. Cancer Immunotherapy with Interleukin 12 and Granulocyte-Macrophage Colony-Stimulating Factor-Encapsulated Microspheres: Coinduction of Innate and Adaptive Antitumor Immunity and Cure of Disseminated Disease. Cancer Res 62(24):7254-7263.
53. de Jong S, Chikh G, Sekirov L, Raney S, Semple S, Klimuk S, Yuan N, Hope M, Cullis P, Tam Y. 2007. Encapsulation in Liposomal Nanoparticles Enhances the Immunostimulatory, Adjuvant and Anti-Tumor Activity of Subcutaneously Administered Cpg Odn. Cancer Immunol Immunother 56(8):1251-1264.
54. Van Herpen CM, Huijbens R, Looman M, De Vries J, Marres H, Van De Ven J, Hermsen R, Adema GJ, De Mulder PH. 2003. Pharmacokinetics and Immunological Aspects of a Phase Ib Study with Intratumoral Administration of Recombinant Human Interleukin-12 in Patients with Head and Neck Squamous Cell Carcinoma: A Decrease of T-Bet in Peripheral Blood Mononuclear Cells. Clin Cancer Res 9(8):2950-2956.
55. Alexander HR, Libutti SK, Bartlett DL, Puhlmann M, Fraker DL, Bachenheimer LC. 2000. A Phase I-Ii Study of Isolated Hepatic Perfusion Using Melphalan with or without Tumor

Necrosis Factor for Patients with Ocular Melanoma Metastatic to Liver. Clinical cancer research 6(8):3062-3070.
56. Bartlett DL, Libutti SK, Figg WD, Fraker DL, Alexander HR. 2001. Isolated Hepatic Perfusion for Unresectable Hepatic Metastases from Colorectal Cancer. Surgery 129(2):176-187.
57. Lienard D, Ewalenko P, Delmotte JJ, Renard N, Lejeune FJ. 1992. High-Dose Recombinant Tumor Necrosis Factor Alpha in Combination with Interferon Gamma and Melphalan in Isolation Perfusion of the Limbs for Melanoma and Sarcoma. J Clin Oncol 10(1):52-60.
58. Torchilin VP. 2010. Passive and Active Drug Targeting: Drug Delivery to Tumors as an Example. Drug Delivery:3-53.
59. Allen TM, Cullis PR. 2004. Drug Delivery Systems: Entering the Mainstream. Science 303(5665):1818-1822.
60. Koten JW, Van Luyn MJ, Cadee JA, Brouwer L, Hennink WE, Bijleveld C, Den Otter W. 2003. Il-2 Loaded Dextran Microspheres with Attractive Histocompatibility Properties for Local Il-2 Cancer Therapy. Cytokine 24(3):57-66.
61. Egilmez NK, Jong YS, Sabel MS, Jacob JS, Mathiowitz E, Bankert RB. 2000. In Situ Tumor Vaccination with Interleukin-12-Encapsulated Biodegradable Microspheres: Induction of Tumor Regression and Potent Antitumor Immunity. Cancer Res 60(14):3832-3837.
62. Sabel MS, Hill H, Jong YS, Mathiowitz E, Bankert RB, Egilmez NK. 2001. Neoadjuvant Therapy with Interleukin-12-Loaded Polylactic Acid Microspheres Reduces Local Recurrence and Distant Metastases. Surgery 130(3):470-478.
63. Sabel MS, Skitzki J, Stoolman L, Egilmez NK, Mathiowitz E, Bailey N, Chang WJ, Chang AE. 2004. Intratumoral Il-12 and Tnf-Alpha-Loaded Microspheres Lead to Regression of Breast Cancer and Systemic Antitumor Immunity. Ann Surg Oncol 11(2):147-156.
64. De Groot CJ, Cadee JA, Koten JW, Hennink WE, Den Otter W. 2002. Therapeutic Efficacy of Il-2-Loaded Hydrogels in a Mouse Tumor Model. Int J Cancer 98(1):134-140.
65. Simpson-Abelson MR, Purohit VS, Pang WM, Iyer V, Odunsi K, Demmy TL, Yokota SJ, Loyall JL, Kelleher RJ, Jr., Balu-Iyer S, Bankert RB. 2009. Il-12 Delivered Intratumorally by Multilamellar Liposomes Reactivates Memory T Cells in Human Tumor Microenvironments. Clin Immunol 132(1):71-82.
66. Samlowski WE, McGregor JR, Jurek M, Baudys M, Zentner GM, Fowers KD. 2006. Regel (R) Polymer-Based Delivery of Interleukin-2 as a Cancer Treatment. Journal of Immunotherapy 29(5):524-535.
67. Fransen MF, Sluijter M, Morreau H, Arens R, Melief CJ. 2011. Local Activation of Cd8 T Cells and Systemic Tumor Eradication without Toxicity Via Slow Release and Local Delivery of Agonistic Cd40 Antibody. Clin Cancer Res 17(8):2270-2280.
68. Allen TM. 2002. Ligand-Targeted Therapeutics in Anticancer Therapy. Nat Rev Cancer 2(10):750-763.
69. Cheng WW, Allen TM. 2008. Targeted Delivery of Anti-Cd19 Liposomal Doxorubicin in B-Cell Lymphoma: A Comparison of Whole Monoclonal Antibody, Fab' Fragments and Single Chain Fv. J Control Release 126(1):50-58.
70. Li C, Wallace S. 2008. Polymer-Drug Conjugates: Recent Development in Clinical Oncology. Adv Drug Deliv Rev 60(8):886-898.

71. Kumar S, Aaron J, Sokolov K. 2008. Directional Conjugation of Antibodies to Nanoparticles for Synthesis of Multiplexed Optical Contrast Agents with Both Delivery and Targeting Moieties. Nat Protoc 3(2):314-320.
72. Dominguez AL, Lustgarten J. 2010. Targeting the Tumor Microenvironment with Anti-Neu/Anti-Cd40 Conjugated Nanoparticles for the Induction of Antitumor Immune Responses. Vaccine 28(5):1383-1390.
73. Zhang M, Yao Z, Dubois S, Ju W, Muller JR, Waldmann TA. 2009. Interleukin-15 Combined with an Anti-Cd40 Antibody Provides Enhanced Therapeutic Efficacy for Murine Models of Colon Cancer. Proc Natl Acad Sci U S A 106(18):7513-7518.
74. Kim YH, Gratzinger D, Harrison C, Brody JD, Czerwinski DK, Ai WZ, Morales A, Abdulla F, Xing L, Navi D, Tibshirani RJ, Advani RH, Lingala B, Shah S, Hoppe RT, Levy R. 2012. In Situ Vaccination against Mycosis Fungoides by Intratumoral Injection of a Tlr9 Agonist Combined with Radiation: A Phase 1/2 Study. Blood 119(2):355-363.
75. Sotomayor EM, Borrello I, Tubb E, Rattis FM, Bien H, Lu ZB, Fein S, Schoenberger S, Levitsky HI. 1999. Conversion of Tumor-Specific Cd4(+) T-Cell Tolerance to T-Cell Priming through in Vivo Ligation of Cd40. Nature medicine 5(7):780-787.
76. Diehl L, den Boer AT, Schoenberger SP, van der Voort EI, Schumacher TN, Melief CJ, Offringa R, Toes RE. 1999. Cd40 Activation in Vivo Overcomes Peptide-Induced Peripheral Cytotoxic T-Lymphocyte Tolerance and Augments Anti-Tumor Vaccine Efficacy. Nat Med 5(7):774-779.
77. Todryk SM, Tutt AL, Green MH, Smallwood JA, Halanek N, Dalgleish AG, Glennie MJ. 2001. Cd40 Ligation for Immunotherapy of Solid Tumours. J Immunol Methods 248(1-2):139-147.
78. van Mierlo GJD, Boonman ZFHM, Dumortier HMH, den Boer AT, Fransen MF, Nouta J, van der Voort EIH, Offringa R, Toes REM, Melief CJM. 2004. Activation of Dendritic Cells That Cross-Present Tumor-Derived Antigen Licenses Cd8+ Ctl to Cause Tumor Eradication. The Journal of Immunology 173(11):6753.
79. Murphy WJ, Welniak L, Back T, Hixon J, Subleski J, Seki N, Wigginton JM, Wilson SE, Blazar BR, Malyguine AM, Sayers TJ, Wiltrout RH. 2003. Synergistic Anti-Tumor Responses after Administration of Agonistic Antibodies to Cd40 and Il-2: Coordination of Dendritic and Cd8+ Cell Responses. J Immunol 170(5):2727-2733.
80. Jackaman C, Cornwall S, Graham PT, Nelson DJ. 2011. Cd40-Activated B Cells Contribute to Mesothelioma Tumor Regression. Immunol Cell Biol 89(2):255-267.
81. Buhtoiarov IN, Lum H, Berke G, Paulnock DM, Sondel PM, Rakhmilevich AL. 2005. Cd40 Ligation Activates Murine Macrophages Via an Ifn-Gamma-Dependent Mechanism Resulting in Tumor Cell Destruction in Vitro. J Immunol 174(10):6013-6022.
82. Buhtoiarov IN, Lum HD, Berke G, Sondel PM, Rakhmilevich AL. 2006. Synergistic Activation of Macrophages Via Cd40 and Tlr9 Results in T Cell Independent Antitumor Effects. J Immunol 176(1):309-318.
83. Lum HD, Buhtoiarov IN, Schmidt BE, Berke G, Paulnock DM, Sondel PM, Rakhmilevich AL. 2006. In Vivo Cd40 Ligation Can Induce T-Cell-Independent Antitumor Effects That Involve Macrophages. J Leukoc Biol 79(6):1181-1192.
84. Turner JG, Rakhmilevich AL, Burdelya L, Neal Z, Imboden M, Sondel PM, Yu H. 2001. Anti-Cd40 Antibody Induces Antitumor and Antimetastatic Effects: The Role of Nk Cells. J Immunol 166(1):89-94.

85. Beatty GL, Chiorean EG, Fishman MP, Saboury B, Teitelbaum UR, Sun W, Huhn RD, Song W, Li D, Sharp LL, Torigian DA, O'Dwyer PJ, Vonderheide RH. 2011. Cd40 Agonists Alter Tumor Stroma and Show Efficacy against Pancreatic Carcinoma in Mice and Humans. Science 331(6024):1612-1616.
86. Kimura K, Moriwaki H, Nagaki M, Saio M, Nakamoto Y, Naito M, Kuwata K, Chisari FV. 2006. Pathogenic Role of B Cells in Anti-Cd40-Induced Necroinflammatory Liver Disease. Am J Pathol 168(3):786-795.
87. Gendelman M, Halligan N, Komorowski R, Logan B, Murphy WJ, Blazar BR, Pritchard KA, Jr., Drobyski WR. 2005. Alpha Phenyl-Tert-Butyl Nitrone (Pbn) Protects Syngeneic Marrow Transplant Recipients from the Lethal Cytokine Syndrome Occurring after Agonistic Cd40 Antibody Administration. Blood 105(1):428-431.
88. Hixon JA, Anver MR, Blazar BR, Panoskaltsis-Mortari A, Wiltrout RH, Murphy WJ. 2002. Administration of Either Anti-Cd40 or Interleukin-12 Following Lethal Total Body Irradiation Induces Acute Lethal Toxicity Affecting the Gut. Biology of Blood and Marrow Transplantation 8(6):316-325.
89. Hixon JA, Blazar BR, Anver MR, Wiltrout RH, Murphy WJ. 2001. Antibodies to Cd40 Induce a Lethal Cytokine Cascade after Syngeneic Bone Marrow Transplantation. Biol Blood Marrow Transplant 7(3):136-143.
90. Wiley JA, Geha R, Harmsen AG. 1997. Exogenous Cd40 Ligand Induces a Pulmonary Inflammation Response. J Immunol 158(6):2932-2938.
91. Bartholdy C, Kauffmann SO, Christensen JP, Thomsen AR. 2007. Agonistic Anti-Cd40 Antibody Profoundly Suppresses the Immune Response to Infection with Lymphocytic Choriomeningitis Virus. J Immunol 178(3):1662-1670.
92. Berner V, Liu H, Zhou Q, Alderson KL, Sun K, Weiss JM, Back TC, Longo DL, Blazar BR, Wiltrout RH, Welniak LA, Redelman D, Murphy WJ. 2007. Ifn-Gamma Mediates Cd4+ T-Cell Loss and Impairs Secondary Antitumor Responses after Successful Initial Immunotherapy. Nat Med 13(3):354-360.
93. Neville ME, Robb RJ, Popescu MC. 2001. In Situ Vaccination against a Non-Immunogenic Tumour Using Intratumoural Injections of Liposomal Interleukin 2. Cytokine 16(6):239-250.
94. Hatzifoti C, Bacon A, Marriott H, Laing P, Heath AW. 2008. Liposomal Co-Entrapment of Cd40mab Induces Enhanced Igg Responses against Bacterial Polysaccharide and Protein. PLoS One 3(6):e2368.
95. Iden DL, Allen TM. 2001. In Vitro and in Vivo Comparison of Immunoliposomes Made by Conventional Coupling Techniques with Those Made by a New Post-Insertion Approach. Biochimica Et Biophysica Acta-Biomembranes 1513(2):207-216.
96. Moreira JN, Ishida T, Gaspar R, Allen TM. 2002. Use of the Post-Insertion Technique to Insert Peptide Ligands into Pre-Formed Stealth Liposomes with Retention of Binding Activity and Cytotoxicity. Pharmaceutical research 19(3):265-269.
97. Allen TM, Sapra P, Moase E. 2002. Use of the Post-Insertion Method for the Formation of Ligand-Coupled Liposomes. Cellular and Molecular Biology Letters 7(2):217-219.
98. Bershteyn A, Chaparro J, Yau R, Kim M, Reinherz E, Ferreira-Moita L, Irvine DJ. 2008. Polymer-Supported Lipid Shells, Onions, and Flowers. Soft matter 4(9):1787-1791.
99. Taraban VY, Rowley TF, Al-Shamkhani A. 2004. Cutting Edge: A Critical Role for Cd70 in Cd8 T Cell Priming by Cd40-Licensed Apcs. J Immunol 173(11):6542-6546.

100. Fattori E, Cappelletti M, Costa P, Sellitto C, Cantoni L, Carelli M, Faggioni R, Fantuzzi G, Ghezzi P, Poli V. 1994. Defective Inflammatory Response in Interleukin 6-Deficient Mice. Journal of Experimental Medicine 180(4):1243-1250.
101. Strassmann G, Fong M, Windsor S, Neta R. 1993. The Role of Interleukin-6 in Lipopolysaccharide-Induced Weight Loss, Hypoglycemia and Fibrinogen Production, in Vivo. Cytokine 5(4):285-290.
102. Rüegg UT, Rudinger J. 1977. [10] Reductive Cleavage of Cystine Disulfides with Tributylphosphine. Methods in enzymology 47:111-116.
103. Kwong B, Liu H, Irvine DJ. 2011. Induction of Potent Anti-Tumor Responses While Eliminating Systemic Side Effects Via Liposome-Anchored Combinatorial Immunotherapy. Biomaterials 32(22):5134-5147.
104. Nowak AK, Robinson BWS, Lake RA. 2003. Synergy between Chemotherapy and Immunotherapy in the Treatment of Established Murine Solid Tumors. Cancer research 63(15):4490-4496.
105. Jackaman C, Nelson DJ. 2012. Intratumoral Interleukin-2/Agonist Cd40 Antibody Drives Cd4(+)-Independent Resolution of Treated-Tumors and Cd4 (+)-Dependent Systemic and Memory Responses. Cancer Immunol Immunother 61(4):549-560.
106. Krieg AM. 2008. Toll-Like Receptor 9 (Tlr9) Agonists in the Treatment of Cancer. Oncogene 27(2):161-167.
107. Krieg AM. 2006. Therapeutic Potential of Toll-Like Receptor 9 Activation. Nat Rev Drug Discov 5(6):471-484.
108. Li JL, Song WR, Czerwinski DK, Varghese B, Uematsu S, Akira S, Krieg AM, Levy R. 2007. Lymphoma Immunotherapy with Cpg Oligodeoxynucleotides Requires Tlr9 Either in the Host or in the Tumor Itself. J Immunol 179(4):2493-2500.
109. Mastini C, Becker PD, Iezzi M, Curcio C, Musiani P, Forni G, Cavallo F, Guzman CA. 2008. Intramammary Application of Non-Methylated-Cpg Oligodeoxynucleotides (Cpg) Inhibits Both Local and Systemic Mammary Carcinogenesis in Female Balb/C Her-2/Neu Transgenic Mice. Current cancer drug targets 8(3):230-242.
110. Reinis M, Simova J, Bubenik J. 2006. Inhibitory Effects of Unmethylated Cpg Oligodeoxynucleotides on Mhc Class I-Deficient and -Proficient Hpv16-Associated Tumours. Int J Cancer 118(7):1836-1842.
111. Lonsdorf AS, Kuekrek H, Stern BV, Boehm BO, Lehmann PV, Tary-Lehmann M. 2003. Intratumor Cpg-Oligodeoxynucleotide Injection Induces Protective Antitumor T Cell Immunity. J Immunol 171(8):3941-3946.
112. Pratesi G, Petrangolini G, Tortoreto M, Addis A, Belluco S, Rossini A, Selleri S, Rumio C, Menard S, Balsari A. 2005. Therapeutic Synergism of Gemcitabine and Cpg-Oligodeoxynucleotides in an Orthotopic Human Pancreatic Carcinoma Xenograft. Cancer Res 65(14):6388-6393.
113. Baines J, Celis E. 2003. Immune-Mediated Tumor Regression Induced by Cpg-Containing Oligodeoxynucleotides. Clin Cancer Res 9(7):2693-2700.
114. Wingender G, Garbi N, Schumak B, Jungerkes F, Endl E, von Bubnoff D, Steitz J, Striegler J, Moldenhauer G, Tuting T, Heit A, Huster KM, Takikawa O, Akira S, Busch DH, Wagner H, Hammerling GJ, Knolle PA, Limmer A. 2006. Systemic Application of Cpg-Rich DNA Suppresses Adaptive T Cell Immunity Via Induction of Ido. Eur J Immunol 36(1):12-20.
115. Fallarino F, Puccetti P. 2006. Toll-Like Receptor 9-Mediated Induction of the Immunosuppressive Pathway of Tryptophan Catabolism. Eur J Immunol 36(1):8-11.

116. Mellor AL, Baban B, Chandler PR, Manlapat A, Kahler DJ, Munn DH. 2005. Cutting Edge: Cpg Oligonucleotides Induce Splenic Cd19+ Dendritic Cells to Acquire Potent Indoleamine 2,3-Dioxygenase-Dependent T Cell Regulatory Functions Via Ifn Type 1 Signaling. J Immunol 175(9):5601-5605.
117. Heikenwalder M, Polymenidou M, Junt T, Sigurdson C, Wagner H, Akira S, Zinkernagel R, Aguzzi A. 2004. Lymphoid Follicle Destruction and Immunosuppression after Repeated Cpg Oligodeoxynucleotide Administration. Nat Med 10(2):187-192.
118. Johnson EE, Buhtoiarov IN, Baldeshwiler MJ, Felder MA, Van Rooijen N, Sondel PM, Rakhmilevich AL. 2011. Enhanced T-Cell-Independent Antitumor Effect of Cyclophosphamide Combined with Anti-Cd40 Mab and Cpg in Mice. J Immunother 34(1):76-84.
119. Stone GW, Barzee S, Snarsky V, Santucci C, Tran B, Langer R, Zugates GT, Anderson DG, Kornbluth RS. 2009. Nanoparticle-Delivered Multimeric Soluble Cd40l DNA Combined with Toll-Like Receptor Agonists as a Treatment for Melanoma. PLoS One 4(10):e7334.
120. Stone GW, Barzee S, Snarsky V, Toppin C, Tran BD, Kornbluth RS. 2006. Treatment of B16 Melanoma Using Peritumoral Injections of Plasmid DNA Encoding Multimeric Soluble Cd40l Combined with Tlr Stimulation. Journal of Immunotherapy 29(6):639-639.
121. Scarlett UK, Cubillos-Ruiz JR, Nesbeth YC, Martinez DG, Engle X, Gewirtz AT, Ahonen CL, Conejo-Garcia JR. 2009. In Situ Stimulation of Cd40 and Toll-Like Receptor 3 Transforms Ovarian Cancer-Infiltrating Dendritic Cells from Immunosuppressive to Immunostimulatory Cells. Cancer Res 69(18):7329-7337.
122. Ahonen CL, Doxsee CL, McGurran SM, Riter TR, Wade WF, Barth RJ, Vasilakos JP, Noelle RJ, Kedl RM. 2004. Combined Tlr and Cd40 Triggering Induces Potent Cd8+ T Cell Expansion with Variable Dependence on Type I Ifn. Journal of Experimental Medicine 199(6):775-784.
123. Kedl RM, Jordan M, Potter T, Kappler J, Marrack P, Dow S. 2001. Cd40 Stimulation Accelerates Deletion of Tumor-Specific Cd8(+) T Cells in the Absence of Tumor-Antigen Vaccination. Proc Natl Acad Sci U S A 98(19):10811-10816.
124. Mauri C, Mars LT, Londei M. 2000. Therapeutic Activity of Agonistic Monoclonal Antibodies against Cd40 in a Chronic Autoimmune Inflammatory Process. Nat Med 6(6):673-679.
125. Schulz O, Edwards AD, Schito M, Aliberti J, Manickasingham S, Sher A, Reis e Sousa C. 2000. Cd40 Triggering of Heterodimeric Il-12 P70 Production by Dendritic Cells in Vivo Requires a Microbial Priming Signal. Immunity 13(4):453-462.
126. Liu H, Kwong B, Irvine DJ. 2011. Membrane Anchored Immunostimulatory Oligonucleotides for in Vivo Cell Modification and Localized Immunotherapy. Angew Chem Int Ed Engl 50(31):7052-7055.
127. Liu H, Zhu Z, Kang H, Wu Y, Sefan K, Tan W. 2010. DNA-Based Micelles: Synthesis, Micellar Properties and Size-Dependent Cell Permeability. Chemistry 16(12):3791-3797.
128. Jewell CM, Lopez SC, Irvine DJ. 2011. In Situ Engineering of the Lymph Node Microenvironment Via Intranodal Injection of Adjuvant-Releasing Polymer Particles. Proc Natl Acad Sci U S A 108(38):15745-15750.
129. Krieg AM, Stein CA. 1995. Phosphorothioate Oligodeoxynucleotides: Antisense or Anti-Protein? Antisense Res Dev 5(4):241.
130. Rutz M, Metzger J, Gellert T, Luppa P, Lipford GB, Wagner H, Bauer S. 2004. Toll-Like Receptor 9 Binds Single-Stranded Cpg-DNA in a Sequence-and Ph-Dependent Manner. European journal of immunology 34(9):2541-2550.

131. Klinman DM. 2004. Immunotherapeutic Uses of Cpg Oligodeoxynucleotides. Nat Rev Immunol 4(4):249-258.
132. Oflazoglu E, Stone IJ, Brown L, Gordon KA, van Rooijen N, Jonas M, Law CL, Grewal IS, Gerber HP. 2009. Macrophages and Fc-Receptor Interactions Contribute to the Antitumour Activities of the Anti-Cd40 Antibody Sgn-40. Br J Cancer 100(1):113-117.
133. Stumbles PA, Himbeck R, Frelinger JA, Collins EJ, Lake RA, Robinson BW. 2004. Cutting Edge: Tumor-Specific Ctl Are Constitutively Cross-Armed in Draining Lymph Nodes and Transiently Disseminate to Mediate Tumor Regression Following Systemic Cd40 Activation. J Immunol 173(10):5923-5928.
134. Rakhmilevich A, Buhtoiarov IN, Lum HD, Malkovsky M, Sondel PM. 2005. Cd40 Ligation in Vivo Induces T Cell Independent Antitumor Effects Even against Immunogenic Tumors. Journal of Immunotherapy 28(6):636-637.
135. Rakhmilevich AL, Buhtoiarov IN, Malkovsky M, Sondel PM. 2008. Cd40 Ligation in Vivo Can Induce T Cell Independent Antitumor Effects Even against Immunogenic Tumors. Cancer Immunol Immunother 57(8):1151-1160.
136. Quezada SA, Peggs KS, Simpson TR, Shen Y, Littman DR, Allison JP. 2008. Limited Tumor Infiltration by Activated T Effector Cells Restricts the Therapeutic Activity of Regulatory T Cell Depletion against Established Melanoma. Journal of Experimental Medicine 205(9):2125-2138.
137. Curran MA, Kim M, Montalvo W, Al-Shamkhani A, Allison JP. 2011. Combination Ctla-4 Blockade and 4-1bb Activation Enhances Tumor Rejection by Increasing T-Cell Infiltration, Proliferation, and Cytokine Production. PLoS One 6(4):e19499.
138. Byrne KT, Cote AL, Zhang P, Steinberg SM, Guo Y, Allie R, Zhang W, Ernstoff MS, Usherwood EJ, Turk MJ. 2011. Autoimmune Melanocyte Destruction Is Required for Robust Cd8+ Memory T Cell Responses to Mouse Melanoma. J Clin Invest 121(5):1797-1809.
139. Turk MJ, Guevara-Patino JA, Rizzuto GA, Engelhorn ME, Sakaguchi S, Houghton AN. 2004. Concomitant Tumor Immunity to a Poorly Immunogenic Melanoma Is Prevented by Regulatory T Cells. Journal of Experimental Medicine 200(6):771-782.
140. Cote AL, Byrne KT, Steinberg SM, Zhang P, Turk MJ. 2011. Protective Cd8 Memory T Cell Responses to Mouse Melanoma Are Generated in the Absence of Cd4 T Cell Help. PLoS One 6(10):e26491.
141. Quezada SA, Peggs KS, Curran MA, Allison JP. 2006. Ctla4 Blockade and Gm-Csf Combination Immunotherapy Alters the Intratumor Balance of Effector and Regulatory T Cells. J Clin Invest 116(7):1935-1945.
142. Peggs KS, Quezada SA, Chambers CA, Korman AJ, Allison JP. 2009. Blockade of Ctla-4 on Both Effector and Regulatory T Cell Compartments Contributes to the Antitumor Activity of Anti–Ctla-4 Antibodies. The Journal of experimental medicine 206(8):1717-1725.
143. Quezada SA, Simpson TR, Peggs KS, Merghoub T, Vider J, Fan X, Blasberg R, Yagita H, Muranski P, Antony PA, Restifo NP, Allison JP. 2010. Tumor-Reactive Cd4(+) T Cells Develop Cytotoxic Activity and Eradicate Large Established Melanoma after Transfer into Lymphopenic Hosts. Journal of Experimental Medicine 207(3):637-650.
144. Mackensen A, Meidenbauer N, Vogl S, Laumer M, Berger J, Andreesen R. 2006. Phase I Study of Adoptive T-Cell Therapy Using Antigen-Specific Cd8+ T Cells for the Treatment of Patients with Metastatic Melanoma. J Clin Oncol 24(31):5060-5069.
145. Yee C, Thompson JA, Byrd D, Riddell SR, Roche P, Celis E, Greenberg PD. 2002. Adoptive T Cell Therapy Using Antigen-Specific Cd8+ T Cell Clones for the Treatment of

Patients with Metastatic Melanoma: In Vivo Persistence, Migration, and Antitumor Effect of Transferred T Cells. Proc Natl Acad Sci U S A 99(25):16168-16173.
146. Mellman I, Coukos G, Dranoff G. 2011. Cancer Immunotherapy Comes of Age. Nature 480(7378):480-489.
147. Cipponi A, Wieers G, van Baren N, Coulie PG. 2011. Tumor-Infiltrating Lymphocytes: Apparently Good for Melanoma Patients. But Why? Cancer Immunol Immunother 60(8):1153-1160.
148. Yuan J, Ginsberg B, Page D, Li Y, Rasalan T, Gallardo HF, Xu Y, Adams S, Bhardwaj N, Busam K, Old LJ, Allison JP, Jungbluth A, Wolchok JD. 2011. Ctla-4 Blockade Increases Antigen-Specific Cd8(+) T Cells in Prevaccinated Patients with Melanoma: Three Cases. Cancer Immunol Immunother 60(8):1137-1146.
149. Byrne KT, Turk MJ. 2011. New Perspectives on the Role of Vitiligo in Immune Responses to Melanoma. Oncotarget 2(9):684-694.
150. Ju SA, Lee SC, Kwon TH, Heo SK, Park SM, Paek HN, Suh JH, Cho HR, Kwon B, Kwon BS, Kim BS. 2005. Immunity to Melanoma Mediated by 4-1bb Is Associated with Enhanced Activity of Tumour-Infiltrating Lymphocytes. Immunol Cell Biol 83(4):344-351.
151. Xu D, Gu P, Pan PY, Li Q, Sato AI, Chen SH. 2004. Nk and Cd8+ T Cell-Mediated Eradication of Poorly Immunogenic B16-F10 Melanoma by the Combined Action of Il-12 Gene Therapy and 4-1bb Costimulation. Int J Cancer 109(4):499-506.
152. Cohen AD, Schaer DA, Liu C, Li Y, Hirschhorn-Cymmerman D, Kim SC, Diab A, Rizzuto G, Duan F, Perales MA, Merghoub T, Houghton AN, Wolchok JD. 2010. Agonist Anti-Gitr Monoclonal Antibody Induces Melanoma Tumor Immunity in Mice by Altering Regulatory T Cell Stability and Intra-Tumor Accumulation. PLoS One 5(5):e10436.
153. Melero I, Murillo O, Dubrot J, Hervas-Stubbs S, Perez-Gracia JL. 2008. Multi-Layered Action Mechanisms of Cd137 (4-1bb)-Targeted Immunotherapies. Trends Pharmacol Sci 29(8):383-390.
154. Lynch DH. 2008. The Promise of 4-1bb (Cd137)-Mediated Immunomodulation and the Immunotherapy of Cancer. Immunol Rev 222(1):277-286.
155. Melero I, Shuford WW, Newby SA, Aruffo A, Ledbetter JA, Hellstrom KE, Mittler RS, Chen L. 1997. Monoclonal Antibodies against the 4-1bb T-Cell Activation Molecule Eradicate Established Tumors. Nat Med 3(6):682-685.
156. Vinay DS, Cha K, Kwon BS. 2006. Dual Immunoregulatory Pathways of 4-1bb Signaling. J Mol Med (Berl) 84(9):726-736.
157. Mittler RS, Foell J, McCausland M, Strahotin S, Niu L, Bapat A, Hewes LB. 2004. Anti-Cd137 Antibodies in the Treatment of Autoimmune Disease and Cancer. Immunol Res 29(1-3):197-208.
158. Sznol M, Hodi F, Margolin K, McDermott D, Ernstoff M, Kirkwood J, Wojtaszek C, Feltquate D, Logan T. 2008 ASCO Annual Meeting, 2008, pp 3007.
159. Houot R, Goldstein MJ, Kohrt HE, Myklebust JH, Alizadeh AA, Lin JT, Irish JM, Torchia JA, Kolstad A, Chen L, Levy R. 2009. Therapeutic Effect of Cd137 Immunomodulation in Lymphoma and Its Enhancement by Treg Depletion. Blood 114(16):3431-3438.
160. John LB, Howland LJ, Flynn JK, West AC, Devaud C, Duong CM, Stewart TJ, Westwood JA, GUO ZS, Bartlett DL. 2012. Oncolytic Virus and Anti-4-1bb Combination Therapy Elicits Strong Anti-Tumor Immunity against Established Cancer. Cancer research.

161. Westwood JA, Darcy PK, Guru PM, Sharkey J, Pegram HJ, Amos SM, Smyth MJ, Kershaw MH. 2010. Three Agonist Antibodies in Combination with High-Dose Il-2 Eradicate Orthotopic Kidney Cancer in Mice. J Transl Med 8:42.
162. Westwood JA, Haynes NM, Sharkey J, McLaughlin N, Pegram HJ, Schwendener RA, Smyth MJ, Darcy PK, Kershaw MH. 2009. Toll-Like Receptor Triggering and T-Cell Costimulation Induce Potent Antitumor Immunity in Mice. Clin Cancer Res 15(24):7624-7633.
163. Takeda K, Kojima Y, Uno T, Hayakawa Y, Teng MW, Yoshizawa H, Yagita H, Gejyo F, Okumura K, Smyth MJ. 2010. Combination Therapy of Established Tumors by Antibodies Targeting Immune Activating and Suppressing Molecules. J Immunol 184(10):5493-5501.
164. Kocak E, Lute K, Chang X, May KF, Jr., Exten KR, Zhang H, Abdessalam SF, Lehman AM, Jarjoura D, Zheng P, Liu Y. 2006. Combination Therapy with Anti-Ctl Antigen-4 and Anti-4-1bb Antibodies Enhances Cancer Immunity and Reduces Autoimmunity. Cancer Res 66(14):7276-7284.
165. Lin GH, Liu Y, Ambagala T, Kwon BS, Ohashi PS, Watts TH. 2010. Evaluating the Cellular Targets of Anti-4-1bb Agonist Antibody During Immunotherapy of a Pre-Established Tumor in Mice. PLoS One 5(6):e11003.
166. Kohrt HE, Houot R, Goldstein MJ, Weiskopf K, Alizadeh AA, Brody J, Muller A, Pachynski R, Czerwinski D, Coutre S, Chao MP, Chen L, Tedder TF, Levy R. 2011. Cd137 Stimulation Enhances the Antilymphoma Activity of Anti-Cd20 Antibodies. Blood 117(8):2423-2432.
167. Kohrt HE, Houot R, Weiskopf K, Goldstein MJ, Scheeren F, Czerwinski D, Colevas AD, Weng WK, Clarke MF, Carlson RW, Stockdale FE, Mollick JA, Chen L, Levy R. 2012. Stimulation of Natural Killer Cells with a Cd137-Specific Antibody Enhances Trastuzumab Efficacy in Xenotransplant Models of Breast Cancer. J Clin Invest 122(3):1066-1075.
168. Palazon A, Teijeira A, Martinez-Forero I, Hervas-Stubbs S, Roncal C, Penuelas I, Dubrot J, Morales-Kastresana A, Perez-Gracia JL, Ochoa MC, Ochoa-Callejero L, Martinez A, Luque A, Dinchuk J, Rouzaut A, Jure-Kunkel M, Melero I. 2011. Agonist Anti-Cd137 Mab Act on Tumor Endothelial Cells to Enhance Recruitment of Activated T Lymphocytes. Cancer Res 71(3):801-811.
169. Dubrot J, Milheiro F, Alfaro C, Palazon A, Martinez-Forero I, Perez-Gracia JL, Morales-Kastresana A, Romero-Trevejo JL, Ochoa MC, Hervas-Stubbs S, Prieto J, Jure-Kunkel M, Chen L, Melero I. 2010. Treatment with Anti-Cd137 Mabs Causes Intense Accumulations of Liver T Cells without Selective Antitumor Immunotherapeutic Effects in This Organ. Cancer Immunol Immunother 59(8):1223-1233.
170. Niu L, Strahotin S, Hewes B, Zhang B, Zhang Y, Archer D, Spencer T, Dillehay D, Kwon B, Chen L, Vella AT, Mittler RS. 2007. Cytokine-Mediated Disruption of Lymphocyte Trafficking, Hemopoiesis, and Induction of Lymphopenia, Anemia, and Thrombocytopenia in Anti-Cd137-Treated Mice. J Immunol 178(7):4194-4213.
171. Schabowsky RH, Elpek KG, Madireddi S, Sharma RK, Yolcu ES, Bandura-Morgan L, Miller R, MacLeod KJ, Mittler RS, Shirwan H. 2009. A Novel Form of 4-1bbl Has Better Immunomodulatory Activity Than an Agonistic Anti-4-1bb Ab without Ab-Associated Severe Toxicity. Vaccine 28(2):512-522.
172. Scott AM, Wolchok JD, Old LJ. 2012. Antibody Therapy of Cancer. Nat Rev Cancer 12(4):278-287.

173. Dubinett SM, Patrone L, Tobias J, Cochran AJ, Wen DR, McBride WH. 1993. Intratumoral Interleukin-2 Immunotherapy: Activation of Tumor-Infiltrating and Splenic Lymphocytes in Vivo. Cancer Immunol Immunother 36(3):156-162.
174. Rosenberg SA, Yang JC, Topalian SL, Schwartzentruber DJ, Weber JS, Parkinson DR, Seipp CA, Einhorn JH, White DE. 1994. Treatment of 283 Consecutive Patients with Metastatic Melanoma or Renal-Cell Cancer Using High-Dose Bolus Interleukin-2. Jama-Journal of the American Medical Association 271(12):907-913.
175. Phan GQ, Attia P, Steinberg SM, White DE, Rosenberg SA. 2001. Factors Associated with Response to High-Dose Interleukin-2 in Patients with Metastatic Melanoma. J Clin Oncol 19(15):3477-3482.
176. Rosenberg SA, Lotze MT, Muul LM, Chang AE, Avis FP, Leitman S, Linehan WM, Robertson CN, Lee RE, Rubin JT. 1987. A Progress Report on the Treatment of 157 Patients with Advanced Cancer Using Lymphokine-Activated Killer Cells and Interleukin-2 or High-Dose Interleukin-2 Alone. New England Journal of Medicine 316(15):889-897.
177. Fyfe G, Fisher RI, Rosenberg SA, Sznol M, Parkinson DR, Louie AC. 1995. Results of Treatment of 255 Patients with Metastatic Renal Cell Carcinoma Who Received High-Dose Recombinant Interleukin-2 Therapy. J Clin Oncol 13(3):688-696.
178. Atkins MB, Lotze MT, Dutcher JP, Fisher RI, Weiss G, Margolin K, Abrams J, Sznol M, Parkinson D, Hawkins M, Paradise C, Kunkel L, Rosenberg SA. 1999. High-Dose Recombinant Interleukin 2 Therapy for Patients with Metastatic Melanoma: Analysis of 270 Patients Treated between 1985 and 1993. Journal of Clinical Oncology 17(7):2105-2116.
179. Fisher RI, Rosenberg SA, Fyfe G. 2000. Long-Term Survival Update for High-Dose Recombinant Interleukin-2 in Patients with Renal Cell Carcinoma. Cancer J Sci Am 6 Suppl 1:S55-57.
180. Yang JC, Sherry RM, Steinberg SM, Topalian SL, Schwartzentruber DJ, Hwu P, Seipp CA, Rogers-Freezer L, Morton KE, White DE, Liewehr DJ, Merino MJ, Rosenberg SA. 2003. Randomized Study of High-Dose and Low-Dose Interleukin-2 in Patients with Metastatic Renal Cancer. J Clin Oncol 21(16):3127-3132.
181. Reeves DJ, Liu CY. 2009. Treatment of Metastatic Renal Cell Carcinoma. Cancer Chemother Pharmacol 64(1):11-25.
182. Krieg C, Letourneau S, Pantaleo G, Boyman O. 2010. Improved Il-2 Immunotherapy by Selective Stimulation of Il-2 Receptors on Lymphocytes and Endothelial Cells. Proc Natl Acad Sci U S A 107(26):11906-11911.
183. Létourneau S, van Leeuwen EMM, Krieg C, Martin C, Pantaleo G, Sprent J, Surh CD, Boyman O. 2010. Il-2/Anti-Il-2 Antibody Complexes Show Strong Biological Activity by Avoiding Interaction with Il-2 Receptor A Subunit Cd25. Proceedings of the National Academy of Sciences 107(5):2171-2176.
184. NCI. 2012. Aldesleukin - National Cancer Institute. http://www.cancer.gov/cancertopics/druginfo/aldesleukin. February 5, 2012
185. King DM, Albertini MR, Schalch H, Hank JA, Gan J, Surfus J, Mahvi D, Schiller JH, Warner T, Kim K, Eickhoff J, Kendra K, Reisfeld R, Gillies SD, Sondel P. 2004. Phase I Clinical Trial of the Immunocytokine Emd 273063 in Melanoma Patients. J Clin Oncol 22(22):4463-4473.
186. Osenga KL, Hank JA, Albertini MR, Gan J, Sternberg AG, Eickhoff J, Seeger RC, Matthay KK, Reynolds CP, Twist C, Krailo M, Adamson PC, Reisfeld RA, Gillies SD, Sondel PM. 2006. A Phase I Clinical Trial of the Hu14.18-Il2 (Emd 273063) as a Treatment for

Children with Refractory or Recurrent Neuroblastoma and Melanoma: A Study of the Children's Oncology Group. Clinical cancer research 12(6):1750-1759.
187. Weiss JM, Back TC, Scarzello AJ, Subleski JJ, Hall VL, Stauffer JK, Chen X, Micic D, Alderson K, Murphy WJ, Wiltrout RH. 2009. Successful Immunotherapy with Il-2/Anti-Cd40 Induces the Chemokine-Mediated Mitigation of an Immunosuppressive Tumor Microenvironment. Proc Natl Acad Sci U S A 106(46):19455-19460.
188. Weiss JM, Ridnour LA, Back T, Hussain SP, He P, Maciag AE, Keefer LK, Murphy WJ, Harris CC, Wink DA, Wiltrout RH. 2010. Macrophage-Dependent Nitric Oxide Expression Regulates Tumor Cell Detachment and Metastasis after Il-2/Anti-Cd40 Immunotherapy. Journal of Experimental Medicine 207(11):2455-2467.
189. Liu LS, Liu SQ, Ng SY, Froix M, Ohno T, Heller J. 1997. Controlled Release of Interleukin-2 for Tumour Immunotherapy Using Alginate/Chitosan Porous Microspheres. Journal of Controlled Release 43(1):65-74.
190. Levin AM, Bates DL, Ring AM, Krieg C, Lin JT, Su L, Moraga I, Raeber ME, Bowman GR, Novick P. 2012. Exploiting a Natural Conformational Switch to Engineer an Interleukin-2/Superkine/'. Nature.
191. Dubois S, Patel HJ, Zhang M, Waldmann TA, Müller JR. 2008. Preassociation of Il-15 with Il-15rα-Igg1-Fc Enhances Its Activity on Proliferation of Nk and Cd8+/Cd44high T Cells and Its Antitumor Action. The Journal of Immunology 180(4):2099-2106.
192. Epardaud M, Elpek KG, Rubinstein MP, Yonekura A, Bellemare-Pelletier A, Bronson R, Hamerman JA, Goldrath AW, Turley SJ. 2008. Interleukin-15/Interleukin-15rα Complexes Promote Destruction of Established Tumors by Reviving Tumor-Resident Cd8+ T Cells. Cancer research 68(8):2972.
193. Weiner LM, Surana R, Wang S. 2010. Monoclonal Antibodies: Versatile Platforms for Cancer Immunotherapy. Nat Rev Immunol 10(5):317-327.
194. Hara I, Takechi Y, Houghton AN. 1995. Implicating a Role for Immune Recognition of Self in Tumor Rejection: Passive Immunization against the Brown Locus Protein. Journal of Experimental Medicine 182(5):1609-1614.
195. Bevaart L, Jansen MJ, van Vugt MJ, Verbeek JS, van de Winkel JG, Leusen JH. 2006. The High-Affinity Igg Receptor, Fcgammari, Plays a Central Role in Antibody Therapy of Experimental Melanoma. Cancer Res 66(3):1261-1264.
196. Saenger YM, Li YY, Chiou KC, Chan B, Rizzuto G, Terzulli SL, Merghoub T, Houghton AN, Wolchok JD. 2008. Improved Tumor Immunity Using Anti-Tyrosinase Related Protein-1 Monoclonal Antibody Combined with DNA Vaccines in Murine Melanoma. Cancer research 68(23):9884-9891.
197. Melero I, Johnston JV, Shufford WW, Mittler RS, Chen L. 1998. Nk1.1 Cells Express 4-1bb (Cdw137) Costimulatory Molecule and Are Required for Tumor Immunity Elicited by Anti-4-1bb Monoclonal Antibodies. Cell Immunol 190(2):167-172.
198. Hanahan D, Weinberg RA. 2011. Hallmarks of Cancer: The Next Generation. Cell 144(5):646-674.
199. Wilcox RA, Tamada K, Strome SE, Chen L. 2002. Signaling through Nk Cell-Associated Cd137 Promotes Both Helper Function for Cd8+ Cytolytic T Cells and Responsiveness to Il-2 but Not Cytolytic Activity. The Journal of Immunology 169(8):4230.